Dynamic Modeling of Apoptosis and its Interaction with Cell Growth in Mammalian Cell Culture

by

Mukesh Meshram

A thesis
presented to the University of Waterloo
in fulfillment of the
thesis requirement for the degree of
Doctor of Philosophy
in
Chemical Engineering

Waterloo, Ontario, Canada, 2011

AUTHOR'S DECLARATION

I hereby declare that I am the sole author of this thesis. This is a true copy of the thesis, including any required final revisions, as accepted by my examiners.

I understand that my thesis may be made electronically available to the public.

Mukesh Meshram

Abstract

In order to optimize productivity of a cell culture it is necessary to understand growth and productivity and couple these features of the culture to extracellular nutrients whose profiles can be manipulated. Also, since growth and productivity are directly affected by cell death mechanisms such as apoptosis, it is imperative to understand these mechanisms. This work describes the development of a differential equation based population balance model of apoptosis in a Chinese Hamster Ovary cell culture producing Anti-RhD monoclonal antibody (mAb). The model was verified in isolation and was then coupled to a metabolic flux model. The model distinguishes between various subpopulations at normal healthy states and at various stages of apoptosis. After finding that glucose and glutamine are not limiting nutrients for this culture, different hypotheses were explored to explain growth arrest. Initially, it was hypothesized that there is some unknown nutrient in either media or serum which is depleted, thus causing growth arrest. Accordingly a first model was developed assuming depletion of this nutrient. Subsequent experiments with different additions of media and serum showed that there is no such nutrient limitation for the media and serum conditions used in most of the experiments. Additional experiments with different culture volumes showed that cell growth was actually controlled by a compound that accumulates and causes pH deviation from its optimal range of operation. Since strong correlations were found between culture volume and growth, it was hypothesized that the compound may be carbon dioxide (CO_2), which is inhibitory for growth and may accumulate due to mass transfer limitations. Following this finding, a second model was proposed to take into account the accumulation of this inhibitor, although the specific inhibiting compound could not be exactly identified. This second mathematical model of cell growth was then integrated with a metabolic flux model to provide for a link between intracellular and extracellular species balances, since the latter are the ones to be manipulated for increasing productivity. This final model formulation was then used to describe mAb productivity. The model was also able to reasonably predict all cell subpopulations, nutrients, metabolites and mAb. In an attempt to mitigate the effect of CO_2 accumulation and renew the cell growth, culture perfusions were performed. Although this approach resulted in some renewal of growth, the cell concentration progressively decreased after each successive perfusion event. This suggests that irreversible cell damage occurs because of CO_2

accumulation. The model was used to describe the perfusion experiments. Agreement between data and model predictions were reasonable. In addition, it was shown that operation with successive perfusions results in a significant increase in productivity and therefore it can be used for further process optimization.

Acknowledgements

It is my great pleasure to thank all the people who contributed in various ways to this thesis.

First and foremost, I would like to express my deepest thank to my supervisor Professor Hector Budman for providing me consistent guidance and support. Thanks professor for your remarkable supervision during normal working days and also for always being available to discuss results of the work even during weekends that helped in development of this thesis. I also would like to extend my sincere thanks to my co-supervisor Brian Ingalls for his excellent input and guidance throughout the years. I also wish to thank another co-supervisor Professor Brendan McConkey for his full support and guidance towards this work. I am greatly obliged to these all my supervisors for all their contributions towards this thesis. They provided me bounteous opportunity to attend conferences where I could meet and exchange ideas with many concurring people. I really appreciate them for the time they spent in reviewing and editing my thesis, papers and presentations.

A special thank goes to Professor Jeno Scharer, who offered his extensive knowledge of bioprocess engineering towards this thesis work.

I also would like to thank my PhD defense and comprehensive examination committee members: Professor Ali Elkamel, Professor Bruce Reed, Professor Jeno Scharer, for agreeing to serve as committee members, providing constructive comments and valuable suggestions. Special thanks to external examiner Professor Alain Garnier for his time, thorough review of thesis and valuable comments. I owe appreciation to Professor Zongwei Chen for serving as a delegate of Professor Ali Elkamel for my PhD defense examination.

Many thanks to all the staff of Chemical Engineering Department and University of Waterloo for making the environment conductive towards the completion of thesis. I would like to extend my thanks to all my colleagues and friends in Biochemical Engineering and Process Systems Engineering Group for the very

friendly and enjoyable environment to work. I express my heartfelt thanks to my friends Jasdeep, Walid-Al-Ghervi, Prashant, Divya, Shankar, Saiedeh Naderi, Bhumika, Santosh Dhule, Arunbabu, Sarang, Mohammad Shams, Rozendo for all the good times I had with them, their advices and for all their little "help" that I required. I am also thankful to my housemates and friends for the time I spent with, support and memorable trips that enriched my stay at Waterloo. I also thank to my other friends back home in India and other locations, my friends during my masters, so called "BPT" group for their constant support, encouragement and wonderful friendship.

Finally and far most, I extend my deepest gratitude to my parents for their boundless love and constant encouragement and support in all my pursuits. I would also like to extend my thanks to all my other family members for their love, support and understanding.

Dedication

To My Family and

Guru

Contents

List of Figures

xiv

List of Tables

Nomenclature

X_v	Viable cell concentration (10^6 cells/mL)
X_{max}	Maximum viable cell concentration (10^6 cells/mL)
x_1	Normal healthy cells (10^6 cells/mL)
x_2	Caspase-8 active cells (10^6 cells/mL)
x_3	Caspase-9 active cells (10^6 cells/mL)
x_4	Caspase-3 active cells (10^6 cells/mL)
x_5	Caspase-8 and caspase-9 simultaneously active cells (10^6 cells/mL)
X_d	Dead cell concentration (10^6 cells/mL)
X_g	Viable growing cell concentration (10^6 cells/mL)
X_{ng}	Viable non-growing cell concentration (10^6 cells/mL)
f_{gr}	Fraction of normal dividing cells
μ_g	Specific growth rate constant (day $^{-1}$)
μ_d	Specific death rate constant (day $^{-1}$)
μ_{dmax}	Maximum specific death rate (day $^{-1}$)
K_{d_A}	Ammonia constant for cell death (mM)
K_s	Tessier apparent saturation constant (mM)
k_4	Specific generation rate constant (day $^{-1}$)
k_5	Specific generation rate constant (day $^{-1}$)
k_{lys}	Specific lysis rate (day $^{-1}$)
k_{sub}	Specific substrate consumption rate (mM (10^6 cells) $^{-1}$ day $^{-1}$)
k_8	Specific generation rate constant (day $^{-1}$)
k_9	Specific generation rate constant (day $^{-1}$)
k_{10}	Specific generation rate constant (day $^{-1}$)
K_i	Nutritional stress constant (mM)

S	Concentration of unknown substrate/component (mM)
Glc	Glucose concentration (mM)
Lac	Lactate concentration (mM)
Gln	Glutamine concentration (mM)
Glu	Glutamate concentration (mM)
Asn	Asparagine concentration (mM)
Asp	Aspartate concentration (mM)
Ala	Alanine concentration (mM)
Amm	Ammonia concentration (mM)
k_{Gln}	Saturation constant of glutamine (mM)
k_{Glc}	Saturation constant of glucose (mM)
k_{Glu}	Saturation constant of glutamate (mM)
k_{Asn}	Saturation constant of asparagine (mM)
k_{Asp}	Saturation constant of aspartate (mM)
k_{Ala}	Saturation constant of alanine (mM)
k_{i1}	Specific production rate of CO_2 by normal growing cells (mM day^{-1} (10^6 cells/mL)$^{-1}$)
k_{i2}	Specific production rate of CO_2 by normal non-growing cells (mM day^{-1} (10^6 cells/mL)$^{-1}$)
k_{i3}	Specific production rate of CO_2 by apoptotic growing cells (mM day^{-1} (10^6 cells/mL)$^{-1}$)
k_a	Accumulation constant (mM^{-1})
I	Inhibition factor concentration (mM)
I_∞	CO_2 concentration in equilibrium with headspace gas phase (mM)
k_{va}	Volumetric mass transfer coefficient (m day^{-1})
k_I	Inhibitory constant (mM)
P	mAb concentration (µg/mL)
q_p	Specific mAb production rate (mM day^{-1} (10^6 cells/mL)$^{-1}$)
a_i	Maximum reaction rate for corresponding nutrient or metabolite (mM day^{-1} (10^6 cells/mL)$^{-1}$) $i = 1…..8$
a_{ii}	Specific utilization or production rate for corresponding nutrient or metabolite (mM day^{-1} (10^6 cells/mL)$^{-1}$) $i = 1…..8$

Chapter 1

Introduction

This thesis is concerned with modeling apoptosis in cell culture, specifically addressing interactions between apoptosis and cell growth. The work is aimed at providing a deeper understanding of cell culture process for optimization of product yield. The work incorporates measurements of various caspases (apoptotic proteins) in culture by flow cytometry. The work investigates cell-cell interaction that triggers apoptosis and develops a comprehensive model of apoptosis, metabolic flux and monoclonal antibody production. This chapter motivates the research discussed in the thesis, beginning with an overview of cell culture technology, and discusses existing efforts towards modeling cell culture processes.

1.1   Mammalian cell culture technology

Cell culture technology has witnessed substantial development in the past few decades and has become an essential part of the biopharmaceutical industry. The products derived from cell culture technology are used in the health care sector to prevent and treat diseases like viral infections, cancer, heredity deficiencies and several chronic diseases. These products have been confirmed to be effective, safe, and economical (Ozturk and Hu, 2006).

Due to the commercial importance of biological products from mammalian cell culture technology there is considerable interest in further research and development of these processes. There are a number of biological products from these cell lines, such as recombinant proteins, monoclonal antibodies (mAb) and nucleic acid based products currently licensed in the market. Among these, monoclonal antibodies have dominated the market with large numbers of antibody-based therapeutic products licensed. The most prominent ones are Rituxan®, Herceptin®, Remicade®, and Synagis® (Brekke and Sandlie, 2003;

Pavlou, 2003). These antibodies have important applications in the management of cancer including diagnosis, monitoring, and treatment of the disease.

1.2   Process improvement in cell culture

Process or productivity improvement in cell culture technology is of primary concern in biopharmaceutical industries. There are various approaches to optimization, such as initial host screening, genetic engineering, and process operation. In process operation, it is important to know the environmental factors in a bioreactor that can affect cell behavior. This thesis investigates a cell culture process for Anti-RhD monoclonal antibody (mAb) production. The mAb productivity in cell culture is determined by viable cell density, culture longevity, and specific mAb production rate. Strategies for process improvement aim at maximizing these parameters by optimizing culture medium and feeding protocol (batch, fed-batch, perfusion and continuous operation, described in further chapters).

The mammalian cell growth system is highly complex, with a complicated intracellular environment consisting of numerous metabolic pathways and reactions occurring simultaneously. Thus understanding of biological activity in bioreactors is limited and trial-and-error experimentation or heuristics for cell culture process improvement are laborious and expensive.

Alternatively, the use of mathematical modeling allows for organization of preliminary experimental information in a logical and systematic manner, thus facilitating process understanding through the identification and quantification of key relationships between process parameters, variables, and product output rates. Analysis of these models can help identify parameters that significantly affect antibody production. Thus this approach can lead to a possible reduction in the required number of experiments with time- and cost-saving implications. In addition, a model can serve in the future to formulate optimal operation strategies.

This thesis focuses on an important factor in cell culture process: apoptosis, or programmed cell death, which is prevalent in cell culture, and affects cell growth and thus final product titer. The aim of this work is to understand the phenomenon of apoptosis and its interconnection with cell growth for mAb production by a model-based approach that will facilitate optimization of cell culture for process improvement.

1.3 Motivation

Cell culture is an efficient way of producing monoclonal antibodies and various other biological products. There has been a rapid increase in the demand for these monoclonal antibody products because of their usefulness and the variety of monoclonal antibodies that are required at high doses for application (Butler, 2005). To meet the current and future demand for monoclonal antibodies, it is necessary to enhance productivity by using the various efficient cell lines available and by developing effective manufacturing processes. The antibody products are, however, typically formed at very low levels because highly specialized culture conditions are required for cell growth and productivity. Host cell lines currently used to produce commercial mAb products include murine hybridoma and myeloma cell lines, CHO cell lines, and human cell lines. Hybridoma technology was first developed by Kolher and Milstein to produce mAb; murine B cells producing a particular antibody were fused to murine lymphoid cells (Kohler and Milstein, 1975). With this technology it was possible to produce mAbs for research, analytical use, and for limited-dose therapeutic products. However, hybridoma cells are generally difficult to engineer for high levels of protein expression and only grow to moderate cell densities in bioreactors (King, 1998), thus resulting in low levels of mAb productivity. To overcome these limitations, Chinese Hamster Ovary (CHO) cell lines came into practice for mAb production. Today, CHO cell lines have become the important workhorses for the production of not only mAbs but also other biological products. Because of the extensive application of these hosts, there is a good understanding of their growth behavior and metabolism in bioreactors, and the possible host-cell related impurities that might occur in the product. Thus an increasing number of products in development are now made using CHO cell lines.

Considering the fact that the dose requirements of these antibodies are high, it is important to enhance the product titer level to more than 1 g/L while culturing the cell lines. There has been substantial work done towards increasing product titer by genetic manipulation of cell lines, e.g. by transcription, post-transcriptional processing, translation, etc. (Bi et al., 2003; Kim et al., 2002; Mangalampalli et al., 2002). Along with genetic manipulation there have also been significant advances over the past few years in the search for optimal cell culture conditions to further improve mAb production (Andersen and Reilly, 2004; Wurm, 2004). Obtaining higher cell density in reactors is considered to be the most important aspect toward increasing productivity. This can be achieved through manipulation of the medium composition and culture conditions.

Programmed cell death, or apoptosis, is one of the key issues that must be addressed if the goal is obtaining higher cell density for enhanced productivity. Apoptosis restricts cell growth and production in

bioreactors and ultimately decreases cell yield. It causes a reduction in cell viability, both directly and indirectly, through the release of harmful metabolites and proteases that damage the remaining viable population and may inactivate the product. Apoptosis is triggered by a cascade of cysteine proteases called caspases, which are activated in response to various insults that may develop in bioreactors during batch or fed batch cultures. It has been observed that apoptosis is a common mode of cell death in CHO culture, especially in the post-exponential growth phase (Franek and Dolnikova, 1991; Golstein et al., 1991; Goswami et al., 1999).

Optimization of cell culture processes for the enhanced productivity of mAb is a highly challenging task and it cannot be easily performed by trial and error. Therefore the work in this research describes the development of a detailed model to be used towards optimization of cell culture. Such an approach would speed up the task of optimization and enhance the understanding of the underlying production process.

Mammalian cell culture involves complex metabolic networks. Previous studies have used metabolic flux analysis to construct mathematical models of mammalian cell culture processes by correlating cell growth to metabolic activities triggered by extracellular nutrient availability (Bonarius et al., 1996; Follstad et al., 1999; Gao et al., 2007). As nutrients are depleted and metabolic activity slows down, growth stops and apoptosis is triggered. Apoptosis accounts for the majority of cell death in bioreactors (Franek and Dolnikova, 1991; Golstein et al., 1991; Goswami et al., 1999) and so it significantly impacts cell density and viability, and thus product titer. A major cause for apoptosis in batch culture is likely depletion of vital nutrients such as glucose (Goswami et al., 1999) and amino acids such as glutamine and asparagine (Sanfeliu and Stephanopoulos, 1999; Simpson et al., 1998b). Precisely which nutritional deficiencies trigger apoptosis is currently unknown. In the models mentioned above, cell death by apoptosis was not explicitly addressed. Instead, the rate of overall cell death (including apoptosis) was correlated to the depletion of primary nutrients (glucose, glutamine) or high levels inhibitory products (ammonia, lactate) formed during the culture process. However, apoptosis can be triggered well before the depletion of glucose, glutamine or even when the levels of inhibitory metabolites like ammonia or lactate are low suggesting that in some cases there are additional factors involved (Ljunggren and Haggstrom, 1994).

Efforts have been devoted in the development of mathematical models of apoptosis (Choi et al., 2007; Eissing et al., 2004; Fussenegger et al., 2000; Spencer and Sorger, 2011). These models address the intracellular signaling networks of apoptosis. Although these generic models are comprehensive, and incorporate the effect of metabolic stress, their use in specific culture settings is limited, since they were not directly correlated with specific extracellular metabolic products, nutrient depletion, or cell density. Moreover, these models are specifically based on single cell level, thus their use may be limited since

each cell in a cell culture will be at different stages of growth, thus preventing its use in the presence of overall cell population in cell culture. The fact that these are single cell models also explains why these models have not been properly verified by experiments.

Operation of the cell culture process in either fed-batch or perfusion modes is another way of enhancing cell density and thus productivity (Detremblay et al., 1992; Lee et al., 2005; Nguang et al., 2001; Trampler et al., 1994). With these modes of operation, it is possible to reach higher cell density and prolonged sustainability of cell viability. However, apoptosis occurs in these modes of operation as well; leading to the accumulation of cell-derived materials in the medium due to membrane disintegration and cell fragmentation, which also result in higher downstream processing cost of the product of interest. In addition, the release of intracellular contents or proteins from the apoptotically lysed cells into the medium can affect the product quality. These effects could be overcome by delaying the onset of apoptosis in the early phase of culture, resulting in high cell density, and high product titer and quality.

In previous studies of mAb-producing hybridoma cell lines it has been observed that the cells continue producing mAb even during the stationary phase indicating that the apoptotic cells also produce mAb, albeit at a different rate than normal viable cells (Dorka et al., 2009). This fact motivated the need for modeling separately the amount of apoptotic and viable cell populations (Linz, 1999).

To address all the above mentioned issues, a model of apoptosis in Chinese Hamster Ovary cell culture was developed and interlinked with a metabolic flux model to arrive at a comprehensive description of mammalian cell culture, thus providing a useful tool for process improvement. Specific objectives and novel contributions of this thesis are:

- *Development and calibration of a model at the cellular level to describe the evolution of key intracellular components involved in apoptosis*

  This model is based on differential equations describing mass balances of the corresponding reactions. Time-course predictions for the concentrations of intracellular components were obtained from the solution of the differential equations. The key parameters of this model were estimated via numerical optimization techniques. The model investigates cell density effect in cell-cell signaling. After finding that glucose and glutamine are not limiting the cell growth, the model investigates the presence of unknown limiting nutrient that is driving the cell growth in the culture.

- *Investigation of volume dependency effect in cell culture*

  Since nutrients such as glucose and glutamine and associated toxic metabolites such as lactate and ammonia were found not to be limiting the growth, the effect of initial culture volume was investigated. It was found that the growth was actually driven by the inhibitory effect of drop in pH possibly due to CO_2 accumulation. The inhibitory effect was more pronounced in higher volume. The model was modified to take this inhibition into account.

- *Coupling of population-based apoptosis model to a dynamic metabolic flux model (developed by another PhD candidate in the group, Naderi et al., 2011) incorporating extracellular metabolites and prediction of mAb concentration with this combined model*

  Previously reported models have only described the extracellular metabolites or the intracellular species separately but have not linked both together into one model as done in this work. This is a novel approach for modeling cell culture process that is expected to provide a more accurate description of the process. The predicted concentrations of species obtained from this combined model of intracellular caspases relevant to apoptosis and metabolic extracellular fluxes were used to describe the mAb production by apoptotic and viable cells present in the culture.

- *Investigation of optimization of mAb concentration and the reversibility of cessation in culture growth*

  Cell growth occurs normally during exponential phase and then the growth stops due to cell cycle regulations influenced by various environmental factors such as nutritional or toxic stress. After investigating the inhibitory effect of pH depression possibly due to CO_2 accumulation in CHO culture under study, the reversibility of cessation in cell growth via full perfusion of culture was investigated as an approach to maximize cell density for higher mAb production.

1.4 Thesis outline

The remainder of the thesis is organized as follows

Chapter 2 presents a literature review of mammalian cell growth, monoclonal antibody production, apoptosis, various methodologies available to assess apoptosis and existing efforts towards intracellular modeling of apoptosis. Chapter 3 describes the materials and methods applied in this research. Chapter 4 presents the work performed towards the investigation of cell density effect as means of cell-cell signaling in cell culture triggering apoptosis. Chapter 5 presents modeling work on apoptosis progression in current CHO cell culture. Chapter 6 describes the investigation of the effect of serum levels on cell culture growth with different initial cell density. Chapter 7 presents the investigation of the effect of cell culture volume on cell behavior. Chapter 8 describes a comprehensive model by connecting an apoptosis model with a metabolic flux model and then to monoclonal antibody production. Chapter 9 presents the investigation of reversibility in growth inhibition for improving viable cell density in culture. Finally, Chapter 10 presents conclusions and provides suggestions for future work.

Chapter 2

Literature review

This chapter reviews literature on cell culture, programmed cell death or apoptosis, various methods of detection of apoptotic proteins, intracellular modeling of apoptotic pathways and summarizes generic mathematical approaches including apoptosis modeling.

2.1 Mammalian cell culture and products

Biological products manufactured from mammalian cell culture have significant importance in medical and clinical applications. The production of viral vaccines was the first application of mammalian cell culture for therapeutic purposes. The cells used were primary cells such as monkey kidney cells and chicken embryo cells. These cells are anchorage dependent, requiring a surface to grow. Furthermore, these cells strictly require growth factors such as serum for growth. This restriction led to the adoption of BHK (Baby hamster kidney) cells, which can be grown in large scale in suspension bioreactors. Although this cell line was accepted for veterinary vaccines it was not initially accepted for human applications because of safety concerns since the cells contain tumorogenic agents and virus-like particles which were unacceptable to regulatory bodies (WHO, FDA). Eventually the use of human diploid cells such WI-38 and MRC-5 was approved for human applications (Petricciani, 1995). These are normal cells, virus-free and contain no carcinogenic components. However, because of their short life span and anchorage-dependent characteristics, growing these cells is challenging for large-scale production. Consequently, continuous cell lines like BHK, myeloma cells (SP2/0, NS0), Chinese hamster ovary (CHO), and human embryonic kidney (HEK) cell were gradually adopted for mammalian cell culture applications. These continuous cell lines can be grown in suspension in agitated and aerated bioreactors, and thus they are suitable for large scale production.

Monoclonal antibodies (mAb) have emerged as potential biopharmaceuticals with significant economic importance. The first mAb to be approved for clinical applications in humans was a murine antibody IgG2, OKT3 (derived from its origin - Ortho Pharmaceutical Corporation, lab of Patrick Kung), also referred to as murumonab (Hooks et al., 1991). This was followed by several chimeric mAbs containing both murine and human regions. These early antibody products posed a moderate risk of immunogenicity to patients from their residual murine components, somewhat limiting their further development. To address this issue, new technologies for creating mAbs, predominately or entirely of human origin, were developed. Currently, almost all antibody products in development are humanized or fully human.

2.2 Characterization of cell culture

Production of biopharmaceuticals from mammalian cell culture is accomplished in various bioreactors for large scale production. The characteristics of cells keep changing during culturing in batch or fed batch mode. Cell morphology (cell size and cell surface structure) is a clear indicator of the state of a cell. Cells usually become larger in size during exponential growth phase and smaller during stationary phase. In the late phase of a batch culture, the membrane surface undergoes typical structural changes. This is later followed by the disappearance of microvilli and appearance of blebs. The variation in cell morphology can be correlated to cell growth and death via the cell cycle. Because of active proliferation with higher proportion of cells in the S-phase of the cell cycle, cells increase in size during the exponential phase (Al-Rubeai et al., 1991; Lloyd et al., 2000).

2.2.1 Cell cycle

In cell culture, heterogeneity exists in terms of the stages at which cells are in the cell cycle. The cell cycle is the process where a cell duplicates its contents and divides into two to produce genetically identical daughter cells. Non-dividing cells are considered to be outside of the cell cycle.

A cell progresses through the four phases of the cell cycle: G1, S, G2 and M (Figure 2.1). The cell cycle begins with the G1 phase (G refers to gap). During this phase a cell feeds on nutrients supplied in the medium, synthesizes RNA and proteins. The cell grows in size and readies itself for DNA replication in S-phase. During the S-phase, the cell synthesizes DNA. This phase ends when the DNA content of the nucleus has doubled and the chromosomes have replicated. The cell then proceeds to the G2-phase where it produces new proteins and grows further in size. Finally, it enters the M-phase during which nuclear division (mitosis) and cytoplasmic division (cytokinesis) occur thus dividing the cell into two daughter cells.

Cell cycle advancement is regulated by CDKs (cycline-dependent kinases which add phosphate to proteins) that get activated by binding of regulatory subunits called cycline (Sherr and Roberts, 1999; Sugimoto et al., 2002). Depending upon the environmental or developmental signals, cells in the G1 phase may leave the cell cycle during which the cells become non-dividing and remain in a quiescent metabolism where protein synthesis and cellular functions continues but where there is no cellular size growth. This quiescent state is referred to as the G0 state.
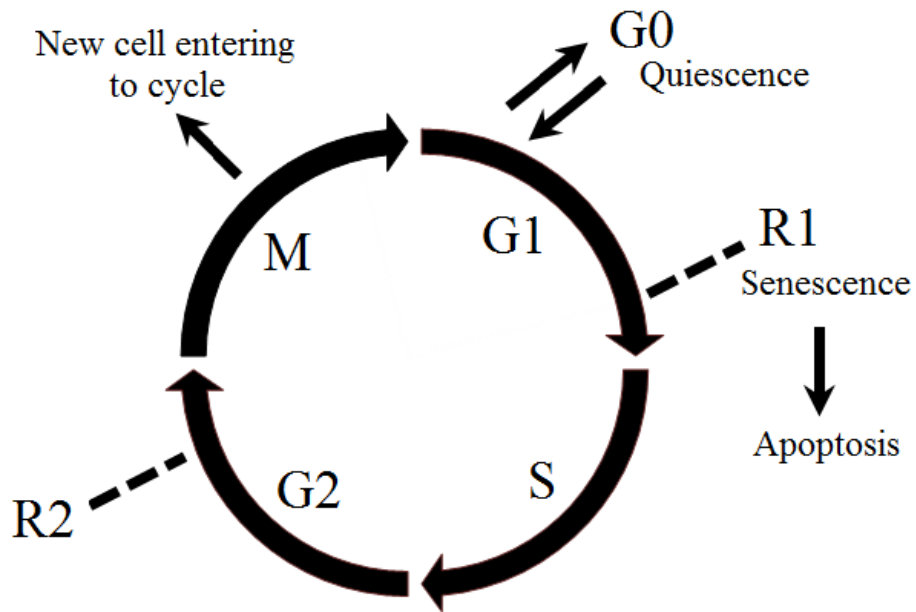
Figure 2.1: Cell cycle (R1, R2: restriction points)

Most of the cells in human body tissues and organs, such as postmitotic neurons and skeletal muscle cells are in non-dividing state. A cell may remain in this state for an indefinite time until signaled to continue through the whole cell cycle. For differentiated neurons this G0 state is permanent (Chanas-Sacre et al., 2000; Yoshikawa, 2000). Growth arrest can be caused by withdrawal of serum growth factors and nutrients. In many cases accumulation of p27 is believed to be the major factor for reversible G0/G1 arrest caused by growth factor deprivation or high cell density in culture (Polyak et al., 1994). But withdrawal of growth factors is not the only way to arrest the cell cycle in G0 state. Induction of CDK inhibitors such as p21, p53, p16, p57 can cause cell cycle arrest in the presence of serum. This form of growth arrest is usually considered to occur during the late G1 phase. The durations of S, G2, and M phases are relatively constant, while the duration of the G1 phase, particularly the early G1 phase, is more variable (Baserga, 1985).

Cellular senescence is a state that occurs in response to DNA damage or degradation that would make the cell nonviable. Nutrient depletion can lead to DNA damage (Weinberger et al., 2007). A protein p53 blocks the cell cycle by inhibiting CDK activity in case of DNA damage and its levels are increased in damaged cells. Activation of p53 allows time and opportunity for DNA repair before DNA replication and mitosis (Hartwell and Kastan, 1994). If the damage is severe and irreparable, p53 induces apoptotic cell death as a mean for eliminating faulty cells.

The cell cycle comprises checkpoints that sense possible defects in DNA synthesis and chromosome distribution for appropriate cell cycle progression. During the developmental G1 stage there may be some errors in functions performed during the cell cycle. At this point the cell may decide whether to proceed to the next phase (S-phase) or not. This is the first checkpoint or restriction point (R1) which is present just before the S-phase (Pardee, 1974). After passing this point, cells are committed to the S-phase. Cellular senescence can be thought of occurring at this check point that can lead to apoptosis.

Another check point is present in the G2-phase referred to as R2. A check is made on the successful replication of DNA that takes place during S phase. If replication stops at any point on the DNA, progress of the cell cycle is halted until the fault is repaired. If not, a cell destroys itself through apoptosis.

A more thorough review on cell cycle progression in mammalian cells can be found in (Fussenegger and Bailey, 1998). A study on the population distribution of hybridoma cells during perfusion was carried out by flow cyometric analysis (Park and Ryu, 1994). It was shown that the proportion of cells in the S-phase decreases during the decline period of a perfusion culture, and the proportion of cells in the G0/G1 phase

increases with decreasing growth rate. Also it was shown that the proportion of cells in the G2/M-phase was relatively constant throughout the perfusion culture.

2.2.2 Cell culture selection for biotherapeutics production

Chinese hamster ovary (CHO), mouse myeloma (NS0), baby hamster kidney (BHK), murine C12, human embryo kidney (HEK-293) or human-retina-derived (PER-C6) cell lines are used for the cell culture production of various recombinant biotherapeutics. However, CHO cell lines are the most used host cells for biotherapeutics production as these cell lines have excellent capability of suspension growth. The other cell lines, except NS0 and HEK-293, are characterized for their anchorage dependent nature and need special efforts to make them adapt to suspension growth environment. CHO cell lines are well-characterized in terms of efficient transfection, amplification and screening for high producer clones. These cell lines are also considered as reasonably safe by regulatory bodies such as FDA. Overall, CHO cell lines are the foremost source organisms for the production of various biological products because of their high capacity for suspension growth, good quality and product safety in therapeutic applications.

Recombinant cell lines transfected with a target gene are used for utilization in cell culture. *dhfr* (di̲hydro̲folate re̲ducatase) and GS (glutamine s̲ynthetase) are the most widely used selectable marker systems for cell lines.

CHO cell lines are customarily used with *dhfr* systems. In *dhfr* systems, a target gene is transfected along with *dhfr* marker gene into a cell line deficient in *dhfr* activity. The *dhfr*⁻ cells are unable to synthesize an essential metabolic enzyme, dihydrofolate reductase, involved in biosynthesis of nucleotide components. After transfection, the transfected cells that express the *dhfr* gene are capable of growing in media in the absence of glycine, hypoxanthine and thymidine. MTX (M̲e̲t̲h̲o̲t̲r̲e̲x̲a̲te), which is an inhibitor of *dhfr* enzyme activity**,** can be used for amplication of the *dhfr* gene (Gandor et al., 1995; Pallavicini et al., 1990). By subjecting the cells to an increasing concentration of MTX for several rounds, amplification of the *dhfr* gene and target gene can be obtained. Thus it is possible to produce a clone with higher specific productivity following an increased gene copy number.

In the GS system, cell lines, having insufficient capability of expressing the GS gene, are co-transfected with the GS gene. The GS enzyme enables the intracellular synthesis of glutamine, thus the cells surviving in a glutamine deficient medium are selected for the production of biological products. CHO cells have the capability to express the GS enzyme to grow in glutamine-free media. High-level expression cell lines can be obtained by subjecting these CHO cell lines to low level of MSX (m̲ethionine

sulpho<u>x</u>imine), a GS inhibitor (Cockett et al., 1990). Myeloma cells (NS0) do not have sufficient capability to express GS since they need glutamine in the media to survive. These cells, after GS transfection and growth in the glutamine-free media, can be selected for high expression clones by using low levels of MSX than that required for CHO cell lines. The advantage of this GS system is that less ammonia is produced thus reducing the toxicity to the cells (Zhang et al., 2006).

2.3   Bioreactor operation modes

The operation of mammalian cell cultivation is an essential aspect of productivity and product quality. The operation modes for cell cultivation can be divided into batch, fed batch, continuous culture with partial cell retention (chemostat or cytostat) and continuous culture with cell retention (perfusion). Figure 2.2 shows the schematics of different modes of operation.

2.3.1 Batch culture

In this mode of cultivation, the cells and medium are charged into a bioreactor and no further addition or withdrawal of cells or medium during the process is done (Figure 2A). At the end of the process the entire reactor content is harvested at once. The cells grow in suspension exponentially consume nutrients (glucose, amino acids etc.) and produce metabolic waste products (e.g. lactate, ammonia and CO_2) until a maximum cell density for a given medium is reached due to nutrient limitation or waste product inhibition.

It is the simplest operation, relatively short in duration and it is the preferable choice of cultivation in much industrial cultivation due to low risk of contamination, while easing implementation, scale up and validation. However, batch processes suffer from problems of nutrient depletion, low cell densities, low productivity and accumulation of toxic metabolites that may hamper product quality. Also, the down-time between batches may be too long resulting in overall less productivity.

Most of the cell lines have been used for cultivation in batch mode. In standard cell culture media cell densities in the range 1-4 x 10^6 cells/mL have reached (Lee et al., 2003; Merten, 1987; Ozturk and Palsson, 1990a). In other studies, significantly higher cell densities of $>10^7$ cells/mL have been reported to be achieved for hybridoma cells (Jo et al., 1993).

2.3.2 Fed-batch culture

To overcome early nutrient depletion, fed-batch mode is usually implemented. Fed-batch culture is characterized by a continuous or intermittent feed of nutrient, thus helping achieve higher cell density and product formation compared to batch operation (Figure 2.2B). Since no cell suspension or supernatant is taken out from the bioreactor during the process, the volume increases till the entire material is harvested at once. With this mode of operation the culture duration is prolonged from a few days to weeks. Generally high productivity is obtained as compared to batch operation due to the prolonged accumulation of product. Optimization of feeding strategies involving optimal feeding solution and feed rate controls are an essential part of this operation to obtain higher product titer by minimizing nutrient depletion and minimizing the formation of toxic metabolites e.g. lactate and ammonia. In CHO cell culture the cell density could be increased by fed-batch operation to 5 x 10^6 cell/mL (Xie et al., 1997). Fed batch has also been applied in large scale in 25000L working volume for large scale production of antibody (Birch and Racher, 2006). In hybridoma cell culture the cell density has been reported to be in the range of 3-17 x 10^6 cell/mL (Xie and Wang, 1996) and productivity to be 10-fold compared to simple batch culture (Robinson et al., 1994; Xie and Wang, 1994). In insect cell fed-batch culture cell density in the range of 5 x 10^6 cell/mL has been reported (Elias et al., 2000).

A review of fed-batch culture in monoclonal antibody and other recombinant protein production can be found in (Wlaschin and Hu, 2006; Bibila and Robinson, 1995; Xie and Wang, 1997).

2.3.3 Continuous culture

In continuous culture or chemostat (<u>chem</u>ical environment is <u>stat</u>ic), fresh nutrient medium is added continuously to the bioreactor with simultaneous partial withdrawal of cell suspension at the same rate, keeping the culture volume in the reactor at constant (Figure 2.2C). The reactor content is well mixed ensuring the concentration of cells, nutrients, and metabolites in the vessel is the same as those in the effluent stream. Because of the continuous addition and removal, the possibility of nutrient depletion and accumulation of toxic metabolite is reduced. While transient changes of most of the parameters are observed in batch culture, continuous operation enables the study of the effect of different culture variables under steady state environmental conditions. A number of studies have been reported in characterization of growth and metabolism over a wide range of dilution rates for CHO cells (Heidemann et al., 1998; Nyberg et al., 1999), hybridoma cells (Frame and Hu, 1991; Ray et al., 1989; Vriezen and van Dijken, 1998) and BHK cells (Carrondo et al., 1999; Hu et al., 2000).

This mode of operation requires a higher level of technical skill to operate as compared to batch or fed-batch cultures. Continuous prolonged operation is subject to genetic changes in cells that can lead to low productivity.

2.3.4 Perfusion culture

In this mode of operation fresh medium is fed in the bioreactor continuously or semi-continuously and cell-free supernatant constantly removed at the same rate while retaining or recycling cells back to the bioreactor (Figure 2.2D). Thus, in this mode of operation, the accumulation of high levels of toxic or inhibitory metabolites that might have negative impact on the productivity is avoided. This mode of operation offers high cells densities and productivities compared to batch, chemostat and even compared to fed-batch. Spin filters, hollow fibers and decanters are used for the retention of cells. The perfusion rate depends on the type and culture behavior of the cell line, the concentration of nutrients in the feed and the level of toxicity. This mode of operation has been used for the production of monoclonal antibodies (Banik and Heath, 1995; Tang et al., 2007; Yang et al., 2000) and recombinant proteins (Al-Rubeai et al., 1999; Avgerinos et al., 1990).
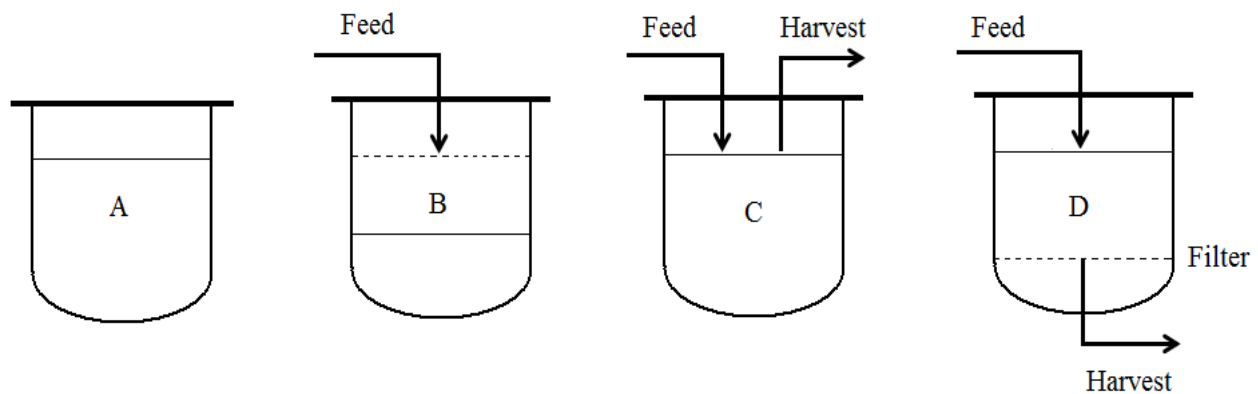
Figure 2.2: Culture operation modes (A) Batch culture operation (B) Fed-Batch culture operation (C) Continuous culture operation (D) Perfusion culture operation

An example of a 500 L industrial perfusion system for monoclonal antibody production by hyridoma is described by (Deo et al., 1996) where the operation continued for 15 to 35 days to achieve commercial production of antibodies with a cell density of >10 x 10^6 cell/mL. Their results have shown that the volumetric productivity of the perfusion process was approximately 10 times that of batch or fed-batch cultures. Large scale cultivations are running at Bayer (Boedecker, 1994), Chiron (Gray et al., 1996), and Novartis (Bachinger et al., 2000) and others. Bayer launched coagulation factor VIII, the first biopharmaceutical produced by recombinant BHK cells using a continuous perfusion culture obtaining a 30-fold increase in cell density that results in a 30-fold higher yield of factor VIII compared to the batch culture, over a period of 185-day production process. This leads to significantly reduced requirements for plant capacity, i.e. a 100-500 L perfusion reactor vs. a 5,000-15,000 L batch reactor (Boedecker, 1994).

The overall advantage of perfusion cultures is that they require smaller scale compared to batch cultures. However, a disadvantage of the perfusion system is the additional time and complexity involved in developing the process and added risk for contamination. Operating a perfusion bioreactor is expensive because of the continuous addition and removal of medium, operating equipment like pumps and membranes to supply medium to the bioreactor and also the extra cost to treat the waste medium (Shuller, 2002).

2.4 Cell death in bioreactors

Cell death occurs as a result of two distinct processes: necrosis and apoptosis.

2.4.1 Necrosis

Necrosis is an accidental, passive, uncontrolled death and is referred as "cell murder" (Darzynkiewicz et al., 1997). This is caused when the cells are exposed to sudden and harsh cellular damage occurring upon severe changes in culture conditions such as shear stress on cell membrane due to collision with the bioreactor wall or stirrer, exposure to high levels of toxic metabolites (Singh et al., 1994).

2.4.2 Apoptosis

Apoptosis is an active, intrinsically controlled cell death and referred as "cell suicide" (Majno and Joris, 1995). It occurs as a regulated response to specific shifts in the culture environment. This non-optimal change, which in some cases is inevitable, is associated to many causes as follows,

2.4.2.1 Nutrient depletion

Depletion of some essential nutrients such as glutamine (Sanfeliu and Stephanopoulos, 1999; Simpson et al., 1998a), glucose (Goswami et al., 1999), growth factors and oxygen (hypoxia) (Ishioka et al., 2007; Malhotra et al., 2001) has been found to trigger apoptosis in cell culture.

2.4.2.2 Serum withdrawal

Serum is an essential component that fulfills an important role in cell growth and cell survival. Serum contains many important growth factors, hormones, vitamins and other nutrients which are essential for the normal growth of the cell. Depletion of specific components in serum triggers nutrient stress leading to apoptosis in hybridoma and CHO cells (Bailey et al., 1999; Even et al., 2006), and plasmacytomas (Singh et al., 1994).

2.4.2.3 Dissolved CO_2 and osmolality

CO_2 in cell culture process is generated by biotic sources i.e. cellular respiration, and abiotic sources such as bicarbonate ($NaHCO_3$) or carbonate (Na_2CO_3) added as a buffer to control the pH of the cell culture medium (Goudar et al., 2006). At high viable cell concentrations in large scale cell culture processes, dissolved CO_2 can accumulate due to low removal rates at reduced bioreactor surface-to-volume ratio (Pattison et al., 2000). As CO_2 accumulates in the bioreactor, it dissolves in the cell culture medium as well as in the cell cytoplasm (i.e., CO_2 passes freely across cell membranes) and dissociates into HCO_3^- and H^+ ions

$$CO_2 + H_2O \leftrightarrow H^+ + HCO_3^-$$
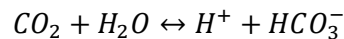
The decreased in pH (increase in H^+ ions) has detrimental effects on cellular metabolism by affecting enzyme activity.

The solubility of a gas in a solvent is directly proportional to the partial pressure of that gas above the solvent and is given by Henry's Law as

$$P_{CO_2} = H_{CO_2}[CO_2]^*$$

where $[CO_2]^*$ is the CO_2 concentration in equilibrium with the gas phase, P_{CO_2} is the partial pressure of CO_2 and H_{CO_2} is Henry's Law constant (Pa/M). The physiological concentration of CO_2 that is required

for the normal growth of cells is 0.04-0.07 atm, i.e., an aqueous phase concentration in equilibrium with a gas phase with a CO_2 partial pressure of .041-0.071 atm (Schmelzer and Miller, 2002).

The HCO_3^- and the base (e.g., NaOH) added to control the pH of cell culture medium contribute to increased medium osmolality. Increased osmolality alters membrane exchange activity to maintain cell volume, leads to increased intracellular solute concentrations (e.g., Na^+ or Cl^-) which can further adversely affect intracellular enzyme activity. Hence, increase in CO_2 accumulation results in increased medium osmolality. The elevated levels of osmolality itself unfavorably affect cell growth and metabolism. It is therefore important to decouple the effect of dissolved CO_2 and osmolality.

Most of the studies related to the effect of CO_2 on cell behavior are actually combined effects of CO_2 and osmolality. In studies of CHO cell culture, a very little or no change in growth rates was observed at higher CO_2 concentrations of 0.18 and 0.26 atm (at an osmolality of 310 mOsm/kg) compared to the control at a CO_2 concentration of 0.05 atm (at an osmolality of 310 mOsm/kg). However, there was a decline in the growth rate by 30% when CO_2 concentration increased from 0.05 to 0.33 atm (at an osmolality of 310 mOsm/kg) (Kimura and Miller, 1996). In studies of CHO cell culture in a 10 L bioreactor, a decrease in the cell viability from 79% to 58% was observed with increasing CO_2 concentration from 0.05 to 0.6 atm (osmolality of 310 to 340 mOsm/kg) (Gray et al., 1996).

On the contrary, investigations conducted with increased osmolality of 357 and 376 mOsm/kg at 0.05 atm CO_2 in CHO cell culture increased the specific death rate by 30% and 60% compared to the control at an osmolality of 310 mOsm/kg (Dezengotita et al., 1998). Combination of elevated CO_2 concentration and osmolality had a detrimental effect on cell growth (Dezengotita et al., 1998; Kimura and Miller, 1996; Zhu et al., 2005). A decrease in growth rate by 45% was observed at 0.33 atm and 376 mOsm/kg compared to the control at 0.05 atm and 310 mOsm/kg in cell culture of CHO cells in T-150 flasks (Kimura and Miller, 1996). It has been shown that apoptosis was the main mechanism of cell death of hybridoma cells at elevated levels of partial pressure of CO_2 and osmolality (DeZengotita et al., 2002).

Aunins and Henzler, (1993) had observed an early cell death in NS0 myeloma cell cultures with a final CO_2 of 0.16 atm. However, the specific production rates of IgG by cells remained unaffected.

2.4.2.4 pH

pH is another parameter that has a large effect on growth in cell culture. During the culture, changes in pH occur that can affect cell growth. As discussed above, CO_2 accumulation in culture medium is a major

cause of decrease in pH during the culture which affects the intracellular pH. Deviation of pH away from its optimal range can have a significant effect on cell growth and productivity via apoptosis. While most of cell culture media offer substantial buffering of pH, cellular metabolism invariably decreases pH due to the secretion of lactic acid and CO_2 accumulation.

The effect of pH shift on cell growth and productivity in batch culture of GS-NS0 mouse myeloma cell line was investigated by Osman et al., (2001) and Osman et al., (2002) over the range of pH 6.5 to 9. The pH shift was obtained by manipulating dissolved CO_2 concentration by CO_2 sparging or CO_2 stripping (nitrogen/air stripping). It was shown that pH shift above 0.2 units can cause a transient increase in apoptotic cell death. The pH shift between the values 7.0 and 8.0 continued the cell growth. On the other hand cultures that shifted below 7.0 and above 8.0 did not recover, resulting in cell death. They found that the maximum specific growth rate and maximum viable cell number occurred at pH 7.3 while product formation was found optimum at pH 7.0. In the studies conducted by Gottlieb, (1996), intracellular pH shift has been described as a trigger of apoptosis in various cell culture systems. Similarly, in the studies carried out by Al-Rubeai and Ishaque, (1998) in hybridoma cell culture, it was found that the intracellular acidification is a clear indication of apoptosis since it induces cellular destruction and cell death.

2.4.2.5 Toxic metabolites

Accumulation of toxic metabolites such as lactate and ammonia during the culture is also responsible for triggering apoptosis. Lactate build-up leads to the acidification of the culture environment. In addition, lactate itself could also be toxic to mammalian cells even under optimal pH values (Hassell et al., 1991; Lao and Toth, 1997; Ozturk et al., 1992; Singh et al., 1994).

2.4.2.6 Cell density

Higher cell density has also been found to trigger apoptosis in cell culture via cell-cell communication (Ishizaki et al., 1994; Mathieu et al., 1995; Saeki et al., 1997). It is hypothesized that the effect of density is due to the lack or reduction of survival signals provoked by direct cell-cell contact or soluble growth factors (autocrine factors) produced by the cells.

2.4.2.7 Oxygen

Other insults like excess oxygen (hyperoxia) have also been found to promote apoptosis (Emery et al., 1995; Laken and Leonard, 2001). Deprivation of oxygen has also been shown to be a trigger for apoptosis (Mercille and Massie, 1994b).

Another form of cell death has also been identified and is being widely studied, this is called autophagy which is a normal cell degradation process without the involvement of caspases (Gozuacik and Kimchi, 2004; Broker et al., 2005). It can be triggered by nutrient depletion, hyperosmotic stress or viral and microbial infection (Mortimore and Poso, 1988; Hwang and Lee, 2008; Han et al., 2010).

2.5 Morphological characteristics of cell death

Cells undergo unique morphological changes during death. In apoptosis, the morphological changes start occurring in the cell nucleus. Simultaneously, the cytoplasm looses water and the cellular cytoskeleton breaks down leading to cell deformation and shrinkage. Then, the chromatin condenses followed by extensive blebbing of the plasma membrane and separation of fragments into apoptotic bodies. This event is referred to as "budding".

Apoptotic bodies consist of cytoplasm with tightly packed organelles with or without a nuclear fragment. The organelle integrity is still maintained and it is enclosed within an intact plasma membrane. These apoptotic bodies can be phagocytosed *in vivo* although *in vitro* they might break apart or accumulate during the cell culture process.

Necrosis on the other hand results in swelling of the cell, rupturing of the plasma membrane, release of cytoplasmic contents to the extracellular environment and cell lysis (Leist and Jaattela, 2001). During necrotic death, neither specific signaling nor particular degradation of DNA has been observed (Mercille and Massie, 1994a). Figure 2.3 shows the morphological changes during the progression of apoptosis and necrosis respectively.

Caspases are the prime mediators of apoptosis. At least 14 different caspases, to date, have been identified in mammalian cells (Droin et al., 2008; Cohen, 1997). Members of the caspase family can be divided into three groups. (1) Initiator caspases (e.g. caspase-2, 8, 9 and 10), executioner caspases (e.g. caspase-3, 6 and 7) and participants in cytokine activation (e.g. caspase-1, 4, 5, 11, 12, 13 and 14). Caspase-8, 9 and 3 have been the most widely studied caspases. Caspases share similarities in their sequences, structure and substrate specificity. Two cleavage events are involved during the activation of caspases. The first event involves cleavage of the protein chain into large and small caspase subunits, and a second cleavage removes the N-terminal pro-domain. The active caspase is a tetramer of 2 large and 2 small subunits, with 2 active sites (Wolf and Green, 1999).
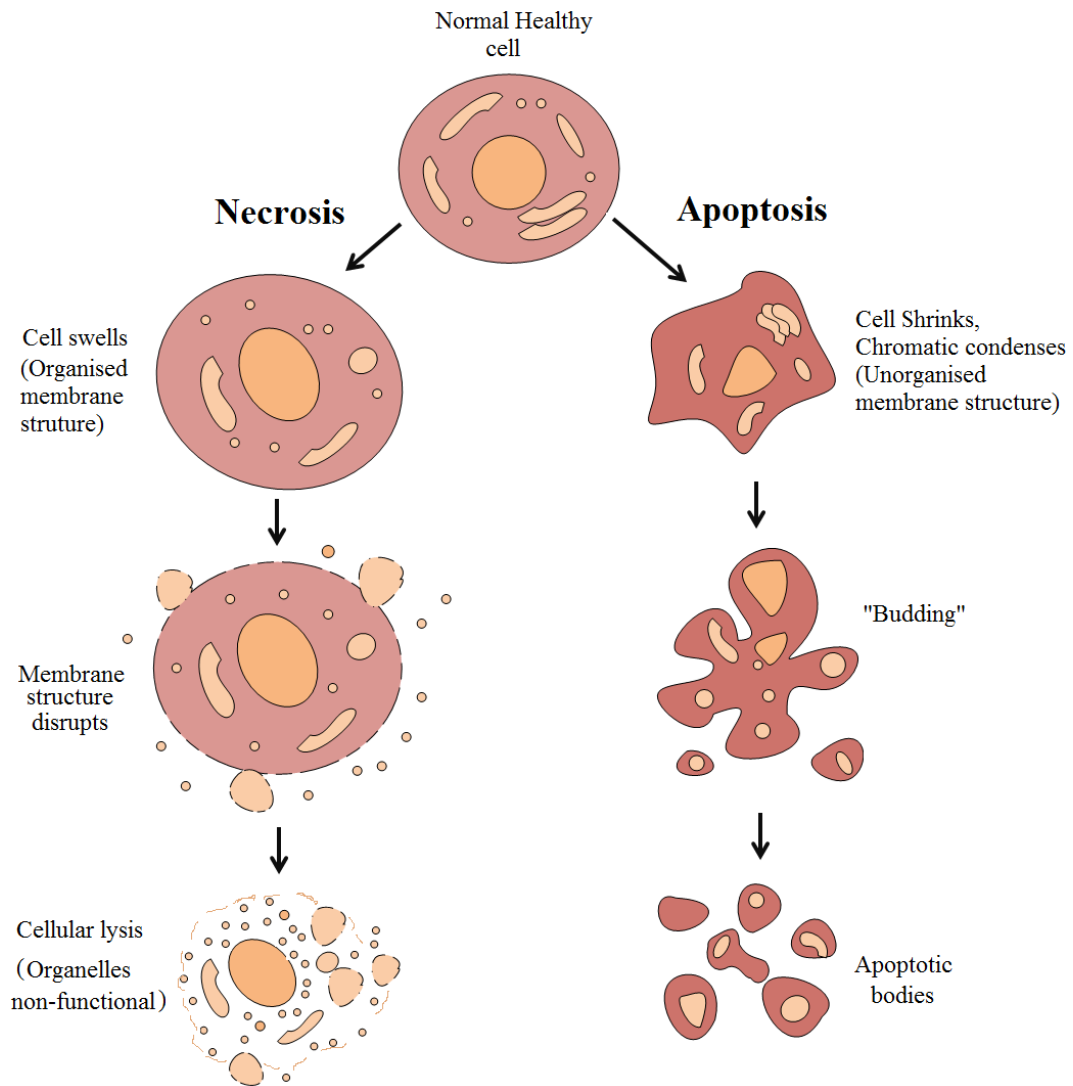
Figure 2.3: Characteristics of apoptosis and necrosis process

2.6 Apoptotic pathways

There are two widely reported main pathways so far through which the apoptotic cascade proceeds. These are the receptor-mediated pathway and the mitochondrial-mediated pathway. These are explained as follows

2.6.1 Receptor-mediated pathway

This pathway of apoptosis is initiated by the binding of some extracellular protein ligands to their cognate transmembrane death receptor proteins (Aggarwal, 2003; Ashkenazi and Dixit, 1998; Schulze-Osthoff et al., 1998). This is also referred to as the extrinsic pathway (Figure 2.4). The receptors involved in this pathway are the members of the tumor necrosis factor (TNF) type I superfamily (Arden and Betenbaugh, 2004; Huerta et al., 2007).

The ligands and their corresponding cognate receptors identified so far are: FASL/CD95L/Apo1L-Fas/CD95/Apo1, Apo2L-DR4, Apo3L-DR3, TNF-α/TNFR1. The death receptors contain a cytoplasmic tail called death domain (DD) which upon ligation recruits an adaptor protein such as FAS associated death domain (FADD) or TNF-related associated death domain (TRADD) (Golstein, 1997; Schulze-Osthoff et al., 1998). This adaptor protein also contains its own death domain (DD) by which it gets recruited to DDs of a death receptor thus forming the so-called death-inducing-signaling complex (DISC). The adaptor protein also contains a death effector domain (DED) which through DED-DED interaction recruits two pro-caspases, which activate each other by proteolytic cleavage. The two caspases that are bound to these adaptor molecules are mainly caspase-8 or caspase-10. These activated caspases stimulate a downstream cascade where other caspases, including executioners caspase-3 or caspase-7 are activated resulting in apoptosis.

The receptor mediated pathway also communicates with the mitochondrial pathway through the small pro-apoptotic Bcl-2 homolog, Bid, which is activated by caspase-8 cleavage to generate truncated Bid (tBid). Activated tBid translocates to the mitochondrial membrane, where it creates pores and stimulates the activation of the mitochondrial apoptosis cascade through an interaction with the pro-apoptotic Bax or Bak proteins (Zha et al., 2000).

2.6.2 Mitochondrial pathway

This pathway is also referred as the intrinsic pathway because it is triggered by signals from the intracellular environment. This however does not mean that the initial stress signals originate in the intracellular area. This pathway is initiated by the release of cytochrome-c from the mitochondria in response to various stresses like nutritional stress, amino acid limitation, hypoxia, exposure to toxic components or UV radiation (Goswami et al., 1999; Kluck et al., 1997; Sanfeliu and Stephanopoulos, 1999; Simpson et al., 1998a).

It is proposed that the release of cytochrome-c can be either permeability transition (PT) pore-dependent or independent. In the permeability transition (PT) pore-dependent mechanism, the pore is opened in response to a stress signal. The pore is formed at sites where the inner and outer membranes of the mitochondria meet. The pore is composed of adenine nucleotide translocase (ANT), the mitochondrial inner membrane protein transporter (Tim), the protein transporter at the outer membrane (Tom), the outer membrane voltage-dependent anion channel (VDAC) and cyclophilin-D (Crompton, 1999).

The opening of a pore can allow molecules smaller than 1.5 kDa to permeate. The entering molecules cause an increase of the osmolar load of the mitochondria which brings more water in. This causes the mitochondria to swell and its outer membrane to rupture resulting in release of cytochrome-c into the cytoplasm (Yang and Butler, 2000). PT pore independent mitochondrial membrane permeabilisation is regulated by the Bcl-2 (B-cell lymphoma 2) family. The members of the Bcl-2 family share at least one common structural features of the four conserved regions termed as Bcl-2 homology (BH) domains (named BH1, BH2, BH3 and BH4) (Chittenden et al., 1995). The Bcl-2 family can be subdivided into anti-apoptotic members such as Bcl-2 and Bcl-xl and pro-apoptotic species.

The anti-apoptotic Bcl-2 proteins (Bcl-2 and Bcl-xl) conserve all four BH domains. Pro-apoptotic members are grouped into two categories based on the expression of BH domains. Multi-domain proteins comprise BH domains 1-3 include Bax, Bak, and Bok. The other sub-group, the BH3-only proteins, consists of Bad, Bik, Bid, tBid, Puma, Bim, Bmf and Noxa. The BH3-only proteins activate multi-domain pro-apoptotic species and disrupt the function of anti-apoptotic Bcl-2 family members (Letai et al., 2002). It is thought that multi-domain Bcl-2 family members form channels in the outer mitochondrial membrane through which cytochrome-c is released into the cytoplasm (Kuwana et al., 2002).
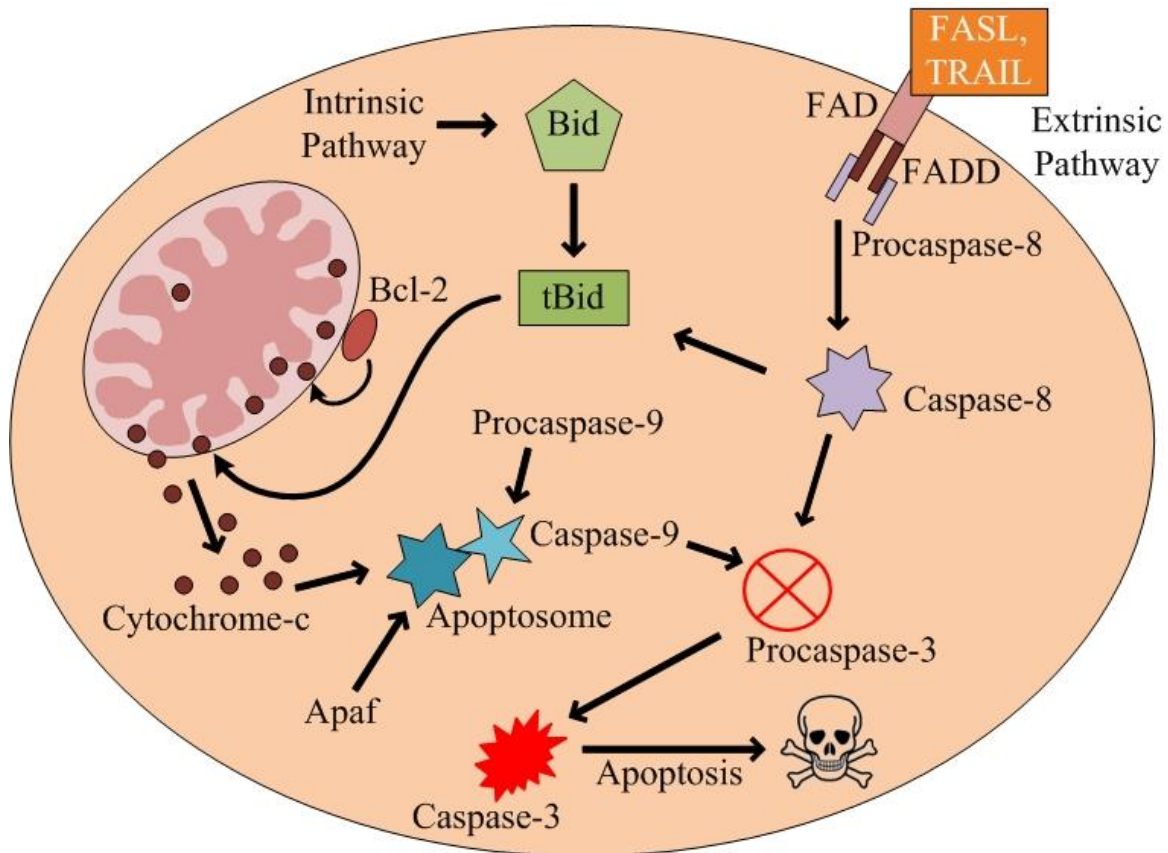
Figure 2.4: Apoptotic pathways

After being released into the cytoplasm, cytochrome-c binds to adenosine triphosphate (ATP) and to an adaptor protein called apoptosis activating factor-1 (Apaf-1) forming a complex to which procaspase-9 is recruited. This entire complex is referred to as an apoptosome complex. This complex in turn facilitates the cleavage and activation of pro-caspase-9 which in turn activates caspase-3. SMAC/DIABLO proteins and apoptosis inducing factor (AIF) are also released into the cytosol from within the mitochondria. SMAC/DIABLO is reported to promote apoptosis by inhibiting IAP (inhibitors of apoptosis proteins) activity (Schimmer, 2004). AIF contributes to DNA fragmentation and subsequent chromosomal condensation, which are prime features of apoptosis (Susin et al., 1999).

The Bcl-2 family members are key players in the regulation of the intracellular caspase cascade. The antiapoptotic proteins resist the activation of caspase-9. They inhibit the release of cytochrome-c from the mitochondria and compete with procaspase-9 for Apaf-1 binding sites. Proapoptotic proteins such Bax or Bid bind to antiapoptotic Bcl-2 family members, thus neutralizing their inhibitive abilities. The ratio of anti-apoptotic versus proapoptotic Bcl-2 family members, for example Bcl-xl to Bax, is tightly controlled by p53 (a gene involved in cell cycle regulation). In response to various stimuli, p53 can cause cell arrest or apoptosis. Depending on the type of stress and its severity, p53 may cause cell arrest (Zhang et al., 2005). However, when stress signals are continual and the cell fails to repair damage through cell cycle arrest, p53 activation triggers apoptosis through mitochondrial stress and degradation following the upregulation of BH3-only pro-apoptotic proteins including; Bax, Noxo, Puma and others (Oda et al., 2000).

A third apoptotic pathway has been reported, but not very widely studied. This pathway originates in the endoplasmic reticulum (ER) which is a specialized site of protein translation, protein folding, modification and transport of secretary/membrane proteins. It is also a specialized site of calcium storage. This pathway can be mediated by mitochondria (because of the proximity of mitochondria) or without mitochondria. In mitochondrial-independent ER pathway, proteins localized to the ER sense the stress signal and activate caspase-12 which subsequently activates caspase-9 (independently of Apaf) which can then activate caspase-3 (Rao et al., 2002). The mitochondrial-dependent pathway is initiated by fluctuations in Ca^{2+} ions in the ER. This leads to the activation of BH3 only proteins which, upon activation, translocate to the mitochondrial membrane leading to apoptosis (Zong et al., 2003). This ER pathway is caused by the severe stresses induced by improper glycosylation, protein misfolding and disturbances in Ca^{+2} fluxes.

2.7   Analytical methods

There are various common analytical methods that can be used for the detection of apoptosis or proteins involved in apoptosis. The applicability of each method depends on its specificity and sensitivity. The following sections describe the various analytical methods useful for the identification of apoptosis, associated proteins and necrosis.

2.7.1 Fluorescence microscopy

Fluorescence microscopy with dual staining of acridine orange and ethidium bromide can be applied to differentiate between physiological states of cells (Giuliano et al., 1998). The dye acridine orange can

penetrate viable and nonviable cells; it fluoresces green when bound to double stranded nucleic acid, i.e. DNA, and fluoresces red if it intercalates into single stranded nucleic acid, i.e. RNA. Ethidium bromide can diffuse only into nonviable cells and fluoresces red when intercalated into DNA. Images of the stained cells can be processed by the Image J software package (Burger and Burge, 2008). The cells thus can be categorized into three groups: (1) Normal viable cells, having organized structure with bright nuclei and translucent green cytosol; (2) Apoptotic cells, either in (i) early apoptosis, -- bearing a condensed or shrunken nucleus with perinuclear chromatin appearing as green patches, or (ii) late apoptosis -- with blebbing on the cell surface, and orange to red condensed or fragmented nuclei; (3) Necrotic cells, having organized structure but with uniformly orange-to-red nuclei. The identification of cells with this methodology applied in this work is shown in Section 4 in Figure 4.4 for a set of experiments.

2.7.2 Flow cytometry

Flow cytometry, also referred as FACS (fluorescence-activated cell sorter), is a very useful technique that is able to make multiple simultaneous measurements at the single cell level. This technique relies upon the measurement of scattered light fluorescence from suitably stained constituents in individual cells in the population. In this method, fluorescently stained cells are passed individually through a focus of high intensity light source. As each cell passes through the focus, a flash of scattered and/or fluorescent light is emitted. This is collected by appropriately positioned lenses. The optical filters direct the emitted light signals to appropriate detectors. The detectors then convert the light flash into an electronic signal which can then be processed by a computer. The data collected on each cell or event is stored in a so-called flow cytometry standard (FCS) format. The data stored in FCS format are "LIST MODE" data, whereby all measurements on each cell are stored separately in a list. Flow cytometry, given a defined threshold intensity, provides quantification of the percentage of cells which are positive or negative for the target protein to be detected within a population of a given amount of sample or alternatively it provides a relative quantification of target proteins.

As mentioned earlier, the various morphological changes that occur during apoptosis take place in an orderly sequence. These can be used to distinguish vital and dying cells, and to analyze the extent and type of cell death. Figure 2.5 shows the morphological changes which are captured by flow cytometry (Vermes et al., 2000). Apoptosis begins with cell shrinkage expressed by changes in cell light-scatter signals. Initially the integrity of cell membrane is intact. The forward light scatter (FSC) is an indicator of cell size, while side angle light-scatter (SSC) reflects the conformation or granularity of inner cellular structures. As a results of these cellular changes, FSC decreases during the initial stages of apoptosis

26

while SSC increases or remains constant. After that, decrease in both FSC and SSC is observed. During necrosis cell swelling occurs due to the loss of membrane integrity. Thus a quick increase in FSC and decrease in SSC are observed.

Flow cytometry is also useful for assessing the cell heterogeneity based on the cell cycle. During the batch culture, the fraction of cells in the G1, S and G2/M phases changes significantly. In the esponential growth phase, most of the cells are in the S and G2 phases, whereas during the decline phases, the majority of the cells are in the G1-phase. By staining the cells with fluorophores such as propidium iodide (PI) and acridine orange (AO), this method can be used to analyse the progress of cell cycle in the culture (Al-Rubeai, 1997; Ramirez and Mutharasan, 1990).
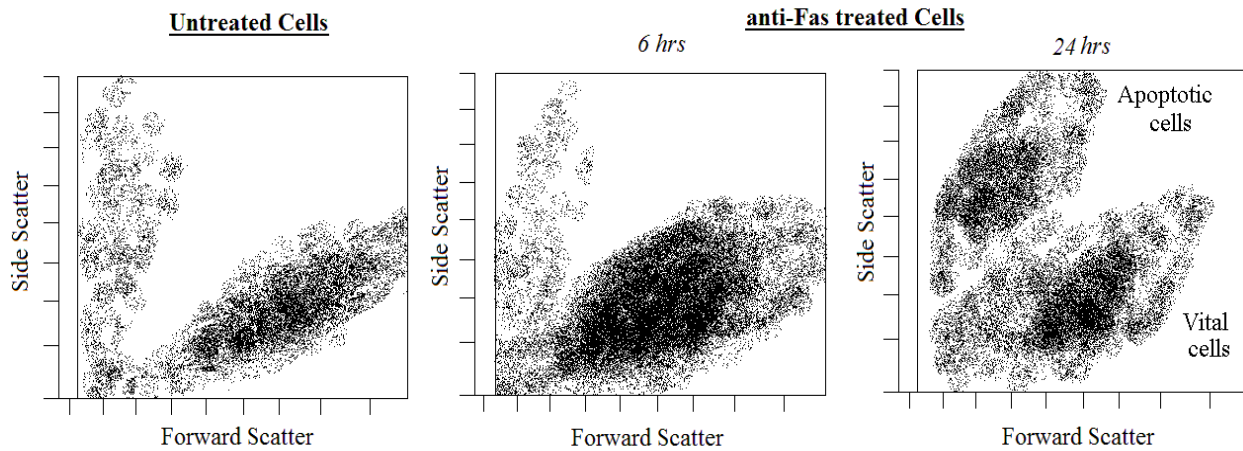
FCM of light scatter of apoptotic cells. Dot plots of forward angle light scatter (FSC) vs side-angle light scatter (SSC) of cultured Jurkat cells. Cells were incubated with 10 ng/ml anti-Fas (anti-CD95, CH11 clone. Immunotech Marseilles, France) for 24 h. After 6 h an increase in SSC becomes visible (middle pannel). After 24 h two of Jurkat cells are visible: vital cell population with unchange scatter signal and apoptotic cell population with decreased FSC and increased SSC signals

Figure 2.5: Analysis of apoptosis with flow cytometry by light scattering of cells (Modified from Vermes et al., 2000)

Flow cytometry is also used to characterize apoptosis based on morphological features by using the annexin-V binding method. This assay detects the loss of plasma membrane integrity, one of the typical features of cells undergoing apoptosis. In cells undergoing apoptosis, the membrane phospholipid phosphatidyl serine (PS) is exposed to the external cellular environment, because it is translocated from the inner to the outer leaflet of the plasma membrane. Annexin-V is a Ca^{2+} dependent binding protein that binds to PS with a strong affinity. Annexin can be conjugated to fluorochromes such as FITC (fluorescein isothiocyanate), APC (allophycocyanin), and PE (phycoerythrin). Another dye, PI (propidium iodide), can also be used to label cells which have lost membrane integrity. Using PI in combination with annexin-V, can provide information to distinguish cells that are at early stages of apoptosis (annexin-V positive, PI negative) from cells that are at a late stage of apoptosis (annexin-V positive, PI positive) (Bakalczuk et al., 2003; Moore et al., 1998; Overbeeke et al., 1998).

Flow cytometry is used extensively for the detection of caspases inside the cells or any others proteins involved in the apoptotic pathway. The FLICA (Fluorochrome inhibitor of caspases) methodology is a very popular method for the detection of caspases in cells by flow cytometry (Arden et al., 2006). The FLICA methodology uses a fluorescent labeled inhibitor consisting of an amino acid sequence that targets a specific caspase. When this FLICA is added to a population of cells, it enters each cell and covalently binds to a reactive cysteine residue of that particular caspase, thereby inhibiting further enzymatic activity. The FLICA reagent is covalently coupled to the enzyme and thus is retained in the cell, while any unbound FLICA reagent diffuses out of the cell and is washed away. The fluorescent signal is a direct measure of the number of active caspase enzymes that were present in the cell when the reagent was added. This technique is referred to as intracellular staining. Flow cytometry detection of caspases can also be carried out by using cell permeable fluorogenic caspase substrates (Benford et al., 2001; Liu et al., 2002). Flow cytometry is also used with an antibody based approach. In this case the technique is referred to as surface staining since it is usually used for the detection of proteins within the membrane surface. FASL, which is a membrane protein, has been detected by flow cytometry by an antibody based method (Lorz et al., 2000; Schulte et al., 2007).

2.7.3 Colorimetry and fluorometry

These methods can be also used for assessing the progress of apoptosis by measuring caspase activities. Many designated substrates and inhibitors have been developed commercially for the investigation of caspases in cell culture undergoing apoptosis. Substrate based methods involve the application of a synthetic tetrapeptide (recognition sequence) conjugated to a colorimetric molecule, p-nitroanilide (pNA) or a fluorescent molecule, 7-amino-4-trifluoromethylcoumarin (AFC). YVAD, VDVAD, VEID, IETD,

and LEHD are commercially designated peptide substrates for caspase-1, 2, 6, 8 and 9 respectively that can be coupled to either *p*NA or AFC to make the complete substrate molecule. DEVD is the peptide substrate for both caspase-3 and caspase-7. There are also caspase specific inhibitors which are developed based on specific caspase substrates. This inhibitor design includes tetrapeptide recognition sequence attached to a functional group aldeyde (CHO), chloromehtylketone (CMK) or fluoromethylketone (FMK). Inhibitors of FMK type, such as z-LEHD-FMK and z-IETD-FMK have been chosen as probes of biological function for various caspases *in vivo*. However, these substrates and inhibitors have limited specificity towards their corresponding caspases. It was shown that these substrates have overlapping activities for different caspases present in a given cell lysate sample (Pereira and Song, 2008). This suggests that the use of these commercially available substrates or inhibitors-based methods is not very efficient for assessing individual caspases' activities.

2.7.4 Western blot

Western blot is a very powerful analytical technique to detect a protein of interest from a mixture of proteins in a given sample of cell extract. With this technique it is possible to identify and locate proteins based on their ability to bind to specific antibodies. In this method a primary antibody is used, which binds to the target protein to be detected. The protein sample is first run in SDS-PAGE. The proteins move based on their molecular weight in the gel. After this step, the separated proteins in the gel are then transferred electrolytically onto a membrane. This step is called *electroblotting*. Nitrocellulose or PVDF are the most commonly used membranes for this purpose. The proteins transferred onto the membrane are then probed with a suitable primary antibody for a specified period of time. The membrane or the blot is then incubated with a secondary antibody. This secondary antibody is tagged to a reporter molecule producing color which can be detected by a suitable scanner machine. All the apoptotic proteins can be detected by western blot method provided that suitable antibodies are available. By assessing the intensity of bands for cells collected at different stages of the cell culture, the progress of apoptosis can be tracked.

2.7.5 DNA laddering assay

Following this method apoptosis can be characterized based on the typical changes occurring in DNA during apoptosis. DNA fragmentation is a hallmark of apoptosis in many mammalian cell types. In the later stages of apoptosis, endonucleases, get activated and translocate into the nucleus and cause DNA fragmentation and internucleosomal cleavage. These nucleases cleave DNA and produce DNA fragments of 180- 200 base-pair. When observed with agarose gel electrophoresis, a characteristic "ladderlike"

appearance can be observed. Flow cytometry also can be used to determine the percentage of cells undergoing DNA breaks by tagging fluorescent molecules to DNA breaks (Li et al., 1995).

2.7.6 DIGE (Differential in gel-electrophoresis) and mass spectrometry

2D differential in gel-electrophoresis is a powerful tool in proteomics that enables accurate analysis of differences in protein expression levels between samples. This method is often used for proteome analysis of molecules regulating apoptosis (Ibuki et al., 2005; Kumar et al., 2008; Wei et al., 2011). The protein samples are labeled with fluorescent dyes (Cy2, Cy3 and/or Cy5), then combined together before 2-D electrophoresis and then subjected to 2-D electrophoresis. These dyes are spectrally distinct allowing the co-separation of different labeled samples in the same gel. This ensures that all samples are subjected to exactly the same first- and second-dimension electrophoresis running conditions. Thus experimental variation or gel-to-gel variation is avoided.

With this method up to two experimental samples can be studied together. These two different samples and an internal standard are run in a single gel. The two different samples are tagged with either Cy3 or Cy5 and the internal standard is tagged with Cy2. The internal standard is prepared by mixing together equal amounts of each sample in the experiment. By including the internal standard in every gel within an experimental series, an accurate analysis of differences in protein expression levels between samples run on different gels can be achieved. The gels are then imaged at the excitation wavelengths of each of the three dyes. These images are then merged and analyzed for the differences in the protein expression levels by using image analysis software. The differentially expressed proteins can then be enzymatically digested with trypsin and readily identified using mass spectrometry. Mass Spectrometry techniques such as Matrix Assisted Laser Desorption Ionisation Time-of-Flight Mass Spectrometry (MALDI-ToF MS) can identify proteins by generating peptide mass fingerprints (PMF) and subsequent database searching.

2.8   Dynamic modeling of bioprocesses

Mathematical modeling of biochemical process has always been an essential tool for making predictions about the process and for defining optimal operation recipes for cell cultures. There have been several mathematical approaches followed for enhancing the understanding and productivity of those bioprocesses, ranging from different empirical model to various dynamic models. However, the use of empirical models is limited as they often fail to illustrate the physiological significance of processes and they are mostly suitable to represent data used for their calibration but less accurate to predict data not used for calibration.

Popular dynamic modeling approaches involve Boolean descriptions, automata and stochastic, partial or ordinary differential equations. (De Jong, 2002; Ventura et al., 2006).

This thesis focuses on ordinary differential equations (ODEs) based model. ODEs do not capture spatial behavior and they are based on the assumption of perfect reactor stirring. State variables progress in a continuous and deterministic fashion. A common representation of ODE based model system can be described as follow

$$\frac{dx_i}{dt} = \dot{x} = \sum_{j=1}^{m} C_{ij} F_j(x, \theta) \qquad\qquad i = 1 \dots n$$

where x represents state variable, grouped into a vector $x \in \mathbb{R}^n$, $C \in \mathbb{R}^{n \times m}$ is the stoichiometric matrix and $F \in \mathbb{R}^m$ is the flux or rate vector which depends on the current state x and the parameter vector $\theta \in \mathbb{R}^k$.

One of the first dynamic models of intracellular mechanisms of apoptosis was developed by Fusseneger. It includes most of the aspects of apoptosis phenomena (Fussenegger et al., 2000). This model describes several parts of the phenomena by including both pathways of apoptosis i.e. death receptor pathway and mitochondrial pathway. The model is able to describe the principle characteristics of process and known regulatory mechanisms. Also in other studies (Harrington et al., 2008) apoptosis was modeled by considering both pathways. Eissing had developed models based on differential equations which solely focused on the extrinsic death receptor pathways (Eissing et al., 2004). Eissing's model was formulated to show the fast caspase activation kinetics occurring at the single cell level. Using bifurcation analysis it was shown that Eissing's model was capable of displaying bistable equilibrium behavior. The parameter values were taken from the literature. It was suggested that the model should include IAP (inhibitor of apoptosis protein) and BAR (bifunctional apoptosis regulator) for effective regulation of death-receptor-mediated apoptosis. In another similar study (Sen et al., 2011), bistability in apoptosis model triggered by mitochondrial pathway was shown. Several other models based on the extrinsic pathway of apoptosis have also been developed (Bentele et al., 2004; Lai and Jackson, 2004; Lavrik et al., 2007; Rangamani and Sirovich, 2007).

Several studies have also been carried out on the modeling of the mitochondrial apoptotic pathway (Bagci et al., 2006; Bao and Shi, 2007; Chen et al., 2007b; Chen et al., 2007a; Cui et al., 2008; Hua et al., 2005; Huber et al., 2007; Legewie et al., 2006; Nakabayashi and Sasaki, 2006; Rehm et al., 2006; Stucki and Simon, 2005). In studies carried out by Rehm et al., (2006) and Hua et al., (2005), the mathematical

model was tested with experimental data. In Rehm' studies, the model prediction was verified qualitatively and quantitatively at single cell level by including the role of XIAP (X-linked-inhibitor-of-apoptosis-protein) and Smac (second mitochondria-derived activator of caspases) in apoptosis regulation in HeLa cancer cells. The same group has also developed software, available through the web, which provides a thorough analysis of mitochondrial-mediated-apoptosis pathway regulation (Huber et al., 2007). This software is able to produce temporal protein profiles, to identify key regulatory proteins and to determine critical threshold concentrations required for the execution of apoptosis in HeLa cancer cells or other cell types. It also provides model predictions for the validation of experimental results.

These models were based on single cell level and consisted of various entities/proteins concentrations as state variables. It should be understood that the single cell behavior is more diverse than the population behavior in cell culture process. Caspase activation is very rapid at the single cell level while in a population of cells caspase activation is in general slow since even when triggering of apoptotic stimulus to a population of identical cells, generally individual cells die at different time points. Also, since, the above models contained various species which cannot be measured, casts less confidence on reliability of parameter values. Thus, the reliability and identifiability of these parameters is somewhat in question with regard to their confidence interval being large. (The identifiability of parameters is explained in the further section).

A key challenge in formulating models used to describe apoptosis is to calibrate the large number of parameters generally present in these models. The reason for this is that the signal transduction pathways involved in apoptosis comprise a very large network of reactions. Thus the number of parameters involved is usually large compared to the amount of experimental data, leading to models that are generally over-parameterized. Thus the identification of parameters for these models is often very difficult. Identification of model parameters from data is a fundamental mathematical problem. Model parameters have physical significance and therefore it is important to know if it is possible to determine their values from the observed data. Addressing the parameters' identifiability problem can be also useful for determining what needs to be measured to determine the model parameters. If there are limitations on what can be measured, this identifiability analysis can at least provide information about the parameters that can be reliably identified from the experimental data. For example, Gadkar's group (Gadkar et al., 2005a; Gadkar et al., 2005b) presented an interesting approach to solving the identification problem by developing an iterative procedure following a state regulator problem.

2.9   Model discrimination

Selection of a best model among the available models should be decided based on a suitable criterion. Sum of squared errors (SSE) may not be the suitable criterion in deciding the best model as different models can have different number of parameters. A model containing higher number of parameters usually offers better fitting thus having low SSE. Thus, it is required to apply a penalty that with take into account the number of parameters.

AIC (Aikaike information criterion) (Akaike, 1973) is a common model selection criteria that was used in the current thesis to choose the best model. This criterion is defined as

$$AIC = -2\ln L + 2p \tag{2.1}$$

Where L is the likelihood function of the model and p is the number of parameters. In the event of least squares analysis where the model error is assumed to be independent and normally distributed, the criterion is given as

$$AIC = n\ln(\hat{\sigma}^2) + 2p \tag{2.2}$$

$$AIC = n\ln\left(\frac{SSE}{n}\right) + 2p \tag{2.3}$$

$$AIC = n\ln\left(\frac{\sum \hat{\varepsilon_i}^2}{n}\right) + 2p \tag{2.4}$$

Where $\hat{\sigma}^2$ is the variance and $\hat{\varepsilon}_i$ are the estimated residuals obtained from model fitting and n is the sample size. If variances are unequal for different time data points then it is recommended to use weighted residuals in place of $\hat{\varepsilon}_i$.

Thus given a set of models, a model that has minimum AIC score is chosen. Thus AIC provides the best tradeoff between a small SSE with a relatively small number of parameters

AIC is corrected for the small sample size (Hurvich and Tsai 1989) and is modified to AICc as follows

$$AICc = AIC + \frac{2p(p+1)}{n-p-1} \tag{2.5}$$

Or

$$AICc = n \ln\left(\frac{SSE}{n}\right) + \frac{2np}{n - p - 1} \tag{2.6}$$

For small sample size AICc is preferred to AIC for model comparison. Also as the sample size becomes relatively larger, the behavior of AICc and AIC converges. Thus use of AICc is always recommended regardless of the sample size. As a rule of thumb, when the ratio of number of sample size and the number of parameters involved in model is less than 40, AICc is preferred to AIC (Burnham and Anderson, 2004).

If the AICc scores of the models differ significantly, then we can conclude that one model is better than the other. However, we cannot confidently choose one model over another if the AICc scores of those two models are close. The probability of choosing the correct model based on AICc scores, is computed as follows (Motulsky and Christopoulos, 2004),

$$Probability = \frac{e^{-0.5\Delta A}}{1 + e^{-0.5\Delta A}} \tag{2.7}$$

where ΔA is the absolute difference in AICc scores of the two models.

Thus if the AICc scores of the two models are equal, then the ΔA will be zero, and both the models will equally likely to be correct.

Another criterion used in the current work for comparing candidate models is BIC (Bayesian information criterion) (Schwarz, 1978) and defined as

$$BIC = -2 \ln L + p \ln(n) \tag{2.8}$$

In the case of independent and normally distributed model error, the criterion reduces to

$$BIC = n \ln\left(\frac{SSE}{n}\right) + p \ln(n) \tag{2.9}$$

Many of the authors have used these criteria in model selection. It was implemented for model selection to describe the data for HIV viral fitness experiments (Miao et al., 2009). Other studies where these

criteria were used include lymphocyte growth regulation (Hawkins et al., 2007), the parotid gland dose-response relationship (Houweling et al., 2010), in tumor cell growth progression (Zhou et al., 2010).

2.10 Parameter sensitivity and identifiability

After modeling a process, analysis should be carried out to assess the model's reliability. Since the main elements of the model are the parameters that depict aspects of the process, analysis is carried out that assesses the reliability of parameters. One such approach is to assess the identifiability of parameters. This is important to carry out to verify how uncertain the parameters in a given developed model are. Since the parameters are developed based on given measurements, the reliability of parameters depends on the quality of the data obtained. However, the measurements are not always accurate; there will always be some error involved in the measurements. These may be due the handling, instruments noise or some undetectable environmental factors. The nosier the measurements are and the lower the number of sampling data points of measurements is, more uncertain these parameters could be. Therefore the model developed with these measurements may not be very accurate and is subjected to some degree of uncertainty in the parameters. The parameters for which no unique solution exists have higher degree of uncertainty, so cannot be unambiguously determined or are non-identifiable. An identifiability test can be implemented for parameters involved in a given model developed. For non-identifiable parameters, their confidence interval would be infinite showing that they cannot be estimated from the given available data.

There are two types of identifiability: theoretical identifiability and practical identifiability. Theoretical identifiability investigates if the parameters in the ODE's based models are identifiable under the assumption of accurate measurement (no measurement noise), while practical identifiability refers to parameter whether they are identifiable from noisy experimental measurements. Accordingly, theoretical identifiability only depends on the characteristics of the model structure, so it is also referred to as structural identifiability analysis. Though structural identifiability analysis is based on the assumption of accurate model structure and no measurement noise, which may not be realistic, it is still useful. Because of the physical significance of parameters it is crucial to know if it is possible to determine their values from measurement information. This analysis can be also useful for experimental design where the inverse problem of what needs to be measured to estimate the model parameters has to be solved.

Identifiability analysis is closely related to sensitivity analysis which examines how sensitive the the model response is to a particular parameter if that parameter is varied by some degree. Low sensitivity typically corresponds to high variability in the calibrated parameter and it is generally found non-identifiable by identifiability analysis.

If the sensitivities of the responses with respect to parameters are linearly independent, the parameters are considered to be identifiable (Beck and Arnold, 1977). Plotting the progression of sensitivity scores with respect to time would give the idea of the identifiability of parameters. If the sum of the sensitivity scores of two parameters on the same response is zero throughout the time, the parameters are considered to be perfectly correlated and cannot be estimated simultaneously.

There are several methods for estimating parameters as described, for example, in Moles et al., (2003), Gadkar et al., (2005a,b), Vayttaden et al., (2004) based on the measurements. In another study, an empirical observability Gramian method was proposed for determining identifiability on a model of biological system of the NF-κB signal transduction pathway (Geffen, 2008). Another approach proposed by Yao et al., (2003) uses an orthogonalization procedure to obtain a set of identifiable parameters applied to a dynamic reactor model for gas-phase ethylene-butene copolymerization. This approach involves the formulation of the sensitivity score matrix as follows

$$
Z = \begin{bmatrix}
\left.\dfrac{\partial x_1}{\partial \theta_1}\right|_{t=t_1} & \cdots & \left.\dfrac{\partial x_1}{\partial \theta_k}\right|_{t=t_1} \\
\vdots & \ddots & \vdots \\
\left.\dfrac{\partial x_n}{\partial \theta_1}\right|_{t=t_1} & \cdots & \left.\dfrac{\partial x_n}{\partial \theta_k}\right|_{t=t_1} \\
\left.\dfrac{\partial x_1}{\partial \theta_1}\right|_{t=t_2} & \cdots & \left.\dfrac{\partial x_1}{\partial \theta_k}\right|_{t=t_2} \\
\vdots & \ddots & \vdots \\
\left.\dfrac{\partial x_n}{\partial \theta_1}\right|_{t=t_m} & \cdots & \left.\dfrac{\partial x}{\partial \theta_k}\right|_{t=t_m}
\end{bmatrix}
\tag{2.10}
$$

where x: state variable, $x \in \mathbb{R}^n$, θ: parameter vector, $\theta \in \mathbb{R}^k$, t: time of sampling, $t \in \mathbb{R}^m$

$\left.\dfrac{\partial x}{\partial \theta_k}\right|_{t=t_m}$: The sensitivity score of the nth response with respect to k^{th} parameter at time t_m.

This method provides two outcomes: it identifies a set of the estimable parameters and also ranks them from the most identifiable to the least one. Because of the possible existence of strong correlations

between the parameters, ranking of parameters is not straightforward. This method starts with finding the most identifiable parameter as the one whose corresponding column has the largest magnitude in terms of sum of squares. Now, if there exists any correlation between this parameter and the remaining parameters, their influences on the response variables are adjusted by orthogonalization of the columns in the Z matrix. This is performed by the following operation

$$\hat{Z}_L = X_L (X_L^T X_L)^{-1} X_L^T Z \tag{2.11}$$

where, $\hat{Z}_L$ is considered as the prediction of the full sensitivity matrix Z based on the most identifiable parameter and X_L is the column for the first most identifiable parameter.

A residual matrix is calculated as $\hat{Z}_L - Z_L$. The next estimable parameter is then chosen corresponding a column which has the largest magnitude in terms of sum of squares in the residual matrix. A column the Z matrix corresponding to this this second most estimable parameter is then augmented in the matrix X_L and is denoted by X_{L+1}. Following operation is then performed to adjust the effect of the second most estimable parameter

$$\hat{Z}_L = X_{L+1} (X_{L+1}^T X_{L+1})^{-1} X_{L+1}^T Z \tag{2.12}$$

This orthogonalization procedure continues until a set value of the sum of squares in the columns of the residual matrix corresponding to the remaining parameters is reached.

The most identifiable parameters correspond to the ones that have a near to unique solution, i.e. their variability is very small. The variability in the parameters can be calculated by the Fisher Information Matrix as follows

$$FIM = \sum_t Z^T V Z \tag{2.13}$$

where V is the inverse of the covariance matrix of measured output error. The Cramer-Rao bound states that the inverse of the FIM represents the error covariance matrix of the minimum variance unbiased estimator (Kay, 1993), and thus a lower bound on the variance of the identifiable parameter can be obtained from the diagonal of the FIM as

$$\sigma^2(\theta_i) \geq (FIM^{-1})_{ii} \tag{2.14}$$

Thus the FIM can be considered as a measure of the information on model parameters gained from an experiment. The FIM can serve as an important tool for constructing an optimal experimental-design using various criteria such as the D-optimality criterion which maximizes the determinant of FIM. This optimality criterion involves obtaining maximum information of or equivalently, minimizing the variance of model parameter estimates.

Chapter 3

Materials and methods

This chapter describes the methods used in thesis work including CHO cell culture experiments for mAb production and measurements of various metabolites, nutrients and caspases involved in apoptosis.

3.1 Cell culture experiments

This section describes the cell line under study and various experiments performed to quantify cell growth and apoptosis.

3.1.1 Cell culture and media

A dihydrofolate reductase-deficient CHO (*dhfr⁻* CHO) cell line transfected with a fully human IgG-Variant gene for anti-RhD mAb (IgG1-r9B8) provided by an industrial partner (Cangene Corporation, Mississauga, Ontario) was used in the current study. This recombinant mAb has shown a higher affinity for the human RhD antigen, thus makes it suitable for therapeutic application (Wiersma, 2000).

The cells were grown in serum free SFX-CHO medium (Thermo Scientific HyClone) in batch mode in spinner flasks. Since the medium does not contain glutamine (Sigma-Aldrich Chemicals), it was supplemented after filter sterilization. The medium was also supplied with Fetal Bovine Serum (Invitrogen).

3.1.2 Maintenance of cells

Maintenance of cell bank reserves was carried out by storing the cells in a cryogenic environment. Dimethyl sulphoxide (DMSO) was used as a cryoprotective agent. Initially, a healthy culture with cell viability higher than 90% was harvested in the mid-exponential phase of growth and then centrifuged. A cryopreservation medium containing 45% fresh medium, 45% conditioned medium and 10% of a cryoprotective agent, DMSO was used to re-suspend the cells to a concentration of approximately 1×10^6 cells/mL. Serum with a concentration of 2% by volume was also added to the fresh medium. The addition of serum helps in improving the post-freezing survival and recovery of the cells. A volume of 1 mL of cell suspension in cryopreservation medium was aliquoted into cryovials. These cryovials were then incubated overnight in a -80°C freezer and then immediately placed to a liquid nitrogen storage container for long term preservation.

3.1.3 Revival of cell line

Revival of cells preserved in a liquid nitrogen tank, was accomplished by thawing a frozen vial of cells in a 37°C water bath for approximately 2 minutes. The vial was swirled gently into the water bath. An anti-microbial reagent (Acryl AquaClean, WAK–Chemie), used as disinfectant, is added to the water bath to avoid any microbial contamination. The vial was removed soon after the contents were thawed and then it was kept within a laminar flow hood after decontaminating it with 70% ethanol. The vial contains approximately 1×10^6 cells in 1 mL of growth medium. The cell suspension in the vial was then transferred into a 25-cm² T-flask containing approximately 4-5 mL of fresh SFX-CHO medium supplemented with 2% serum. Prior to the transfer of the cell suspension from the vial, the T-flask containing medium was placed in a CO_2 incubator (Sanyo IR Sensor, 37°C, 5% CO_2) for sufficient time to attain optimal temperature and pH conditions. The T-flask with the cell suspension was then incubated for 1-2 days depending on the cell growth. In mid-log phase (usually two or three days), the cells were harvested and passaged to another T-flask containing fresh medium every two or three days (i.e. sub-culturing). The following method was used:

1. Initially, all the supernatant was removed from T-flask. A dissociating agent TrypLE (Invitrogen) was added to the flask at a ratio of 1 mL to 20 mL of medium of T-flask used in the previous passage for culturing.
2. The flask was then gently shaken for a few seconds so that TrypLE covers all the surface area of the bottom of flask covering all the cells.

3. The flask was then incubated at 37 °C for approximately 5 minutes. This incubation facilitates cell dispersal and so reduces the enzyme exposure period relative to that when kept without incubation at 37° C. Cell detachment was confirmed by observing the flask under an inverted phase-contrast microscope.

4. After the complete detachment of cells was observed, 5 mL of fresh medium and 5mL of spent medium, i.e. a total 10 mL of medium, was added to the flask. The spent medium was added to supplement the next sub-culture with the components which cells might have previously produced for cell growth during the course of the cell culture.

5. The cells were mixed homogeneously by aspirating through gentle pipetting. Inactivation or removal of TrypLE by centrifugation was not required as TrypLE has a gentle effect on cells and its concentration is negligible after dilution.

6. Approximately 1 mL of cell sample was removed by pipette and transferred to an eppendorf to count the cells. Cell concentration was then measured by a hemocytometer.

7. Based on cell concentration, a new subculture was prepared with a cell concentration of $0.2x10^6$ cells/mL. The original serum concentration in the flask (2%) was gradually reduced to 0.5% or less during the following subculturing steps.

3.1.4 Culturing in spinner flask as suspension culture

The cells were cultured in spinner flasks as suspension cultures for further experiments. For this purpose, the cells were adapted to suspension culture before starting the experiments in spinner flask by growing them in suspension in smaller volumes (starting from 80 mL to 250 mL) in a 250 mL spinner flask and then scaled up to 500 mL culture volumes in 500 mL spinner flask. A trypsinized monolayer culture from T-flask was seeded with a final cell concentration of $(0.1-0.3) x10^6$ viable cells/mL in the spinner flask. The culture was agitated at 100 RPM stirring speed. The agitation rate of 100 RPM was same throughout all the experiments. A 4-position magnetic stirrer was installed inside the CO_2 incubator to provide agitation. Being inside the incubator, the spinners were maintained at the conditions of temperature, humidity and CO_2 atmosphere as that used for T-flask cultures. The viable cell concentration and viability was checked every 2-3 days. At the beginning the serum level was kept at 2% depending on the growth of suspension culture and then it was gradually reduced to 1% after the growth rate stabilized to suitable levels.

3.2 Monitoring of cell culture

Samples were taken at different time points during the cell culture and analyzed for viable cell concentration, viability, apoptosis, nutrient, metabolites etc. These assays are described below.

3.2.1 Cell count and viability measurement

Samples were taken at regular time intervals. The cell density was determined using a hemocytometer. Cell concentration and viability was determined by the trypan-blue dye exclusion method (Phillips, 1973). In this method, trypan blue dye is used to estimate viability by distinguishing viable from dead cells. The dye is used at a concentration of 0.5% mixed in PBS. This dye can only diffuse through membranes of nonviable cells, making them appear blue. A 100μL sample was taken from the cell suspension in eppendorf and diluted in 1:1 with trypan blue dye. The stained cells were counted within 3 minutes of the addition of the trypan blue to the cell sample with the hemocytometer positioned under a light microscope. The viability of cells was quantified by the ratio of viable cell count to total cell count.

3.2.2 Caspase assay

Samples from the spinner flask cultures were also taken for flow cytometry analysis of caspases. Progression of apoptosis in the culture was tracked via flow cytometric analysis of caspases using an apoptosis detection kit (Immunochemistry Technology, LLC). The detection is based on a fluorescent inhibitor of caspases (FLICA™) methodology. Altogether four caspase assays were used: a green (carboxyfluorescein) FLICA caspase-8 assay kit, a green FLICA caspase-9 assay kit, a red (sulforhodamine) FLICA Caspase-3 & 7 kit and a red (sulforhodamine) FLICA caspase-9 assay kit (ImmunoChemistry Technologies, LLC). (Caspase-7 is not considered in this study, since it is not as widely studied as caspase-3). The FLICA reagent was supplied as 150X. Before conducting flow cytometry analysis, the cells were treated with FLICA reagent. The cells were treated as per the instructions provided with the kit.

Flow cytometry analysis was set up by inducing apoptosis in an exponentially growing culture. Staurosporine, a protein kinase inhibitor, has been the most frequently used reagent *in vitro* to induce apoptosis in different cell types. This reagent is widely known to induce apoptosis via caspase-9 activation (Chattopadhyay et al., 2011; Manns et al., 2011; Zhang et al., 2004). In addition metal-based reagents are also available which can induce apoptosis in cells. Nickel acetate has also been widely reported to induce apoptosis via caspase-9 activation (Cai et al., 2010; Dally and Hartwig, 1997; Shiao et

al., 1998). It is also reported to induce apoptosis via caspase-8 activation when used in a concentration of 320µM (Kim et al., 2002).

In this study, staurosporine was used to induce apoptosis in culture for calibration of flow cytometry method. It was used at a concentration of 1µM and then the culture was incubated for around 2 hrs. Nickel acetate (II) was also used to treat cells to make sure apoptosis was induced via caspase-8 activation. It was used at a concentration of 320µM as used by Kim, et al., (2002). The treated culture was then incubated for around 12 hours.

After incubation the cells were subjected to flow cytometry analysis of caspases. The following samples were prepared for setting up the method

1. unstained cells (treated and untreated)
2. cells stained with only (green) caspase-8 FLICA reagent (treated and untreated)
3. cells stained with only (green) caspase-9 FLICA reagent (treated and untreated)
4. cells stained with only (red) caspase-3 FLICA reagent (treated and untreated)
5. cells stained with only (red) caspase-9 FLICA reagent (treated and untreated)
6. cells stained with both (green) caspase-8 and (red) caspase-3 FLICA reagent (treated and untreated)
7. cells stained with both (green) caspase-9 and (red) caspase-3 FLICA reagent (treated and untreated)
8. cells stained with both (green) caspase-8 and (red) caspase-9 FLICA reagent (treated and untreated)

The above samples were prepared as per the instructions provided with the kit as described below

An amount of 0.3×10^6 cells were taken for the analysis. Since the FLICA should be used as 30X, it was diluted to 30X with PBS. An amount of 10µL of this 30X FLICA was added to the cell sample. Cells were mixed (by flicking) so that the FLICA was distributed uniformly throughout the sample. The tubes containing this sample were then incubated at 37^0C and 5% CO_2 for 45 min in the incubator and protected from light. Since the cells might settle during incubation, the tubes were flicked twice during this period, after every 15 min. At the end of incubation period, the cells were washed twice with wash buffer provided with the kit. Finally, after centrifugation, the cells were suspended into 400µL of wash buffer and analyzed by a flow cytometer (BD FACSVantage SE). For each sample, the fluorescence of 25,000 cells (events) was measured on a flow cytometer. Data were acquired and analyzed using the WinMDI 2.9 software (The Scripps Research Institute, CA, USA).

3.2.3 Western blot

This analytical technique was used for the analysis of death ligand proteins suspected to be involved in the extrinsic pathway of apoptosis. Analysis of these ligand proteins is necessary as it can provide important information on the onset of apoptosis and this information could be potentially included as an input into the mathematical model. FASL, which is a transmembrane protein, is a widely studied ligand protein in the death-receptor-mediated (extrinsic) apoptotic pathway. Therefore western blot was carried out for both the detection of FASL and caspases. Since there are no CHO specific primary antibodies available, the success of western blot to detect these proteins was questionable. Consequently, a number of trials were done to confirm the presence of these proteins in the CHO culture samples. Some primary antibodies are available from mouse or human, which as per the manufacturers' explanations can detect mouse, rat and human version proteins. Different antibodies were tried until successful detection of FASL was obtained. A procedure was developed and is described below

3.2.3.1 Cell lysis

Cells samples were collected at different times from the spinner flask for western blot analysis. After sampling, cells were first washed twice with cold PBS (at approximately 4^0C) then stored at -80^0C until analyzed. The cell lysis was carried out on ice. Approximately 10 µL of lysis buffer per 1×10^6 cells was used. An inhibitor cocktail mix (Sigma Chemicals) was also added to avoid any inhibition of proteins which might occur during the lysis process. This inhibitor mix was added to the cell sample before adding the lysis buffer. An amount of 1 µL of inhibitor mix per 1×10^6 cells was used. After adding the lysis buffer and inhibitor mix, the cell sample was mixed well. The cells get lysed during this time. The sample was then centrifuged for 10 min at 14000 RPM, sufficient time to obtain a clear supernatant (cell lysate). The supernatant obtained was then used for western blot analysis.

3.2.3.2 SDS-PAGE gel electrophoresis

For western blot analysis, proteins were separated using SDS-PAGE. 25 mL of 12% polyacrylamide gel was used for SDS-PAGE analysis. Cell lysate proteins were loaded into the wells of the SDS-PAGE gel using loading tips and then run with pre-stained protein molecular weight marker. Electrophoresis was carried at 20 mA/gel until the dye front ran off the gel. The composition of 12% gel of 25 mL is shown below

12% Polyacrylamide Running gel (25 mL)

Component	Volume (mL)
Water	8.2
30% acrylamide	10
1.5M Tris (pH 8.8)	6.3
10% SDS	0.25
10% ammonium persulfate	0.25
TEMED	0.01

And the stacking gel (5 mL):

Component	Volume (mL)
Water	3.4
30% acrylamide	0.83
1.0M Tris (pH 6.8)	0.63
10% SDS	0.05
10% ammonium persulfate	0.05
TEMED	0.005

3.2.3.3 Protein transfer

After electrophoresis was complete, the transfer of protein was carried out. For this purpose a nitrocellulose membrane was used. The transfer assembly, including sponges and blots, was soaked in transfer buffer. The composition of the transfer buffer was as follows

Component	Composition
Glycine	192 mM
Tris Base	25 mM
Methanol	20%
SDS	0.1%

The gel was then sandwiched into the transfer cassette as shown in Figure 3.1. The cassette was then arranged into the transfer tank and then transfer/electroblotting was carried out at a constant voltage of 30 V overnight in a cold room.

3.2.3.4 Blot analysis by antibodies

After transfer, the membrane was then washed with water on a rocker for about 10 min. Ponceau staining was used to check the success of the transfer. Following the staining of the membrane, it is possible to cut the membrane into horizontal strips of individual samples to investigate the properties of different sizes of proteins on the same membrane. This stain can then be removed with 1X TBST (Tris Buffered Saline with Twen-20) made from 10X TBS (Tris Buffered Saline) with the following composition

10X TBS	Components	Composition
	Tris-HCl pH 7.6	200 mM
	NaCl	2.0 M

1X TBST (1L)	Components	Volume
	10X TBS	100 mL
	20% Tween	5 mL
	Make up to 1 L	

Black side of cassette	Cathode
Sponge	
Blotting paper	
Gel	
Membrane	
Blotting paper	
Sponge	
White side of cassette	Anode
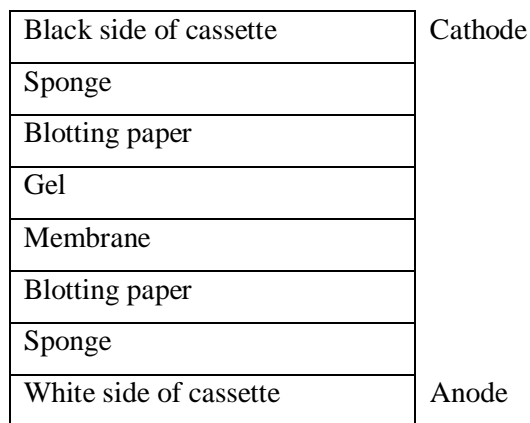
Figure 3.1: Assembly of Western blot transfer cassette

After destaining, the blot or membrane was subjected to blocking with 3% Bovine serum albmin (BSA). (BSA was made in 1X TBST and this solution was filtered before using it for blocking). Blocking was done for 2 hrs at room temperature. Blots were then probed with 1:200 dilution of rabbit polyclonal primary antibody (Santacruz Biotechnology, 200 μg/mL) and incubated for either 2 hrs at room temperature or overnight at 4^0C.

The washing of the blot was done with 1X TBST after primary antibody incubation. The blot was rinsed twice with two changes of 1X TBST and then washed for 5 min for three times with fresh changes of 1X TBST. After these washing steps, the blot was incubated with 1:25000 dilution of an HRP labeled anti-rabbit secondary antibody for 1 hr at room temperature. Washing was done in the same way as done after the primary antibody incubation. After this step, the detection was carried out in a dark environment using an enzyme linked chemiluminescence plus detection reagent (ECL Plus: GE healthcare, USA). The detection solutions A and B were mixed in a ratio of 40:1 to provide an amount that is sufficient for covering the blot at 0.1 mL/cm^2. The membrane was then exposed to this detection mixture for about 5 min and then the blot was scanned with a Typhoon9400 scanner (GE healthcare, USA).

3.2.4 Monoclonal antibody assay

The Enzyme-Linked Immunosorbent Assay (ELISA) was used for the measurement of total human IgG1 antibody concentration in cell culture samples. The method developed by Cangene for this IgG1 was used in this study. A goat anti-human IgG (Jackson ImmunoResearch Laboratories, Inc.) was used as primary antibody and alkaline-phosphatase conjugated goat-anti-human IgG (Jackson ImmunoResearch Laboratories, Inc.) was used as secondary antibody. A substrate used for alkaline-phosphatase was *p*-nitro-phenyl (Sigma Aldrich Ltd.). The assay was performed in 96-well flat-bottom microtiter plates (Immulon$^®$ 2HB). Human IgG1 myeloma (Calbiochem) was used as standard. Various dilutions of standard were made to construct standard curve of absorbance to quantify the amount of IgG1 in cell culture samples. The absorbance was measured at 405 nm in a spectrophotometer (DU 520 UV/Vis, Beckman Coulter).

3.2.5 Glucose assay

Glucose in cell culture samples was measured by an enzymatic method using a glucose kit (Megazyme Glucose Test Kit) according to provided directions. The assay is based on the glucose oxidase/peroxidase reactions. Glucose determination reagent provided with the kit was added to the sample and the mixture was then incubated for 20 min at 40°C. The absorbance of the assay mixture was read at 510 nm against

the reagent blank. The color intensity of the dye produced after the reaction period is proportional to glucose concentration.

3.2.6 Lactate assay

Lactate assay was performed by using lactate strips in a Lactate Plus meter (Nova Biomedical, USA). In this method, the strip is dipped into a drop of sample. The meter reads the concentration of lactate in the sample. The meter contains a lactate oxidase biosensor with a measurement range of 0.3-25 mmol/L.

3.2.7 Amino acid assay

Amino acids in cell culture samples were assayed by high-performance reverse-phase chromatography. The pre-column derivatization technique using phenylisothiocyanate (PITC) was employed to analyze the free amino acids in culture. The method involves reaction of PITC with amino acids forming phenylthiocarbamyl (PTC) amino acid derivatives (Bidlingmeyer et al., 1984) which can be detected by ultraviolet absorbance. The derivatization reaction is shown in Appendix A. The method started with drying of samples and standard amino acids solutions (Sigma-Aldrich Chemicals) under vacuum. A volume of 10µL sample and standard amino acid solutions at a concentration of 2.5 µmol/mL was used in micro-centrifuge tubes for drying. This was followed by addition of 20 µL of solution of ethanol, water and triethylamine (TEA) in the ratio of 2:2:1 respectively. The samples were dried again under vacuum. A freshly prepared derivatization reagent (solution of ethanol, TEA, water and PITC in the ratio of 7:1:1:1 respectively) was added to the dried samples. PITC is unstable in air, so this addition was performed in a nitrogen environment. A volume of 20 µL of this derivatization reagent was added to the samples to obtain the PTC-amino acids derivatives. These samples were then incubated sealed for 20 min at room temperature. After completion of reaction period of 20 min, the samples were subjected to vacuum drying to remove any un-reacted reagent. After the completion of drying, the derivatized samples could be stored dry and frozen without significant degradation.

Before HPLC analysis, the dried derivatized samples and amino acid standards at various dilutions were then dissolved in 500 µL of mixture of 50mM sodium acetate, pH 6.35 (containing 400µL of TEA per liter of buffer) and acetonitrile (ACN). These standards at various dilutions were used for constructing the calibration curve. The chromatography system was a Varian ProStar reverse phase HPLC (Varian analytical Instruments, USA). Eclips Plus C18 column (150×4.6 mm, I.D.) was used for separation. A volume of 10 µL of each sample and standards was subsequently injected into the column using an autosampler. The column was maintained at 40°C and the UV detector was set at 254 nm. The solvent

system consisted of two eluents: Solvent A, an aqueous buffer, was 50mM sodium acetate containing 0.4 mL/L TEA which titrated to pH 6.35 using glacial acetic acid and Solvent B was a 60% solution of acetonitrile in water. The two eluents were run at a flow rate of 1.0 mL/min. A gradient mixer of solvent system adopted by Gheshlaghi et al., (2008) was used optimal separation of amino acids. This gradient profile consisted of starting the run with a 90% A / 10% B solution and then gradually changing the concentration to 49% A / 51% B. This gradient was set for a period of 20 min, followed by the injection of a 100% B solution to flush the column to remove any residual sample component from it.

3.2.8 Ammonia assay

The dissolved ammonia concentration in cell culture samples was measured with an Ammonia Ion-Selective electrode (VWR) using a pH/ISE meter model 710A. The electrode contains a hydrophobic gas-permeable membrane that separates the sample solution from an electrode internal standard solution of ammonium chloride. The method involved increasing the pH of sample above 11 with an ionic strength adjustor (ISA) also called alkaline reagent. 10M NaOH solution was used as an alkaline reagent (ISA) and was added to the sample solution just before the measurement was taken. A volume of 10 µL of ISA was added to 1 mL volume of cell culture sample for ammonia measurement. This converts the dissolved ammonium in the sample to the gaseous form (NH_3), which then diffuses through the electrode membrane until the partial pressure of ammonia will be proportional to its concentration. The resulting change in the pH of internal solution is measured by the pH electrode. Calibration curve was prepared by using standard ammonia solutions (NH_4Cl) with known concentrations.

3.2.9 Dissolved oxygen (DO) assay

A VWR symphony Dissolved Oxygen probes designed for use with VWR symphony series Dissolved Oxygen Meters was used to measure DO in cell culture samples. The electrode calibration (one point calibration at 100%) was performed in water-saturated air in a special calibration chamber provided with probe.

Chapter 4

Investigation of cell density effect on growth and apoptosis

4.1 Introduction

This part of the work involved investigating different factors that trigger apoptosis in the CHO cell line under study. The TNF super-family members such as FASL and TNF-α, as mentioned in Section 2.5.1 are responsible, for triggering the extrinsic apoptosis pathway by cell-cell interaction. Initially, a qualitative analysis of death ligand proteins by western blot was carried out to test whether these proteins are responsible for triggering the death-receptor-mediated apoptotic pathway in CHO cell cultures. After a number of preliminary unsuccessful trials with different primary and secondary antibodies, a primary antibody (rabbit polyclonal from Santa Cruz Biotechnology, USA) and secondary antibody (ECL plus, GE Healthcare) antibody led to relatively successful identification. The result obtained by using these antibodies for the detection of FASL is shown in Figure 4.1. From comparison to the marker protein bands it was found that the band observed in the blot corresponds to ~40kD which is the approximate molecular weight reported for FASL. This seems to confirm the presence of FASL protein in the cell culture thus indicating activation of the extrinsic apoptotic pathway. This result was obtained by incubating the membrane with primary antibody for two hours. The result was also corroborated by subjecting the membrane to overnight primary antibody incubation.

Although the correct band was found, the band clarity was not well defined because of background and non-specific binding. Thus the technique needs further improvement to reduce this background and non-

specific binding that was observed on the membrane. By decreasing this background, the signal-to-noise ratio could be increased. Improvements could be achieved by decreasing the blocking time, and by varying the concentrations of the primary or secondary antibodies. A well-defined band with a high signal-to-noise ratio is necessary if densitometry measurements, for the quantification of protein through intensity measurement, are to be carried out.

This result, which suggests the presence of FASL in the CHO cell culture, is important evidence of the presence of cell-cell communication effects that are responsible for triggering the extrinsic pathway of apoptosis.
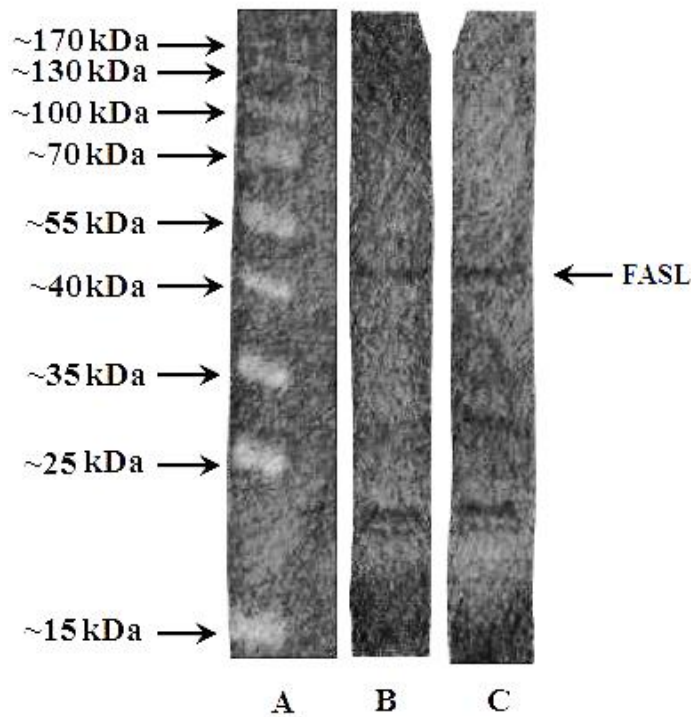
Figure 4.1: Western blot analysis of FASL (A) Marker (B) sample incubated with primary antibody for 2 hrs (C) sample incubated overnight with primary antibody

Since FASL could not be satisfactorily detected from western blot experiments with higher signal-to-noise ratio sufficient for quantification, it was proposed to investigate the effects of cell density on apoptosis based on the premise that higher density may be directly related to cell-cell interaction due to cell proximity and higher release into the medium of proteins involved in cell-cell interactions. In previous reports, cell density has been found to be a trigger for inducing apoptosis in cell culture via cell-cell communication (Ishizaki et al., 1994; Mathieu et al., 1995; Saeki et al., 1997). Cell density could also lead to apoptosis as a result of nutrient depletion occurring in high density cultures. However, it was found in an earlier work by our group (Naderi et al., 2011), by experimenting with varying concentrations of glutamine, glucose or with concentrated media, that growth arrest or apoptosis are not significantly correlated with nutrient limitations in the CHO cell culture used in this study. Then, having found that apoptosis was not correlated to nutrient limitations, experiments were designed to investigate both the density effect and correlations between apoptosis and the accumulation of toxic metabolites, such as ammonia, that have been reported to trigger the intrinsic apoptotic pathway (Lao and Toth, 1997; Ozturk et al., 1992).

4.2   Materials and methods

4.2.1   Cell culture and experimental design

Each set of batch cultures with working volume of 500 mL was carried out in 500 mL spinner flasks in a humidified incubator at $37^{\circ}C$ with 5% CO_2 and agitated at 100 rpm on a magnetic stirrer inside the incubator. Each spinner flask was inoculated with a common seed culture. Regular, daily sampling was performed to assess cell growth, viability, apoptosis and metabolite analysis. HyClone SFX-CHO medium was the basal medium used to perform sub-culturing and to perform the final growth experiments. Batch cultures were set up in four 500 mL spinner flasks, labeled SP1, SP2, SP3 and SP4, with different initial cell densities out of common seed culture. The preparation of this common seed culture is described as follows

- Two cultures of 500 mL volumes were grown each separately in 500 mL capacity spinner flasks and one of 1000 mL volume in a 1000 mL capacity spinner flask.
- The cultures, during the exponential phase, were harvested and added in a separate 2000 mL sterilized vessel with 50 mL pipette. Since only the pipette of maximum capacity available was 50 mL, it was used to mix the whole culture by aspirating in and out. This was performed till homogeneity of seed culture is assured.

- Individual volumes of 50 mL of seed culture were pipetted out from the 2 liter vessel into separate 50 mL centrifuge tubes.
- The tubes were centrifuged at 300 g for 5 min. After centrifugation, supernatant was removed and then fresh SFX-CHO medium was added to each tube to suspend the cells remained at bottom after centrifugation. The suspension was mixed homogenously by aspirating in and out with a 25 mL pipette. The well mixed suspension from each tube was then added to the respective spinner flasks (SP1-SP4) in quantities as required to achieve the desired initial cell densities. Additionally, the tubes were rinsed with some more fresh medium to suspend leftover cells. This suspension was added again to spinner flask to avoid the loss of cells.

The intended initial cell concentrations were $0.25x10^6$, $0.5x10^6$, $0.5x10^6$ and $1.0x10^6$ cells/mL cell concentrations respectively but the actual initial concentrations (reported below) were slightly different. For each batch culture a calculated volume of seed culture, according to the above mentioned initial cell density, was centrifuged, supernatant was discarded and the settled cells were then suspended in fresh medium in the corresponding spinners. Then, after seeding the spinners the medium in each spinner was supplemented with serum and glutamine, with different concentrations according to the initial cell density used in each particular spinner. The lowest cell density culture spinner (SP1) was supplemented with 1% serum and 1mM glutamine. The same initial ratios of serum and glutamine per cell were provided in the remaining three spinner flasks (SP2-4) to avoid the possibility of nutrient depletion in higher–cell-density spinners. For instance, the concentration of serum and glutamine was four-fold higher in the highest cell density culture (SP4) compared to the lowest cell density culture (SP1) but the ratio between glutamine to serum was maintained the same in the four spinners.

As mentioned above, the measured initial cell densities in the four spinner flasks, $0.15x10^6$, $0.30x10^6$, $0.26x10^6$ and $0.77x10^6$ cells/mL respectively, were slightly different from the projected values due to experimental variability during the inoculation. The two intermediate initial concentration values of $0.30x10^6$ and $0.26x10^6$ cells/mL were originally designed as replicates. The actual initial cell concentrations deviated from the projected ones. This deviation can be attributed to the insufficient centrifugation (300 g for 5 min) due to which the cells might have lost in the supernatant. It can also be attributed to the loss by possible removal of cells from the settled clump of cells along with the removal of supernatant while aspirating out with pipette.

4.2.2 Caspase assay

The caspase assay was performed by flow cytometry by measuring intracellular caspase activity levels. The FLICA based methodology (Immunochemistry Technology, LLC) was used for this purpose. Altogether four caspase assays were used: a green (carboxyfluorescein) FLICA caspase-8 assay kit, a green FLICA caspase-9 assay kit, a red (sulforhodamine) FLICA Caspase-3 & 7 kit and a red (sulforhodamine) FLICA caspase-9 assay kit (Caspase-7 is not considered in this study, since it is not as widely studied as caspase-3). Flow-cytometry analyses began approximately 1 day after seeding at which time the cultures had entered exponential phase. For each spinner flask, three aliquots were collected at each time point. One was tested for levels of caspase-8 and caspase-3 activation, the second for activated caspase-9 and caspase-3 and the third for caspase-8 and caspase-9 activation. Although the simultaneous testing of all three caspases would be preferred, no such three channel assay is currently commercially available. For each sample, the fluorescence of 25,000 cells (events) was measured on a flow cytometer (Becton Dickinson FACS Vantage SE). Analyses of flow cytometry data were performed using WinMDI v2.9 (Scripps Research Institute, CA, USA). To classify cells based on their caspase activation status, intensity thresholds for each caspase were set by single-dye negative controls prepared at day one. For each test, cells were then categorized into four sub-populations, resulting in a total of twelve cell conditions: $C8^- C3^-$, $C8^+ C3^-$, $C8^+ C3^+$, $C8^- C3^+$ and $C9^- C3^-$, $C9^+ C3^-$, $C9^+ C3^+$, $C9^- C3^+$ and $C8^- C9^-$, $C8^+ C9^-$, $C8^+ C9^+$, $C8^- C9^+$. The experimental results showed that whenever cells were positive for caspase-3, they were also positive for caspases-8 and 9. That is, the $C8^- C3^+$ and $C9^- C3^+$ subpopulations were negligible. This is likely a result of cross-talk between the two pathways. A population-based model describing the progression of caspases over time and its correlation to apoptosis from these experimental observations was developed as described in Chapter 5.

4.3   Results and discussion

Figure 4.2 shows the changes of viable cell concentration over time for the four batch experiments with different initial concentrations as described above. For the lowest initial cell density culture (SP1), a lag phase is clearly noticeable. The cells may exhibit extended G1 phase or temporarily enter into G0 phase during this lag period. On the other hand there is no observable lag in the higher cell density cultures. The observed lag phase in the low initial cell density culture can be attributed to higher magnitude of growth factors (auto-stimulatory compounds released into medium) reduction following medium dilution after inoculation as opposed to higher cell density cultures (SP2-4). Thus it can be interpreted that in the high initial cell density, cultures overcome a limiting value of growth factors that is required for continued

exponential growth of cultures. It can be also seen in Figure 4.2 that the viable cell concentration in SP4 reaches more rapidly its maximum as compared to the other cultures, but also declines more rapidly. Cell growth was assessed determining specific growth rate (Table 4.1) which was calculated as average quantity during the exponential growth phase. Since it is not possible to accurately separate the two phases of growth i.e. exponential and stationary phase, the numbers are approximate. It was found that the average specific growth rate was inversely correlated to the initial cell density (Table 4.1). Thus, the specific growth rate was higher in the lower initial cell density culture and it decreased as the initial cell density increased. Similar observations have been reported for hybridoma batch cultures in T-flask where the specific growth rate increased for increasing initial cell densities up to a certain initial cell density value and then decreased beyond that critical value (Lee, 2000). Regardless of the differences in growth rates, the maximum cell density values were similar for the higher initial cell density cultures (SP4, SP2 and SP3), though these peak concentrations were reached at different times. On the other hand, significant differences were observed in terms of nutrient depletion and metabolite production rates. These rates were calculated as average quantities throughout the whole culture period from the slope of the plot of nutrient /metabolites/product concentration vs. time integral of viable cells. Since lactate production remained constant after certain period of culture, its specific production rate was calculated only upto the period where its production starts becoming constant. The procedure for calculation of these rates is shown in Appendix B. The specific glucose consumption rate (q_{Glc}) in the lowest initial cell density culture was significantly higher than for the highest initial cell density cultures (Table 4.2). Figure 4.3 shows the progression with time of glucose, lactate, glutamine, and ammonia concentrations in the four spinners. As shown in this figure, when the viable cell concentration maxima were reached, neither glucose nor glutamine was completely depleted suggesting that they were not limiting growth. From Table 4.2, it can be observed that the specific glucose consumption rate was lowest in highest initial cell density culture (SP4), while it was highest in lowest initial cell density culture (SP1). This can be attributed to the specific growth rates in these cultures: the specific glucose consumption rate was higher in higher specific growth rate cultures and lower in lower specific growth rate cultures. Similar observation can be made with other cultures (SP2 and SP3) where the glucose consumption rates were lower than in the lower initial cell density culture SP1. The same interpretation can also be made with specific lactate production rate (q_{Lac}) which was also correlated to the specific growth rate, i.e. higher in the higher specific growth rate culture and lower in lower specific growth rate culture. Similar observations have been reported for hybridoma in perfusion culture where it was found that specific glucose consumption and specific lactate production rates are highly correlated to the specific growth rate of the culture (Banik and Heath, 1995).
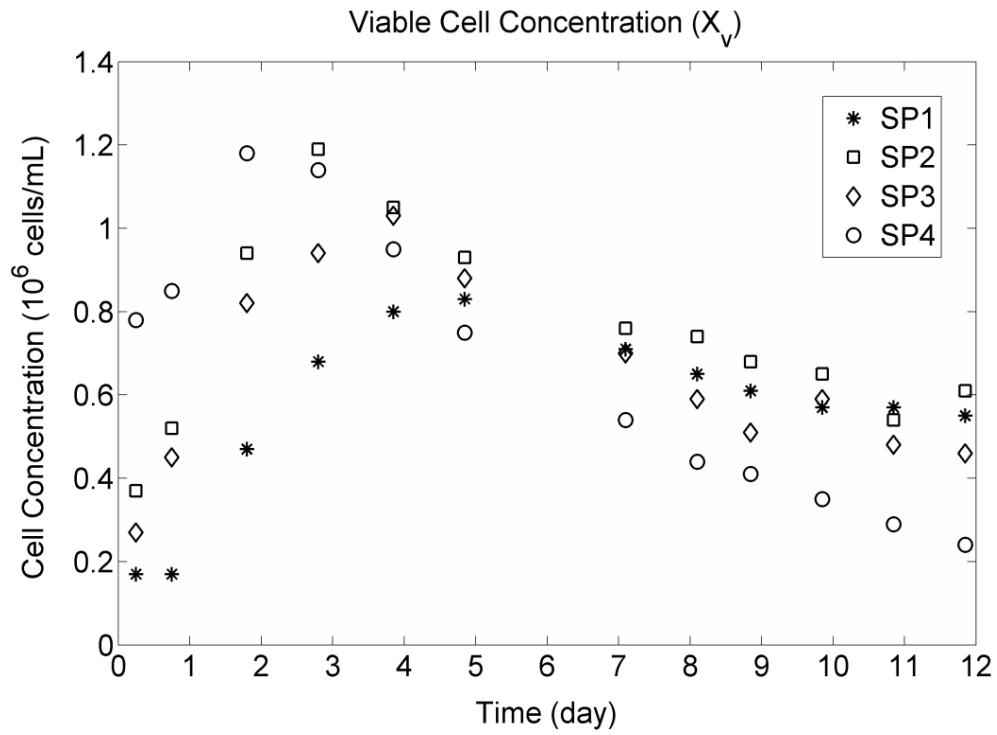
Figure 4.2: Viable cell concentration profile in different initial cell density cultures

Table 4.1: Average specific growth rates in different initial cell density cultures

	SP1	SP2	SP3	SP4
Initial cell density (cells/mL)	0.15×10^6	0.3×10^6	0.26×10^6	0.77×10^6
Average specific growth rate (day $^{-1}$)	0.50	0.38	0.40	0.20

Table 4.2: Specific glucose uptake (q_{Glc}) and lactate production rates (q_{Lac}) in different initial cell density culture

	SP1	SP2	SP3	SP4
q_{Glc} (mM/10^6 cells/mL day)	1.48	1.07	1.15	0.9
q_{Lac} (mM/10^6 cells/mL day)	3.95	2.56	2.26	1.76
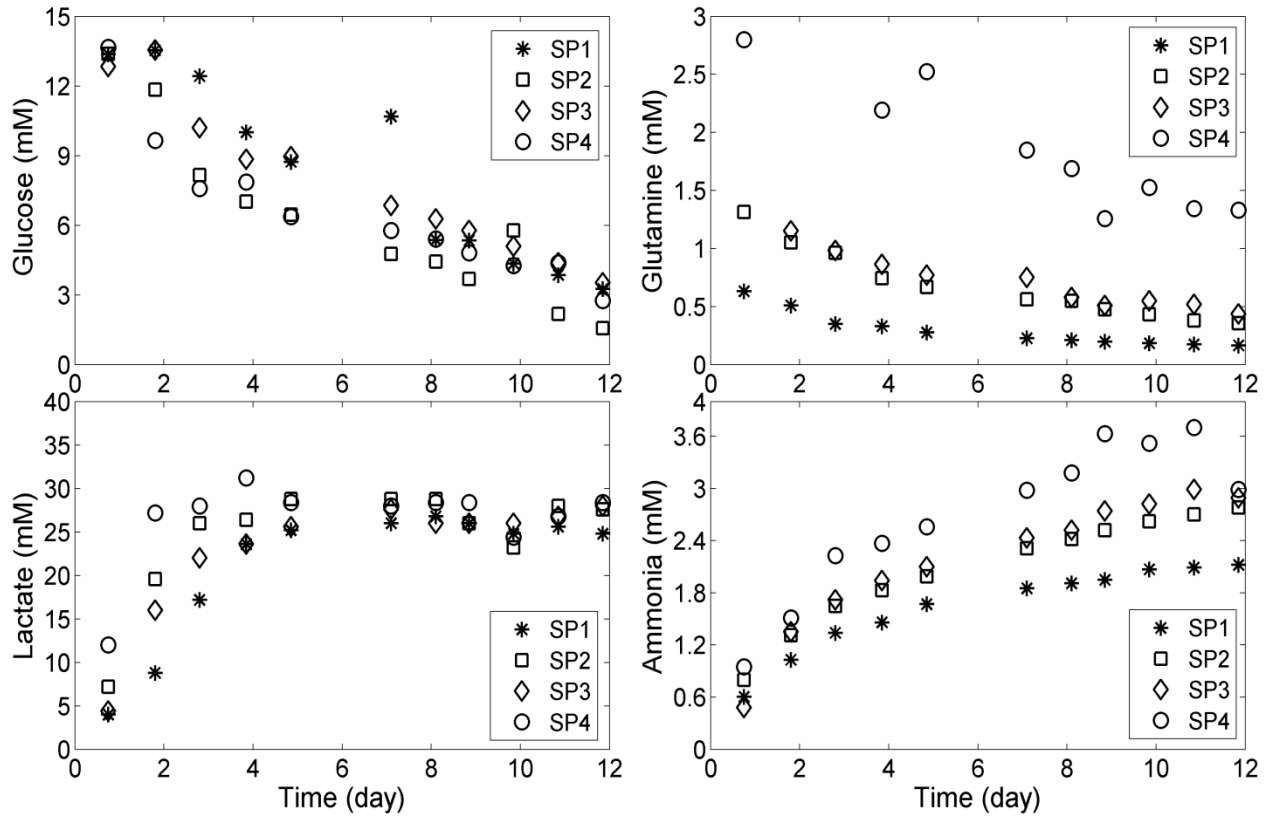
Figure 4.3: Time course of glucose, glutamine, lactate and ammonia evolution in different initial cell density culture

In a parallel investigation to the current one (Naderi, 2011) the evolution of apoptosis was monitored by tracking morphological cell changes characteristic of apoptosis using fluorescence microscopy with ethidium bromide (EB) and acridine orange (AO) as markers. It was found that there were relatively few necrotic cells (appearing red and round in fluorescence images) and their number did not increase significantly with time. Figure 4.4 shows a fluorescence microscopic image of the current CHO cell culture in stationary phase obtained with dual staining of ethidium bromide and acridine orange, showing the difference between apoptotic dead cells, which were abundant, and necrotic dead cells ,which occur in smaller amounts. Thus, that work confirmed that most of the cell death occurs by apoptosis rather than by necrosis.

In addition apoptosis was also monitored based on flow-cytometry scattering parameters. Forward scatter (FSC) characterizes cell size whereas side scatter (SSC) characterizes granularity in cell structure. When a cell becomes apoptotic its size decreases. Consequently FSC decreases during this change while SSC remains constant or increases. Figure 4.5 shows characteristic flow cytometry forward scatter-side scatter (FSC-SSC) plots in the low initial cell density culture (SP1). The distribution in the plot indicates subpopulations involving cells that decrease in size thus resulting in a decrease in FSC and an increase in SSC indicating the initiation of apoptosis. According to these flow cytometry measurements apoptosis appears to become significant after the exponential phase (after day 3) in this culture). Figure 4.6 shows, based on flow cytometry measurements, that the degree of apoptosis was more significant in the high cell density culture SP4 than in the low cell density culture SP1 (~45% at day 7 and day 11).

Necrosis is often associated to cells swelling, leading to an increase in FSC and a decrease in the SSC signal. As can be seen from Figures 4.5 and 4.6, there was only a very small increase in FSC. This indicated that there was negligible necrosis in the CHO cell culture system under investigation, confirming the aforementioned results obtained by fluorescence microscopy with ethidium bromide and acridine orange (Figure 4.4).

Figures 4.7 and 4.8 show bivariate distributions of fluorescence intensities of green and red FLICA markers stained for caspase-8 and caspase-3 in spinner SP1 (low initial cell density culture) and spinner SP4 (high initial cell density culture) respectively. The dual color fluorescence data are displayed as dot-plots of log intensity of green fluorescence of caspase-8 on the *x*-axis and red fluorescence of caspase-3 on the *y*-axis. This dot-plot was sub-divided into four quadrants, corresponding to four cell-subpopulations as follows. The lower left quadrant represents cells that show neither caspase-8 nor caspase-3 fluorescence ($C8^- C3^-$), the lower right quadrant represents cells that are active for caspase-8 but non-active for caspase-3 ($C8^+ C3^-$), the upper right quadrant represents cells that show simultaneous

activity of caspase-8 and caspase-3 ($C8^+ C3^+$), and the upper left quadrant represents the cells that show activity for caspase-3 but not for caspase-8 ($C8^- C3^+$). Similarly, when the cell sample was stained for caspase-9 and caspase-3 (not shown), four subpopulations within four quadrants was identified: $C9^- C3^-$, $C9^+ C3^-$, $C9^+ C3^+$, and $C9^- C3^+$. As the culture proceeded, there was an increase in the amount of data points in the lower right and upper right quadrants indicating a corresponding increase in activation of caspase-3 which is the executioner caspase at the end of the apoptotic pathways. Also, based on Figures 4.6 and 4.7, it is possible to infer that there was a larger proportion of apoptotic cells in the high cell density culture SP4 as compared to the lower initial cell density culture SP1.

The degree of apoptosis, quantified by percentages of the total amount of cells passed through the flow cytometer (25,000 cells), was obtained from each quadrant corresponding to each subpopulation in the above plots. Using these percentages, the evolutions of the caspase-8, caspase-9 and caspase-3 subpopulations in each of the spinners were determined (Figures 4.9-11). Based on the definition of the subpopulations, the total caspase-8 subpopulation corresponds to ($C8^+ C3^-$) + ($C8^+ C3^+$), the total caspase-9 subpopulation corresponds to ($C9^+ C3^-$) + ($C9^+ C3^+$) and the total caspase-3 subpopulation was taken as the average of ($C8^- C3^+$) + ($C8^+ C3^+$) and ($C9^- C3^+$) + ($C9^+ C3^+$). In principle ($C8^- C3^+$) + ($C8^+ C3^+$) and ($C9^- C3^+$) + ($C9^+ C3^+$) should be identical since both represent the total population of $C3^+$. However, these subpopulations were slightly different due to experimental error caused by the calibration of the thresholds used to separate the different subpopulations and therefore the average was taken.

In general, Figures 4.9 to 4.11 shows that caspase activation is correlated to initial cell density, i.e. higher initial cell density corresponds to higher caspases' activation. However, it should be pointed out that the dynamics of apoptosis in the culture, as quantified by monitoring the evolution of these cell sub-populations, is significantly different compared to the evolution of apoptosis in individual cells. In a culture of cells, a slow gradual activation of caspases along several days is observed but this reflects an average over many cells each at different stage of apoptosis. In contrast, caspase activation at the cell level is very fast occurring in a matter of few hours (Goldstein et al., 2000; Rehm et al., 2002).
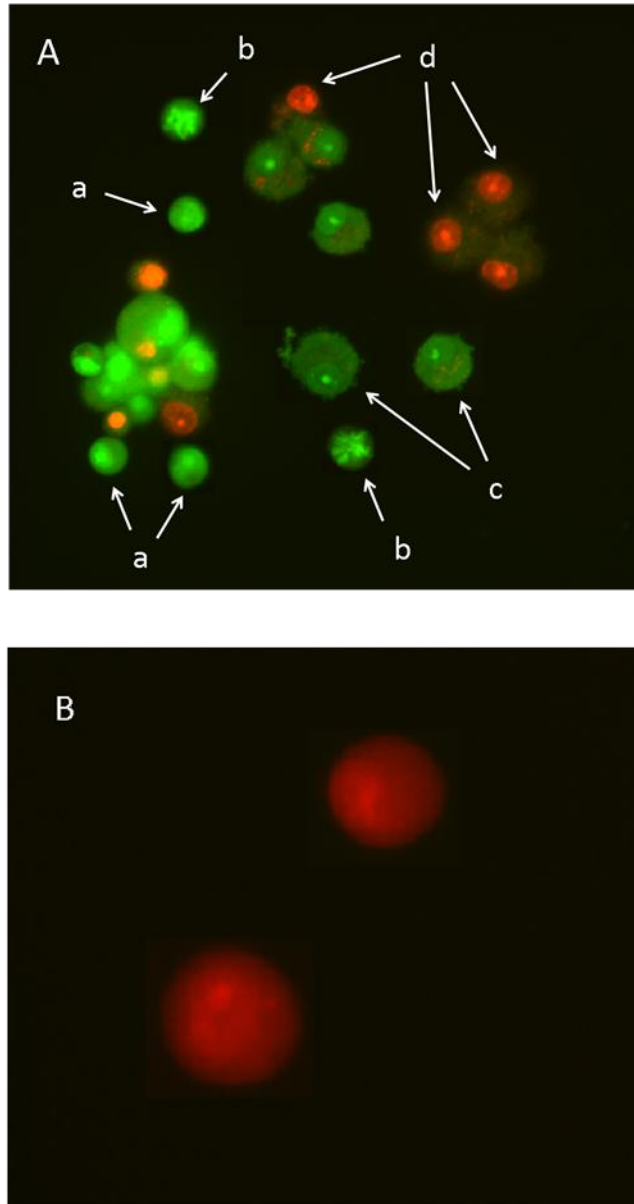
Figure 4.4: Fluorescence micrograph of CHO cell culture obtained with dual staining of ethidium bromide and acridine orange (A) Different physiological states: (a) Normal Viable cells (b) Early apoptotic cells (c) late apoptotic cells (approaching death) (d) Dead cells resulting from apoptosis (the cell membrane is ruptured and structure is not organized) (B) Necrotic cells
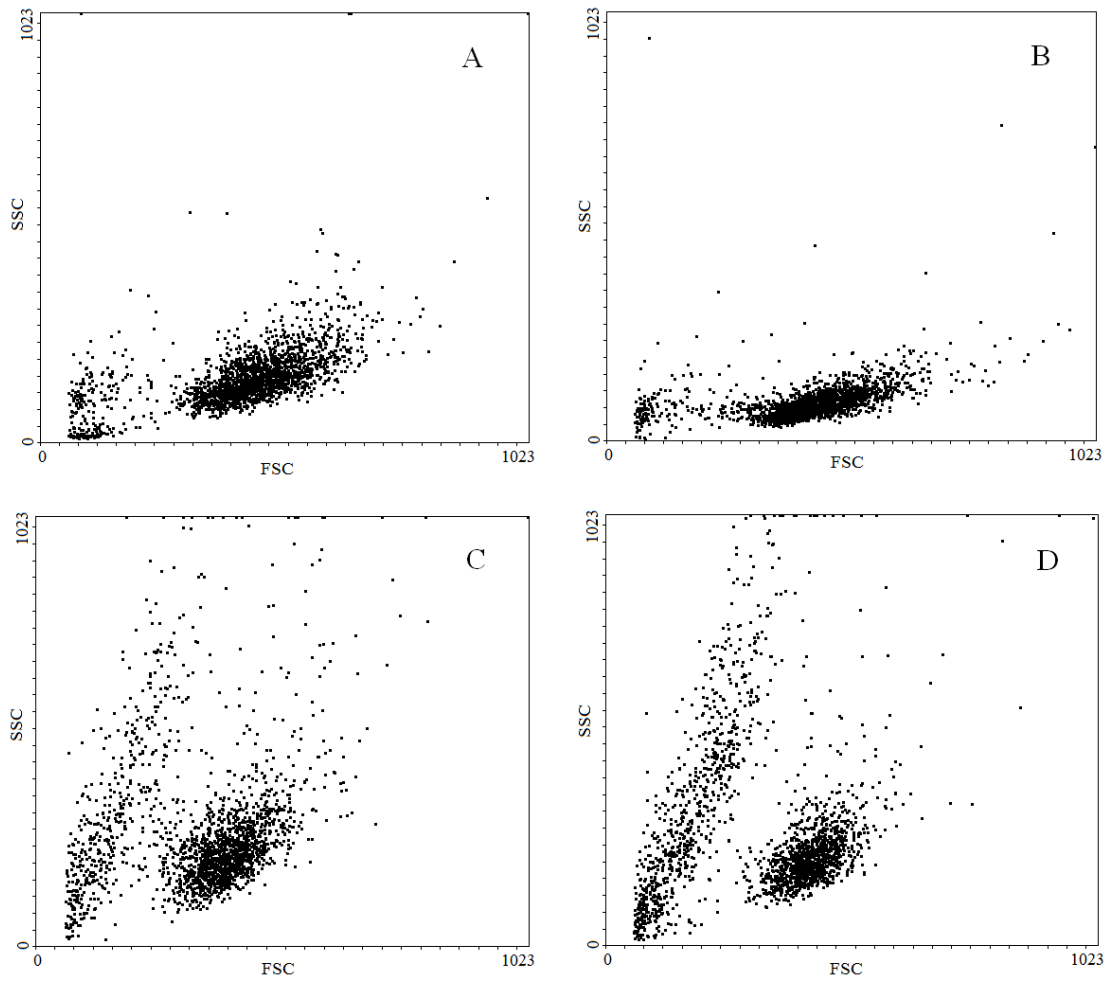
Figure 4.5: Bivariate distributions of cell samples for SSC vs. FSC in the low cell density culture SP1

(A) day 1 (B) day 3 (C) day 7 (D) day 11
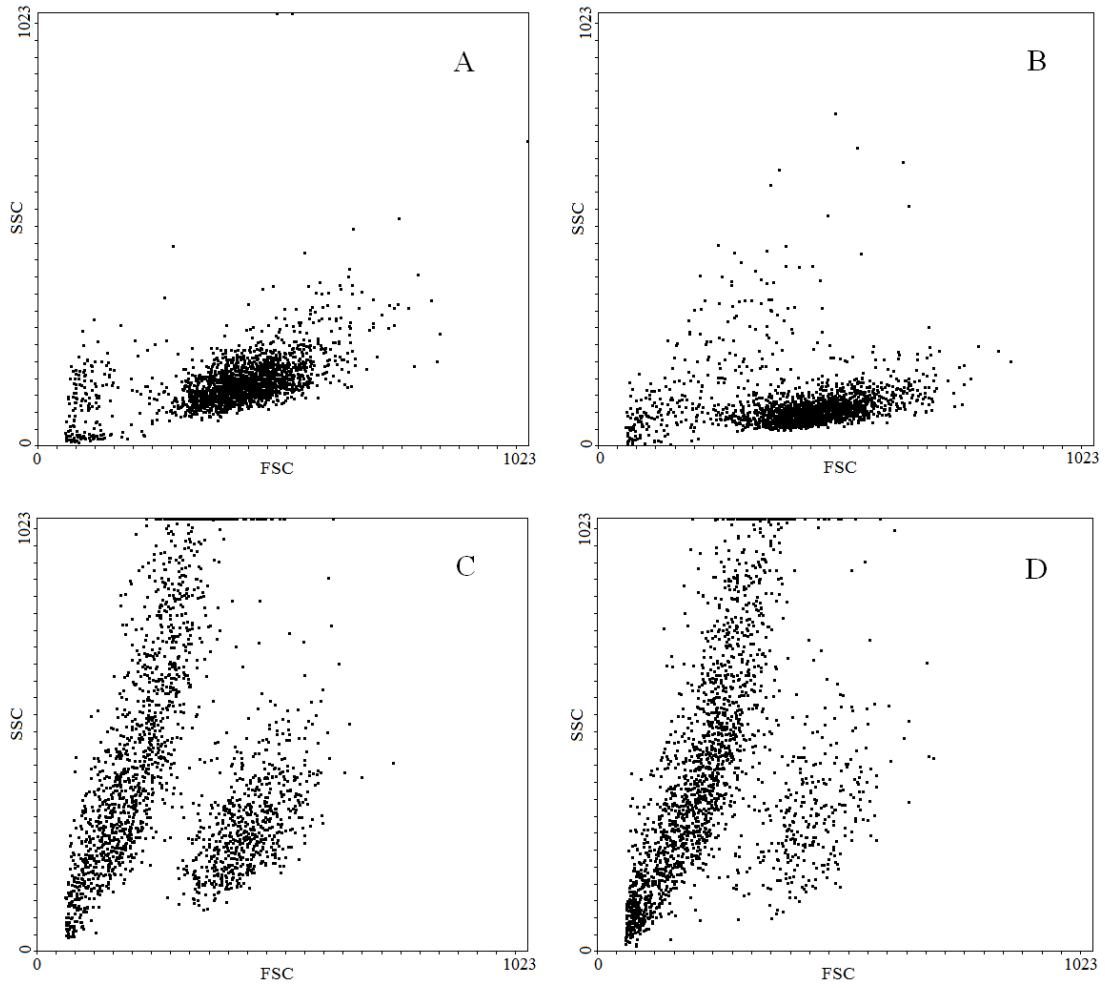
Figure 4.6: Bivariate distributions of cell samples for SSC vs. FSC in the high cell density culture SP4

(A) day 1 (B) day 3   (C) day 7   (D) day 11
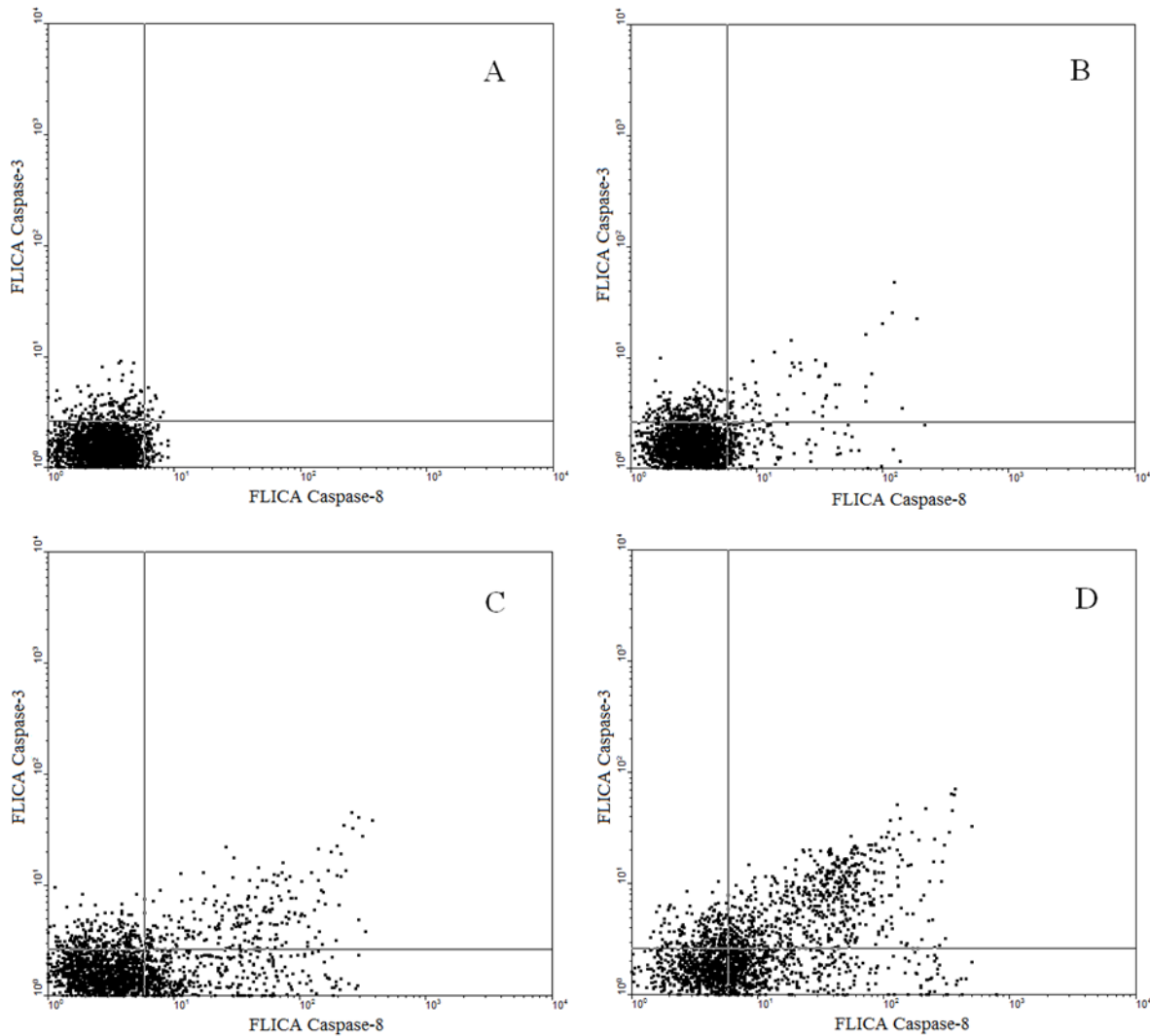
Figure 4.7: Dual fluorescence staining flow cytometric analysis of simultaneous caspase-8 and caspase-3 activation in CHO cell culture in the low cell density culture SP1. The four quadrants represent different subpopulations based on caspase-8 and caspase-3 activity. The four scatter diagrams show caspase activation during the culture (A) day 1 (B) day 3 (C) day 7 (D) day 11. As the culture proceeds, the clusters of data points become increasingly denser on the right of these figures.
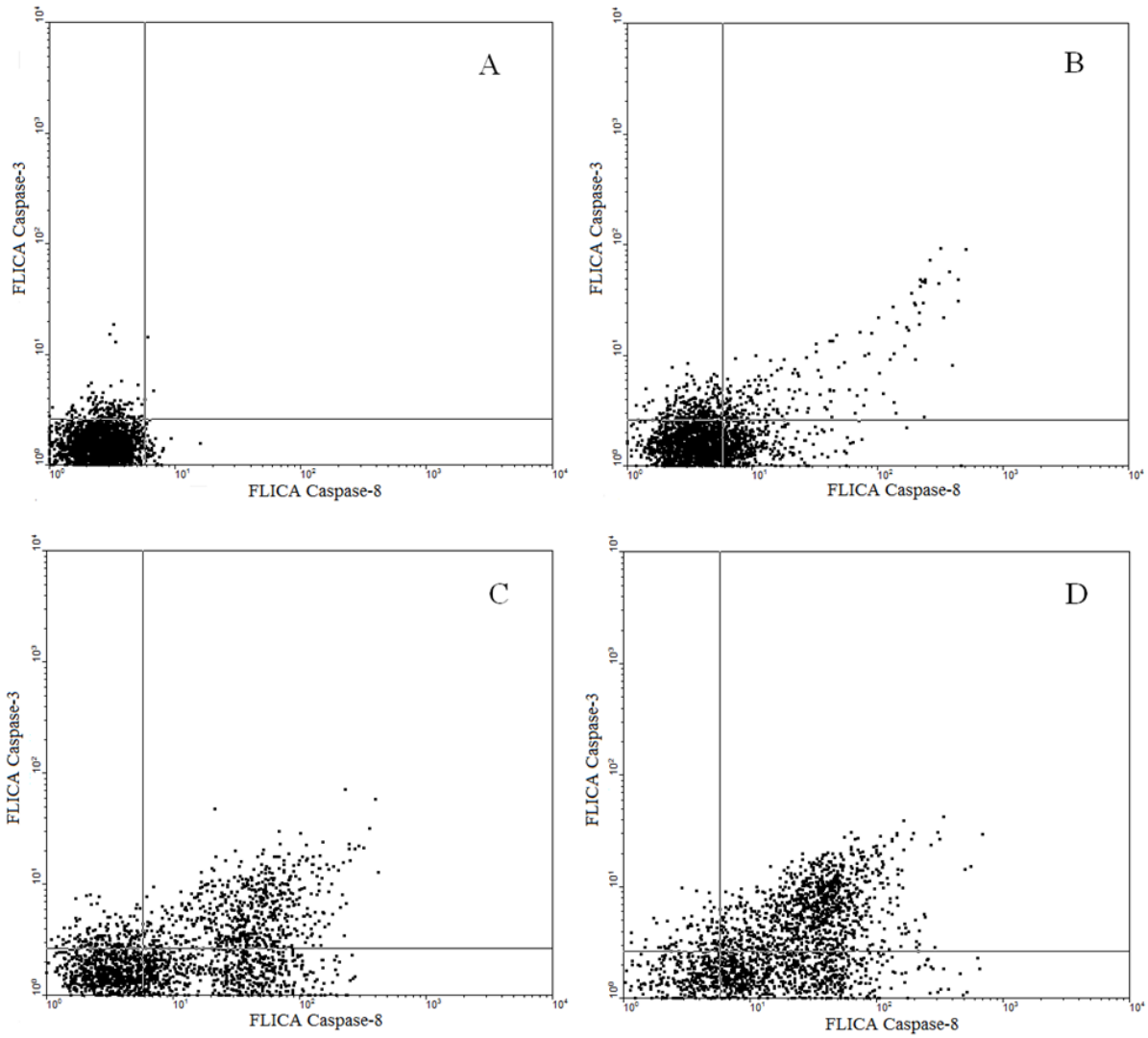
Figure 4.8: Dual fluorescence staining flow cytometric analysis of simultaneous caspase-8 and caspase-3 activation in CHO cell culture in the high cell density culture SP4. The four quadrants represent different subpopulations based on caspase-8 and caspase-3 activity. The four scatter diagrams show caspase activation during the culture (A) day 1 (B) day 3   (C) day 7   (D) day 11
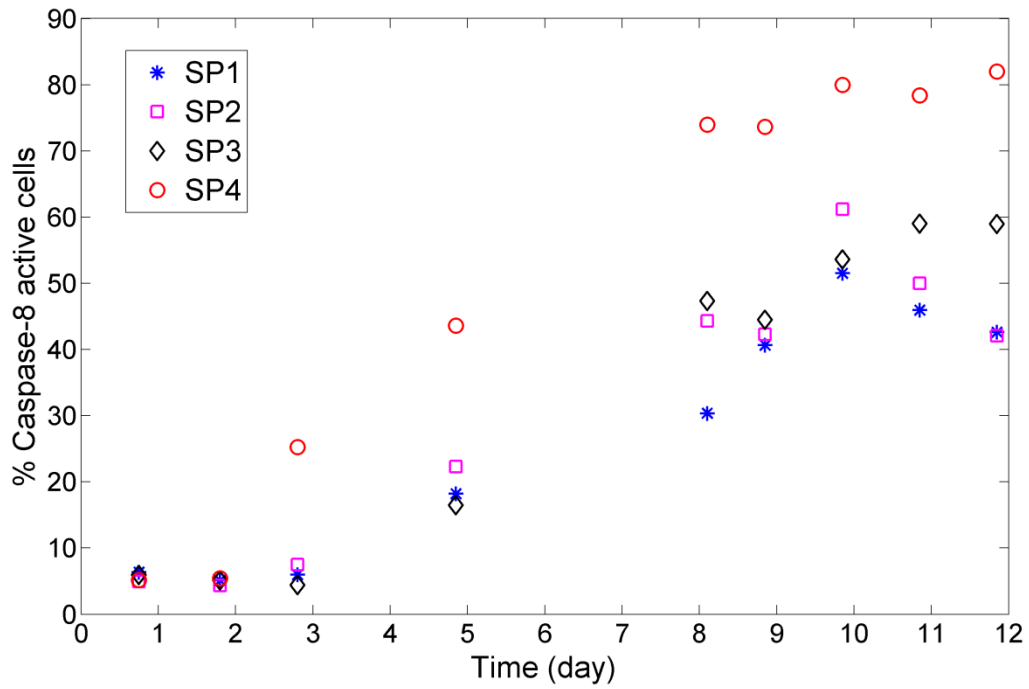
Figure 4.9: Caspase-8 subpopulation progression in different initial cell density culture
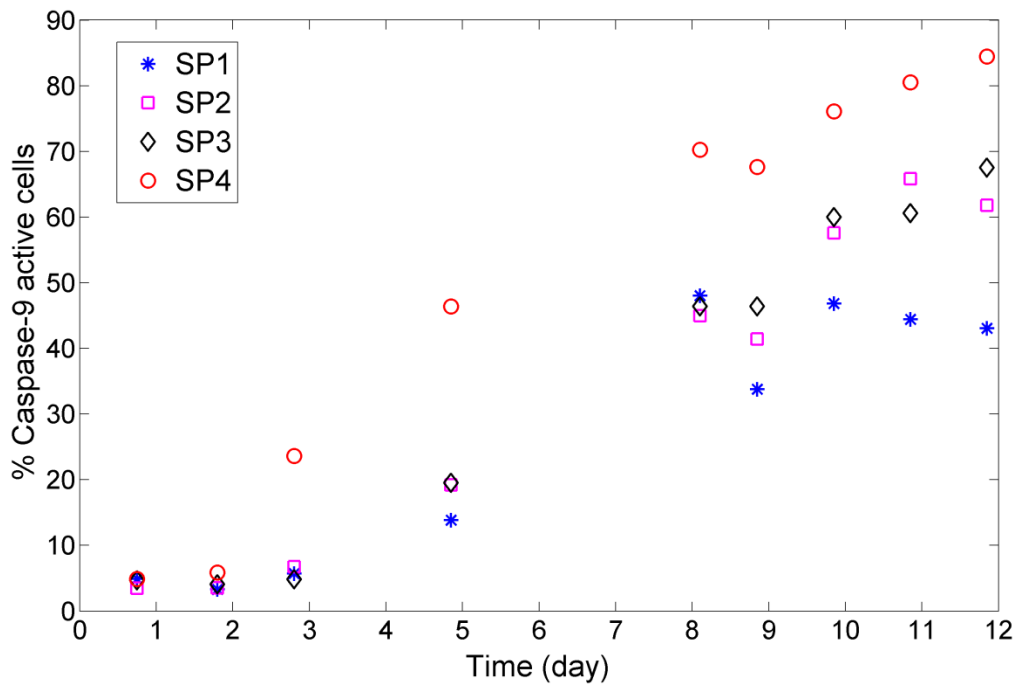
Figure 4.10: Caspase-9 subpopulation progression in different initial cell density culture
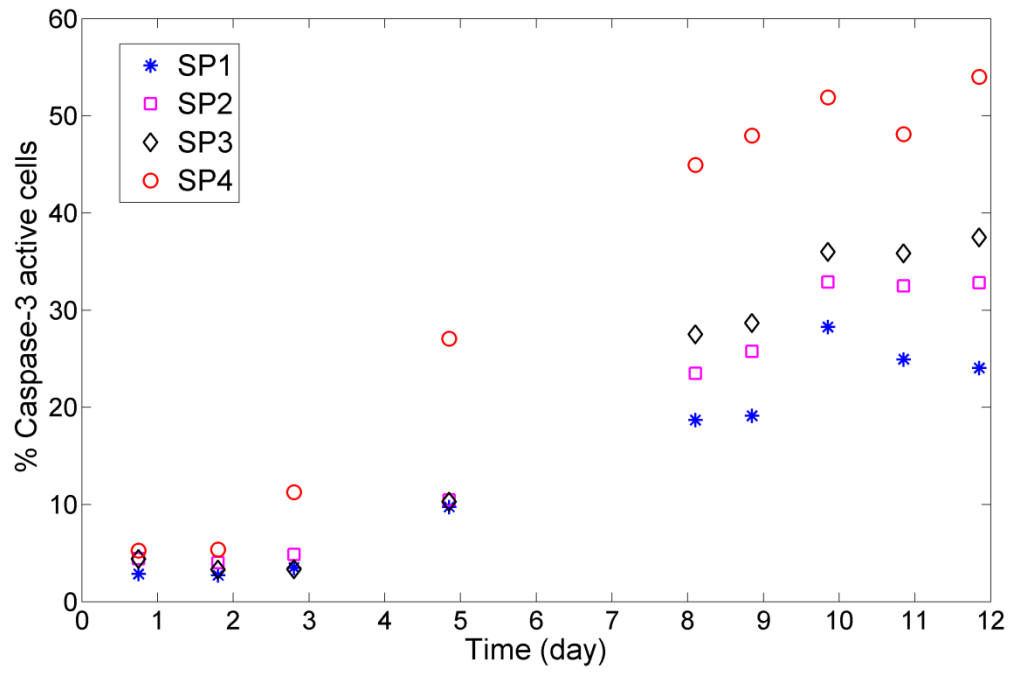
Figure 4.11: Caspase-3 subpopulation progression in different initial cell density culture

Chapter 5

Modeling the progression of apoptosis

Based on the experimental observations in different initial cell density cultures a population-based model was developed to describe the dynamic evolution of the different apoptotic subpopulations identified by flow cytometry.

5.1 Materials and methods

The lowest initial cell density culture (SP1) and highest initial cell density culture (SP4) were used for calibrating the apoptosis population-based model. The details of these cultures are given in the previous chapter (Chapter 4). The prediction capability of this model was assessed by validating this model against data from the remaining two spinner flasks SP2 and SP3 and four additional experiments with different operating conditions. The operating conditions of these four additional experiments are given in Table 5.1.

5.1.1 Model development

A subpopulation balance based model was developed to describe the evolution with time of the different subpopulations identified in the flow cytometry experiments described in Chapter 4 corresponding to different combinations of activated caspases. The estimate of each subpopulation obtained in percentages from in each quadrant after dot-plot analysis of flow cytometry results was transformed to concentration with corresponding viable cell concentration (X_v) obtained using the trypan blue method.

Since the specific dependencies of caspase activations with respect to factors such as cell density, nutrients' levels and toxicants' concentration were not known *a priori* it was decided to formulate a number of different model structures that assume different functionalities of caspase activation with respect to the aforementioned factors. Then, the most suitable structure was identified by analyzing the quality of fit between model predictions and data and by assessing the prediction accuracy of each one of the assumed model structures. A total of twenty-four variants of population-based model were considered based on combinations of different hypotheses regarding different triggering mechanisms for apoptosis, cross-talk between pathways and the presence of a limiting nutrient. These variants are described later in the Chapter.

For modeling purposes, cell subpopulations corresponding to the different mathematical states in the model are defined in terms of caspase activity as follows:

- Normal healthy cells: $x_1 = C8^- C9^- C3^-$
- Apoptotic cells testing positive for caspase-8 but negative for caspase-9: $x_2 = C8^+ C9^- C3^-$
- Apoptotic cells testing positive for caspase-9 but negative for caspase-8: $x_3 = C8^- C9^+ C3^-$
- Apoptotic cells positive for caspase-8 and -9 but negative for caspase-3: $x_5 = C8^+ C9^+ C3^-$
- Apoptotic cells testing positive for caspase-3: $x_4 = C8^+ C9^+ C3^+$

The modeling scheme is shown in Figure 5.1. According to this scheme, it is proposed that normal healthy cells (x_1) undergo apoptosis via either of the two pathways as described above: the extrinsic pathway, forming caspase-8 active cells (x_2) and the intrinsic pathway, forming caspase-9 active cells (x_3). Eventually these two subpopulations progress either directly into caspase-3 active cells (x_4), or "cross-talk" between the pathways results in an intermediate state $(x_5 = C8^+ C9^+ C3^-)$ as shown in Figure 5.1. Finally the apoptotic cells (x_4) undergo death thus converting into the final population (x_6). These dead cells eventually disintegrate by lysis. A separate necrosis process acting in parallel to the apoptotic events was not included, since, as mentioned in Chapter 4, the examination of this cell culture by fluorescence microscopy and flow cytometry confirmed that there are very few necrotic cells (appearing red in fluorescence images) in the culture, and their numbers do not increase significantly with time. All living cells are capable of mAb production and so are considered viable $(X_v = x_1 + x_2 + x_3 + x_4 + x_5)$. Rather than correlate the onset of apoptosis with the cessation of growth, the viable cell population was divided into two subpopulations: viable dividing/growing cells and viable non-dividing/non-growing or resting cells. The latter consume substrate for maintenance but not for growth. The fraction of viable cells in the growing state (f_{gr}), decreases as the culture grows. It was initially hypothesized that growth

rate decrease and eventual growth arrest was due to a nutrient in either the medium or the serum that gets depleted. Accordingly, the fraction of growing cells was described by a modified form of the Tessier growth model (Moser, 1985) as follows,

$$f_{gr} = 1 - e^{-\frac{S}{X_v K_s}}$$ (5.1)

where K_s is a constant and S represents a limiting nutrient. The dependence on the cell density (X_v) accounts for a reduction in the specific growth rate at high cell density as a result of increased energy requirements for cell maintenance (Lee, 2002).

Since it was found in earlier investigations that neither glucose nor glutamine are limiting in the culture conditions used in experiments, the identity of the assumed limiting nutrient(s) was not known. Goudar et al., (2005) were also unable to find a growth rate limiting nutrient for their CHO cell line and employed a logistic model. So it was chosen to represent the residual fraction of a currently unknown limiting nutrient, denoted by S. Later in this chapter, a model comparison analysis is presented that aims to determine whether this limiting nutrient is contained in the medium or in serum. However, at later stages of this research it was found that growth arrest is mostly correlated to large changes in pH that are possibly due to accumulation of carbon dioxide in the medium. Since the mathematical model for the growth fraction as either a function of an unknown nutrient or an inhibitory compound is of similar mathematical structure, the model presented in this section follows the unknown nutrient assumption (Equation 5.1) to describe the change in the fraction of growing cells. However, later in a chapter (Chapter 8, Equation 8.2), the above was replaced by a dependency with respect to an inhibitor (accumulation of CO_2) instead of the unknown nutrient.

Following the definition of the fraction of growing cells, the growth rate of normal viable healthy cells is expressed as:

$$v_1 = \mu_g\, f_{gr}\, x_1$$ (5.2)

where μ_g is a constant parameter.

Cells that are not yet caspase-3 active $(x_2, x_3$ and $x_5)$ are assumed to be growing as well. Cells in these populations may not be actively undergoing apoptosis. Because dividing cells may continue at least one round of division while entering the apoptotic process (Meikrantz and Schlegel, 1995), growth of these sub-populations was allowed for in the model. Their growth rates are given by

$$v_{2_g} = \mu_g \, f_{gr} \, x_2 \tag{5.3}$$

$$v_{3_g} = \mu_g \, f_{gr} \, x_3 \tag{5.4}$$

$$v_{5_g} = \mu_g \, f_{gr} \, x_5 \tag{5.5}$$

On the other hand, cells that have progressed further along the apoptotic pathway (x_4) as indicated by activation of caspase-3 are considered to be growth-arrested.

The fraction of limiting substrate S decays according to its consumption during cell growth:

$$\frac{dS}{dt} = -k_{sub} \, f_{gr} \, (x_1 + x_2 + x_3 + x_5) \tag{5.6}$$

To account for cell-cell signaling activity, the rate of activation of the extrinsic pathway, v_2 is taken to be dependent on the cell density (Hardy and Stark, 2002) as per the following nonlinear equation

$$v_2 = (\mu_e \, (\text{signalling cell density})^\alpha) x_1 \tag{5.7}$$

where μ_e and α are constant parameters. Since it is unclear whether these apoptosis-inducing signals are sent from all cells or just cells that have committed to apoptosis, several cases were considered. In one case, just cells with active caspase-3 were considered in Equation (5.7),

$$v_2 = (\mu_e \, x_4^\alpha) x_1 \tag{5.8}$$

In a second case, all cells were considered to be exchanging these signals

$$v_2 = (\mu_e \, X_v^\alpha) x_1 \tag{5.9}$$

For comparison purposes, a third case was considered in which signaling is not density-dependent as follows

$$v_2 = \mu_e \, x_1 \tag{5.10}$$

The intrinsic pathway has been shown to be triggered via nutritional stress (Goswami et al., 1999; Sanfeliu and Stephanopoulos, 1999; Simpson et al., 1998b), and so this rate dependent on the limiting nutrient S can be described as

$$v_3 = \mu_i \frac{1}{1 + K_i S} x_1 \tag{5.11}$$

where μ_i and K_i are constants. In contrast, and as mentioned in earlier chapters, some studies have shown that the accumulation of toxic metabolites may trigger this pathway. Accordingly, an alternative formulation was considered in which the intrinsic pathway is triggered by the accumulation of ammonia:

$$v_3 = \mu_i \, Amm \, x_1 \tag{5.12}$$

Experimental measurements of ammonia concentration were linearly interpolated for incorporation into model. Ammonia is inhibitory to mammalian cell growth at concentrations as low as 2.4–2.8 mM (Hansen and Emborg, 1994; Newland et al., 1994). Ammonia concentrations reached as high as 4 mM at the end of experiments; the concentration range was 1.5-2.0 mM when an increase in caspase-9 activity was first observed. The observations of lactate show that its levels follow a trend similar to ammonia, reinforcing the possibility that the increase in caspase-3 sub-population may be correlated to other toxic metabolites that may be involved in triggering the intrinsic pathway.

The rates of internal apoptosis progression, as indicated in Figure 5.1, are presumed linear for simplicity, so that

$$v_4 = k_4 x_2 \tag{5.13}$$

$$v_5 = k_5 x_3 \tag{5.14}$$

$$v_8 = k_8 \, x_2 \tag{5.15}$$

$$v_9 = k_9 \, x_3 \tag{5.16}$$

$$v_{10} = k_{10} \, x_5 \tag{5.17}$$

where k_4, k_5, k_8, k_9 and k_{10} are parameters.

The death rate of caspase-3 active cells (v_6) is given as

$$v_6 = \mu_d x_4 \tag{5.18}$$

where μ_d is a parameter.

In the preliminary investigations, the dependence of this death rate on the ammonia concentration was explored and found based on the model identifiability analysis presented in the next section that any ammonia effect was negligible, and so it was not included.
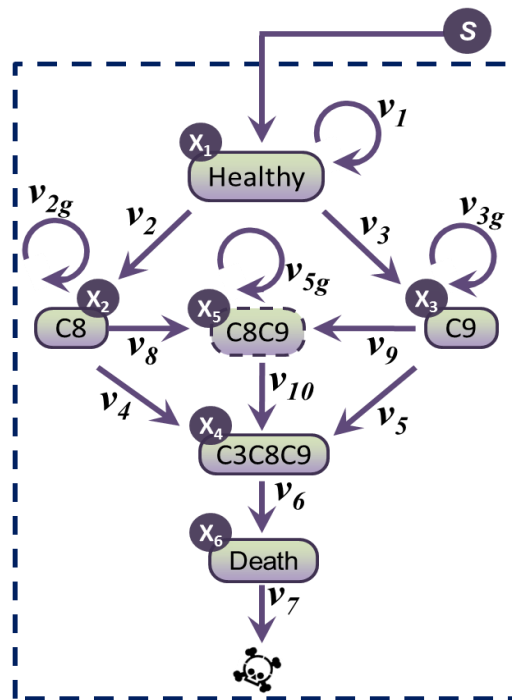
Figure 5.1: Balance between apoptotic subpopulations. Healthy cells begin apoptosis by activation of the intrinsic pathway (C8) of the extrinsic pathway (C9). The cells eventually trigger caspase-3, leading to late apoptosis and eventually death. Cross-talk between the two pathways may lead to the presence of early apoptotic cells in which both initiator caspases are active. 'S' represents limiting substrate.

Finally, the lysis rate of dead cells is given as

$$v_7 = k_{lys} x_6 \qquad (5.19)$$

where k_{lys} a parameter.

As a final variant for model comparison, a model was considered in which the cross-talk between the two apoptotic pathways is negligible, so that the caspase-8 and -9 active population (x_5) is absent. This is equivalent, according to Figure 5.1, to setting k_8 and k_9 to zero.

The initial conditions for all the state variables were also estimated along with the model parameters. The initial condition for the limiting nutrient S was chosen to reflect hypotheses about the source of this nutrient. In the first variant, the nutrient is presumed to be contained in the medium, and so the initial condition for S is fixed (at 1, units arbitrary). In the second variant, the limiting nutrient is presumed to be contained in serum, and so depends on the initial serum concentration (at a level of 100 times the percentage serum level).

To summarize, a total of twenty-four different model formulations were constructed involving the different hypotheses described above which in terms of the model variables are as follows:

1. Limiting nutrient S present in medium or in serum (initial value of S is identical for all spinners or depends on initial serum concentration)

2. Cross-talk (x_5) absent or present

3. Extrinsic pathway triggered by apoptotic signaling from all cells, caspase-3 active cells, or at a fixed rate ($v_2 = (\mu_e * x_4^\alpha) x_1$ or $v_2 = (\mu_e * x_v^\alpha) x_1$ or $v_2 = \mu_e x_1$)

4. Intrinsic pathway triggered by nutrient limitation or toxic stress by ammonia accumulation ($v_3 = \mu_i \frac{1}{1+K_i S} x_1$ or $v_3 = \mu_i \, Amm \, x_1$)

Each of the 24 model formulations was calibrated against the training data set, consisting of the experimental data in SP1 and SP4. The models were then compared based on their ability to predict the outcomes of the validation data set (the remaining experiments: SP2, SP3). Additional data set was also considered for validation to see the robustness of the developed model in terms of its prediction

73

capability. These additional dataset were obtained from experiments labeled SP5-8. The experimental conditions are given below (Table 5.1). (More details of these experiments are given in the next chapter).

Table 5.1: Experimental conditions in additional validation data set

experiment	Initial cell density (10^6 cells/mL)	Glutamine (mM)	Serum (%)
SP5	0.18	1	0.5
SP6	0.15	1	2
SP7	0.64	4	0.5
SP8	0.71	4	2

5.1.2 Model fitting

A system of differential equations was set up by applying material balances based on the model shown in Figure 5.1. The model was simulated in MATLAB (Mathworks, USA). The integration of differential equations was performed using *ode23s* in MATLAB. Parameter fitting began with the use of a genetic algorithm to obtain approximate values of the optimal model parameters. In view of the nonlinearity of the resulting optimization problem, various initial guesses of parameters were provided for the minimization of the objective function. The sum of squared errors (SSE) was used as an objective function and was generated by comparing the model predictions to the data and weighting each squared residual by the size of the concentration (resulting in a relative measure of error):

$$SSE(k) = \sum_{i=1}^{r} \sum_{t=1}^{m} \left[\frac{y_i(t) - \hat{y}_i(t)}{y_i(t)} \right]^2 \qquad (5.20)$$

where k are the parameters involved in the model, y is the output that corresponds to the system measurements, $y \in \mathbb{R}^r$ obtained at sampling time points at t, $t \in \mathbb{R}^m$ and $\hat{y}$ are the predicted outputs obtained by solving differential equations.

In each case, the final set of parameters obtained via the genetic algorithm was refined by subsequent application of a constrained nonlinear optimization function (MATLAB routine: *fmincon*).

For minimizing the relative sum-of-squares errors (SSE) towards parameter estimation, the model state variable x_1, which represents the population of viable non-apoptotic cells, was compared to subpopulation C8⁻ C9⁻ since a negative test for caspases indicates that a cell is not undergoing apoptosis as yet. Subpopulation C8⁻ C3⁻ was compared to the sum of states x_1 and x_3 where the latter is defined as being caspase-9 positive, while C9⁻ C3⁻ was compared to the sum of states x_1 and x_2 where the latter is defined as being caspase-8 positive. In the case of x_4, due to experimental error there was generally a small discrepancy between the measured population of caspase-3 active cells corresponding to either the sum of C8⁺ C3⁺ and C8⁻ C3⁺ or the sum of C9⁺ C3⁺ and C9⁻ C3⁺ although they should have been equal as explained in Chapter 4. Hence, the state x_4 was compared against the average of these two values. Finally, in the five-state model C8⁺ C3⁻ was compared to the sum of x_2 and x_5 , while C9⁺ C3⁻ was compared to sum of x_3 and x_5, while in the four-state model, x_2 was compared to C8⁺ C3⁻ , and x_3 to C9⁺ C3⁻ . The dead cell population x_6 was compared to the dead cell count obtained from the trypan blue exclusion method.

It was found necessary to add an additional weight to the second time point (at day 1.8) for the high-density culture in spinner SP4. The early dynamics for populations C8⁻C9⁻ , C9⁻C3⁻ and C8⁻C3⁻ in this spinner were not well resolved by the measurements; an additional weighting (by a factor of 80) was required in order to force the early peaks observed in behavior.

5.1.3 Model comparison and parameter identifiability analysis

Because the model formulations involve different numbers of state variables and parameters, the fits to the experimental data were compared using the AICc, the small-sample-size corrected version of the Akaike information criterion. This measure allows for comparison of model fits while taking into account the fact that some model formulations can take advantage of more degrees of freedom to fit the data, while others are constrained by additional comparisons to the data. Presuming the errors are independent and normally distributed, the AICc is defined by

$$AICc = n \ln\left(\frac{SSE}{n}\right) + \frac{2np}{n-p-1} \tag{5.21}$$

where SSE is the minimized sum of squared errors, n is the sample size, and p is the number of model parameters. Also the AIC and the BIC (Bayesian information criterion) were applied and leading to similar results.

Identifiability analysis was performed to assess confidence in the best-fit parameter values. Identifiability was assessed by parametric sensitivity analysis, which indicates how variation in parameter values influences the behavior of the system. (Low sensitivity typically corresponds to low confidence in the calibrated parameter value). Overall sensitivity measures for each parameter were determined as in (Brun et al., 2002). The general procedure is as follows. Consider the following system of differential equations

$$\dot{x} = f(x, k, t) \text{ and } y = h(x)$$

where x is the state vector, k is the parameter vector, t is time, and y is the output that corresponds to the system measurements. The sensitivity of the jth parameter on the ith output variable at sampling time t is given by the coefficient

$$M_{ij}(t_m) = \left. \frac{\partial y_i}{\partial k_j} \right|_{t=t_m} \tag{5.22}$$

These can be organized into a sensitivity score matrix M, as follows:

$$M = \begin{bmatrix} M_{11}(t_1) & \cdots & M_{1p}(t_1) \\ \vdots & \ddots & \vdots \\ M_{1r}(t_1) & \cdots & M_{rp}(t_1) \\ M_{11}(t_2) & \ldots & M_{1p}(t_2) \\ \vdots & \ddots & \vdots \\ M_{r1}(t_m) & \ldots & M_{rp}(t_m) \end{bmatrix} \tag{5.23}$$

where the model has r outputs and p parameters, and measurements were taken at m time-points.

In order to determine the identifiability of model parameters, the individual sensitivity scores in the sensitivity score matrix M, were scaled as

$$M_{ij}^s(t_m) = \frac{k_j}{y_i} M_{ij}(t_m) = \left. \frac{k_j}{y_i} \frac{\partial y_i}{\partial k_j} \right|_{t=t_m} \tag{5.24}$$

The orthogonalization method proposed by Yao et al., 2003 (as mentioned in Chapter 2, Literature review) was applied on this scaled sensitivity matrix to determine identifiable parameters.

After determining identifiability of parameters, confidence intervals for these parameters were obtained via the Fisher Information Matrix (FIM). FIM is based the linearization of each of the responses in the neighborhood of the optimal parameter set k and signifies the amount of information contained in experimental measurements. The Fisher Information Matrix (FIM) was constructed from the original sensitivity score matrix given in Equation (5.23) by

$$FIM = \sum_t M^T V M$$

(5.25)

where V is the inverse of the covariance matrix of measured output error. The variance was estimated by using measurement replicates of the initial time-point to determine a coefficient of variation associated with the experimental assays (flow cytometry and trypan blue cell counting).

The Cramer-Rao bound states that the inverse of the FIM represents the error covariance matrix of the minimum variance unbiased estimator (Kay, 1993), and thus a lower bound on the variance of the identifiable parameter can be obtained from the diagonal of the FIM as

$$\sigma^2(k_i) \geq (FIM^{-1})_{ii}$$

(5.26)

A 95% confidence interval for an identifiable parameter can then be obtained as

$$k_i \pm 1.96 \sqrt{\sigma^2(k_i)}$$

(5.27)

These confidence intervals reflect the degree to which each parameter value is constrained by the data. Parameters for which the sensitivity is low give rise to large confidence intervals, since their values are not well-constrained by the model outputs that correspond to data in this study.

The overall parameter sensitivity score was calculated as follow (Brun et al., 2002).

$$\delta_j = \sqrt{\frac{1}{m} \sum_t^m \sum_i^r [M_{ij}(t)]^2}$$

(5.28)

5.2 Results and discussion

Table 5.2 represents the minimal SSE scores for the 24 model variants and AICc measures, which incorporate both the training and prediction fits. As shown in the table, the best model variant (i.e. lowest AICc value, denoted in bold) has the limiting nutrient S present in the medium, incorporates cross-talk, has the rate of the extrinsic pathway expressed as a function of caspase-3 active cells, and has the rate of the intrinsic pathway expressed as a function of ammonia. The parameter values obtained after optimization for this best model variant are shown in Table 5.3, along with sensitivity measures, identifiability scores, and confidence intervals. Figure 5.2 shows the fit of the model to the experiments SP1 and SP4. Figure 5.3-5.5 shows the model prediction for experiments SP2-8. Overall, the model successfully predicts the dynamic behavior of the culture subpopulations for all initial cell densities. However, for the low cell density and high initial serum levels in SP6, the progression of apoptosis was not well captured.

5.2.1 Model comparison results

The five-state model out-performed the four-state model, even after taking into account, in the Akaike criterion calculation, the additional degree of freedom provided by the increased number of fitting parameters and the increased number of comparison used to fit the five-state model. This suggests that cross-talk is occurring between the two apoptotic pathways in the current CHO cell culture. The best model performance occurred in the case where the signals that trigger the extrinsic pathway are generated by caspase-3 active cells (x_4), suggesting that actively apoptotic cells are responsible for triggering apoptosis in the rest of the culture. This model variant was also compared with other variants based on AICc scores by computing the probability as per Equation (2.7), and found that this model variant was 99.99% correct than the other model variants. The model sensitivity and identifiability analysis (discussed in the next section) shows that the parameter associated with cell density dependence has a strong effect on model behavior, indicating the prominent effect of cell density on apoptosis. The models performed significantly better when the intrinsic pathway was presumed dependent on the accumulation of ammonia. This suggests that build-up of toxic metabolites, rather than nutrient depletion, is responsible for triggering the intrinsic apoptotic pathway in this culture.

The model comparison suggests that the liming nutrient is not present in serum. Nevertheless, the current CHO cell line would not grow in the absence of serum. It was determined that the maximum specific growth rate was not serum-dependent for serum between 0.5% and 1.0%. The peak viable population

density was essentially the same for 0.5% to 1.0% serum, it increased by 40% with serum concentrations above 1%. It was observed that the time where growth arrest occurred was not dependent on the serum levels (since the maximum cell concentration reached at the same time of day in both serum level cultures of 0.5% and 2%, Chapter 6, Figure 6.1) but the progression of apoptosis was. Together with the model comparison results, these observations suggest that when the serum is above 1% the growth-limiting nutrient is present in the medium, but some components of serum affect the dynamics of apoptosis. Later in this work it was found that spinner volume had an effect on the cell density peak. Based on this observation and after measuring low levels of pH during growth arrest it was later hypothesized that arrest may be related to inhibition by carbon dioxide. To account for these observations, the mathematical model was kept the same except that the limiting nutrient concentration (S), used in the calculation of the fraction of growing cells (f_{gr}), as in Equation (5.1), was substituted by (1-I) where I is the inhibitor concentration. The results of the model using this correction are presented in Chapter 8.

5.2.2 Model identifiability analysis

Taking the best-performing model variant, an identifiability analysis via the orthogonalization method was applied to parameter sensitivities as described earlier. The results of identifiability analysis are indicated in Table 5.3, along with the normalized 95% confidence intervals as determined via the FIM. The identifiability scores were calculated from the model itself, while the confidence intervals incorporate the experimental observations. Consequently, the rankings of the parameters by these two measures are only approximately consistent. Not surprisingly, the growth parameters scored highest in terms of identifiability. The least identifiable parameters are k_{lys}, K_s and k_8. The first of these, k_{lys}, is difficult to determine since lysed cells are not available for observation. Parameter K_s represents the impact of nutrient S on the growth rate. As described above, the growth profile shows a complex dependence on serum level, indicating that this aspect of the culture requires further investigation. Finally, k_8 describes triggering of the intrinsic pathway by the extrinsic pathway. While the data seems unable to characterize this particular interaction, that does not impact the model's ability to predict the overall progression of apoptosis.
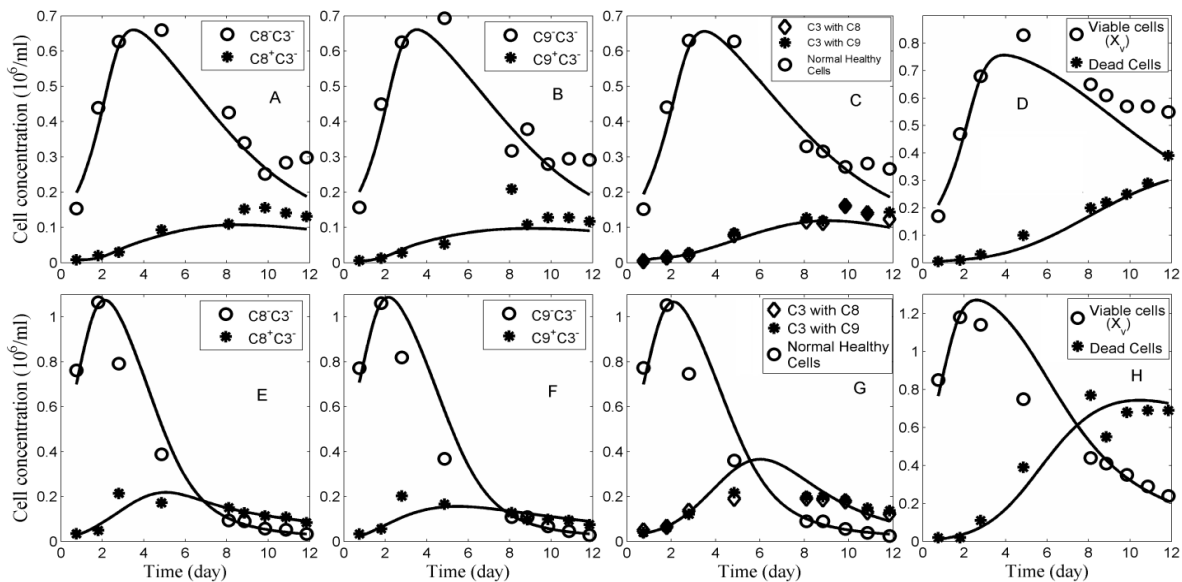
Figure 5.2: Comparison of experimental observations with simulated profiles from the best-fit model variant. A-D: SP1 and E-H: SP4. The solid curves represent the simulated profiles and the data points represent the experimental observations.
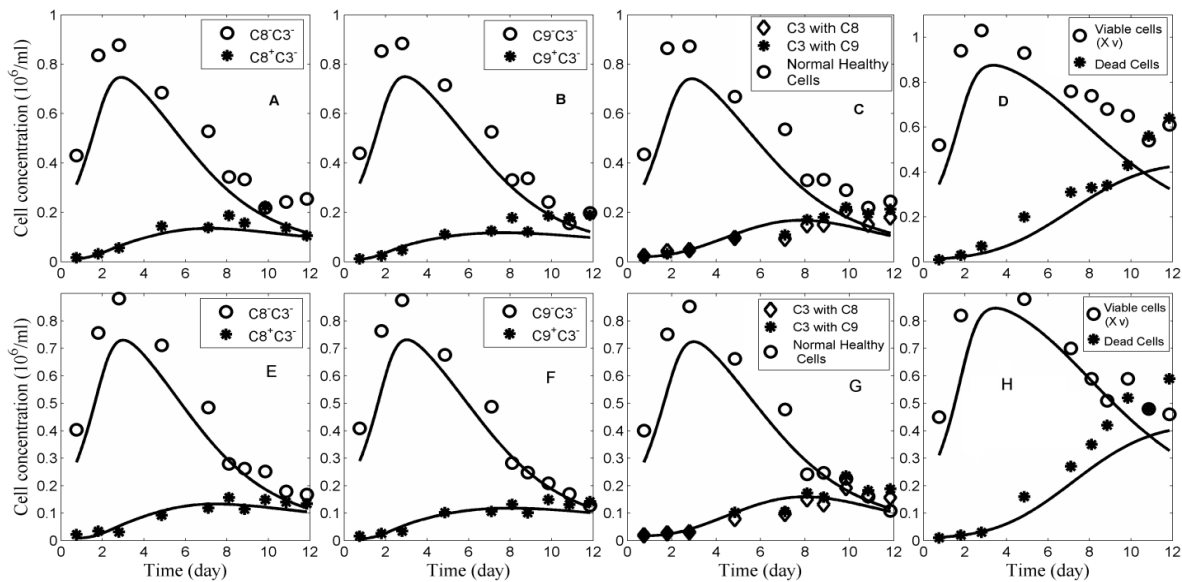
Figure 5.3: Comparison of experimental observations with simulated profiles from the best-fit model variant. A-D: SP2 and E-H: SP3. The solid curves represent the simulated profiles and the data points represent the experimental observations.
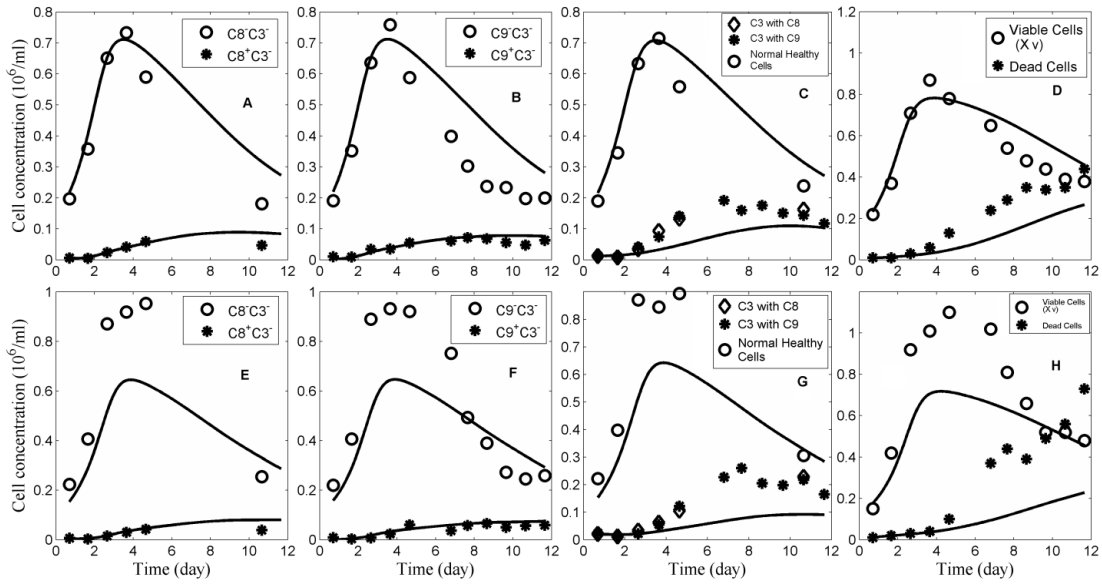
Figure 5.4: Comparison of experimental observations with simulated profiles from the best-fit model variant. A-D: SP5 and E-H: SP6. The solid curves represent the simulated profiles and the data points represent the experimental observations.
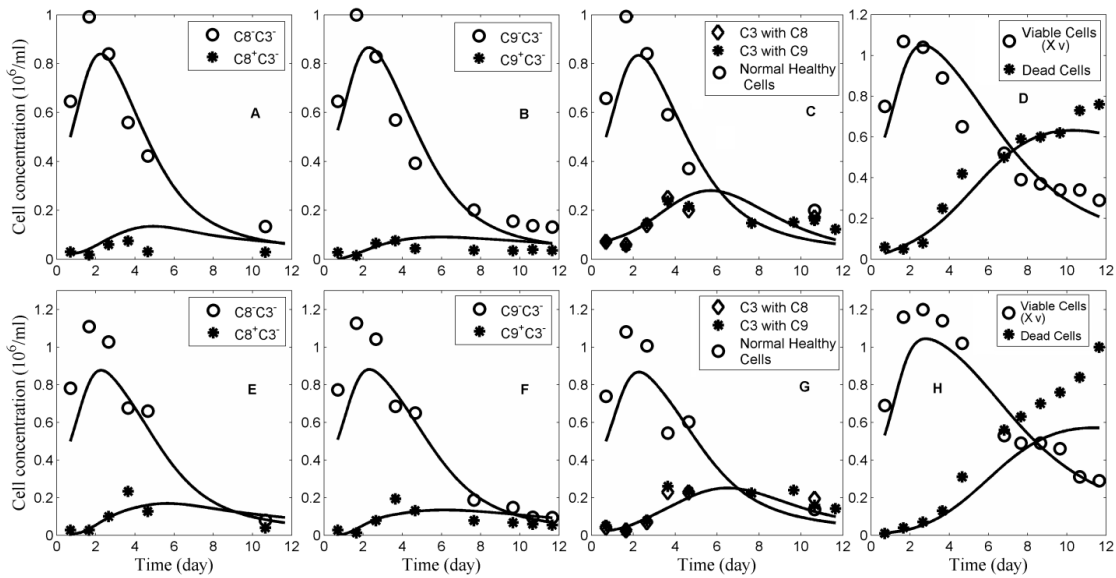
Figure 5.5: Comparison of experimental observations with simulated profiles from the best-fit model variant. A-D: SP7 and E-H: SP8. The solid curves represent the simulated profiles and the data points represent the experimental observations.

Table 5.2: SSE and AICc measure obtained for different model variants

| Intrinsic pathway | Extrinsic pathway | S present in medium | | | | S present in serum | | | |
| | | Four state model | | Five state model | | Four state model | | Five state model | |
		SSE	AICc	SSE	AICc	SSE	AICc	SSE	AICc
Nutritional stress (S)	Constant signaling	115.41 $p = 11$ $n = 424$	-529.07	161.18 $p = 14$ $n = 564$	-677.66	128.81 $p = 11$ $n = 424$	-482.52	184.15 $p = 14$ $n = 564$	-602.52
	Caspase-3 active cells signaling	104.98 $p = 12$ $n = 424$	-567.14	105.03 $p = 15$ $n = 564$	-917.12	111.13 $p = 12$ $n = 424$	-542.97	111.75 $p = 15$ $n = 564$	-882.12
	All the viable cells signaling	120.09 $p = 12$ $n = 424$	-510.10	179.95 $p = 15$ $n = 564$	-613.43	120.33 $p = 12$ $n = 424$	-509.26	158.97 $p = 15$ $n = 564$	-683.35
Toxic metabolite stress (Amm)	Constant signaling	146.13 $p = 10$ $n = 424$	-431.13	147.92 $p = 13$ $n = 564$	-728.20	143.49 $p = 10$ $n = 424$	-438.85	184.34 $p = 13$ $n = 564$	-604.05
	Caspase-3 active cells signaling	107.37 $p = 11$ $n = 424$	-559.70	87.77 $p = 14$ $n = 564$	**-1020.46**	88.84 $p = 11$ $n = 424$	-640.04	106.50 $p = 14$ $n = 564$	-911.38
	All the viable cells signaling	145.45 $p = 11$ $n = 424$	-430.99	159.75 $p = 14$ $n = 564$	-682.69	144.81 $p = 11$ $n = 424$	-432.85	143.17 $p = 14$ $n = 564$	-744.49

Table 5.3: 95% confidence interval of parameters involved in the best model variant obtained after model comparison

Parameter	Parameter Values	Sensitivity score	Identifiability score	Confidence interval
α	1.27	14.34	3085.7	0.5206
μ_g	0.69 day $^{-1}$	3.77	95.9	0.3667
μ_d	0.5 (cell/mL) $^{-1}$ day $^{-1}$	5.40	68.2	0.1737
μ_i	0.04 day $^{-1}$	2.67	52.6	0.8689
k_4	2.66 day $^{-1}$	2.1	26.7	0.8046
k_{sub}	1.17 mM $^{-1}$ (cell/mL) $^{-1}$ day $^{-1}$	3.29	12.4	0.3842
μ_e	1.53 (cell/mL) $^{-1}$ day $^{-1}$	7.14	10.8	0.5717
k_{10}	0.15 day $^{-1}$	1.33	3.6	0.6168
k_9	5.1 day $^{-1}$	0.87	1.8	4.6677
k_5	4.06 day $^{-1}$	1.56	1.1	5.4017
k_{lys}	0.1 day $^{-1}$	0.25	0.7	0.6770
K_s	0.47 mM	0.33	0.3	1.4185
k_8	0.003 day $^{-1}$	0.006	1.6×10^{-5}	118.1408

Chapter 6

Investigation of the effect of serum on growth

Serum contains essential nutrients, growth factors, hormones and vitamins which are important for cell growth. As mentioned in earlier sections (Chapter 2) depletion of one or more components of serum could be a factor that leads to apoptosis. Hence, experiments were performed to assess the effect of different levels of serum in CHO cell culture, along with different initial cell densities.

6.1   Materials and methods

All experiments were performed with regular HyClone SFX-CHO medium. Batch cultures were set up in four 500mL spinner flasks, labeled SP5-8. The experiment in SP5 was designed to start with 0.25×10^6 cells/mL of cell density supplied with 0.5% of serum and 1mM glutamine, SP6 with 0.25×10^6 cells/mL supplied with 2% of serum and 1mM glutamine; SP7 with 1×10^6 cells/mL supplied with 0.5% of serum and 4mM glutamine; SP8 with 1×10^6 cells/mL supplied with 2% of serum and 4mM glutamine. A calculated volume of seed culture according to the above mentioned initial cell densities, was centrifuged, supernatant was discarded and the settled cells were then suspended in fresh medium in respective spinner flasks and then supplemented with serum and glutamine. The measured initial cell density in the four spinner flasks turned were slightly different from the projected values (0.18×10^6, 0.15×10^6, 0.64×10^6 and 0.71×10^6 cells/mL respectively) due to experimental variability during the inoculation.

6.2   Results and discussion

Figure 6.1A shows the viable cell concentration profile in each case. As can be seen, for the higher initial cell density cultures, the cell culture quickly reached to a maximal density. For the same higher cell

84

density cultures but different serum levels (SP7 and SP8) the differences in terms of maximum cell concentration were not significant, thus indicating a negligible effect of serum concentration. For the lower serum level culture (SP7) the specific growth during the exponential phase, which was expected to be lower if there was a serum effect, turned out to be slightly higher compared to SP8, indicating no pronounced effect of serum (Table 6.1). In addition, the specific growth rate in SP8 was similar to the growth observed for SP4, described in Chapter 4, which used a higher serum level (4%) with similar initial cell density. In terms of viability, SP4, SP7 and SP8 exhibited similar values indicating no effect of serum.

On the other hand, for the lower cell density cultures (SP5 and SP6), there was an effect of serum. The maximum viable cell concentration (shown in Table 6.1) reached in SP6 (2% serum, $X_{max} = 1.24$ x 10^6 cells/mL) was higher as compared to SP5 (0.5% serum, $X_{max} = 0.87$ x 10^6 cells/mL). While comparing SP5 with SP1 (1% serum, as described in Chapter 4, $X_{max} = 0.83$ x 10^6 cells/mL), no significant difference was found in the maximum viable cell concentration reached thus indicating small effect of serum when working with low serum concentrations of less than 1%.

After comparing viability in the four different cultures (Figure 6.1B), it can be observed that viability is mostly correlated to initial cell density but is not significantly correlated to the initial levels of serum. Accordingly, the viability in SP5 is similar to SP6, and the viability in SP7 is similar SP8.

Figure 6.2-6.3 shows flow cytometry forward scatter-side scatter (FSC-SSC) plots for the lower and higher initial serum level, SP5 and SP6 respectively. As the culture proceeds, the healthy culture disassociates into a less healthy culture containing more apoptotic cells as indicated by an increase in SSC of these cells. As can be seen in these graphs between days 1 and 3 most of the culture is still healthy as observed by a single cluster corresponding to lower values of SSC. Then, in the following days, an additional cluster appears with increased SSC values as compared to the SSC values of the healthy cells thus indicating increased number of apoptotic cells. Estimation of these apoptotic group of cells (in percentage), after gating, shows that there was not much difference in the overall degree of apoptosis for two different initial serum levels.
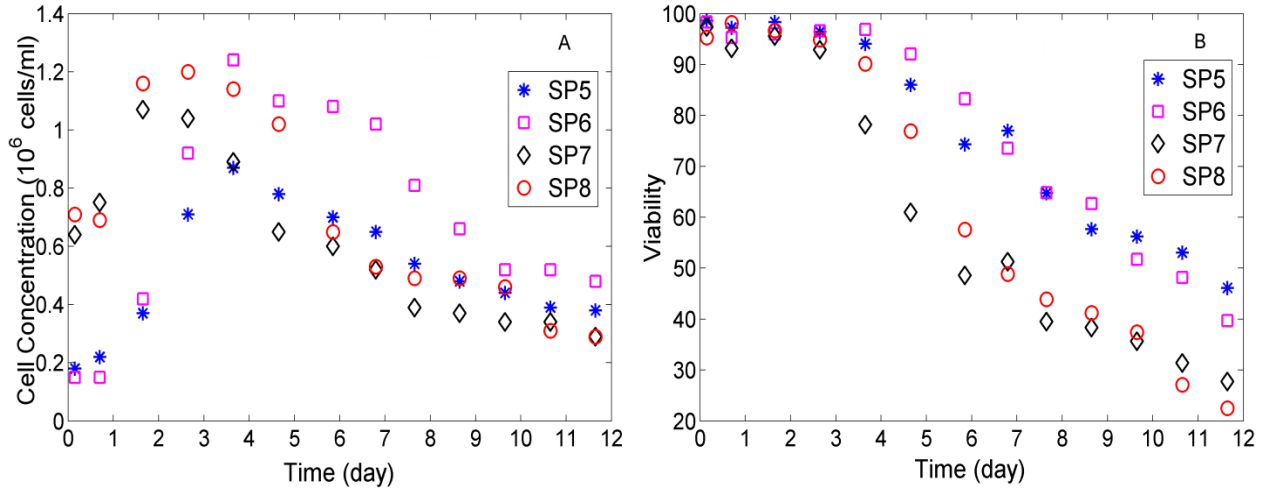
Figure 6.1: (A) Viable cell concentration (B) Viability

Table 6.1: Characteristic parameters

	SP5	SP6	SP7	SP8
Initial cell density (10^6 cells/mL)	0.18	0.15	0.64	0.71
Specific growth rate (day $^{-1}$)	0.49	0.68	0.30	0.23
X_{max} (10^6 cells/mL)	0.87	1.24	1.07	1.2
q_{Glc} (mM/10^6 cells/mL day)	1.29	0.94	1.03	0.78
q_{Lac} (mM/10^6 cells/mL day)	3.91	2.78	1.62	1.45
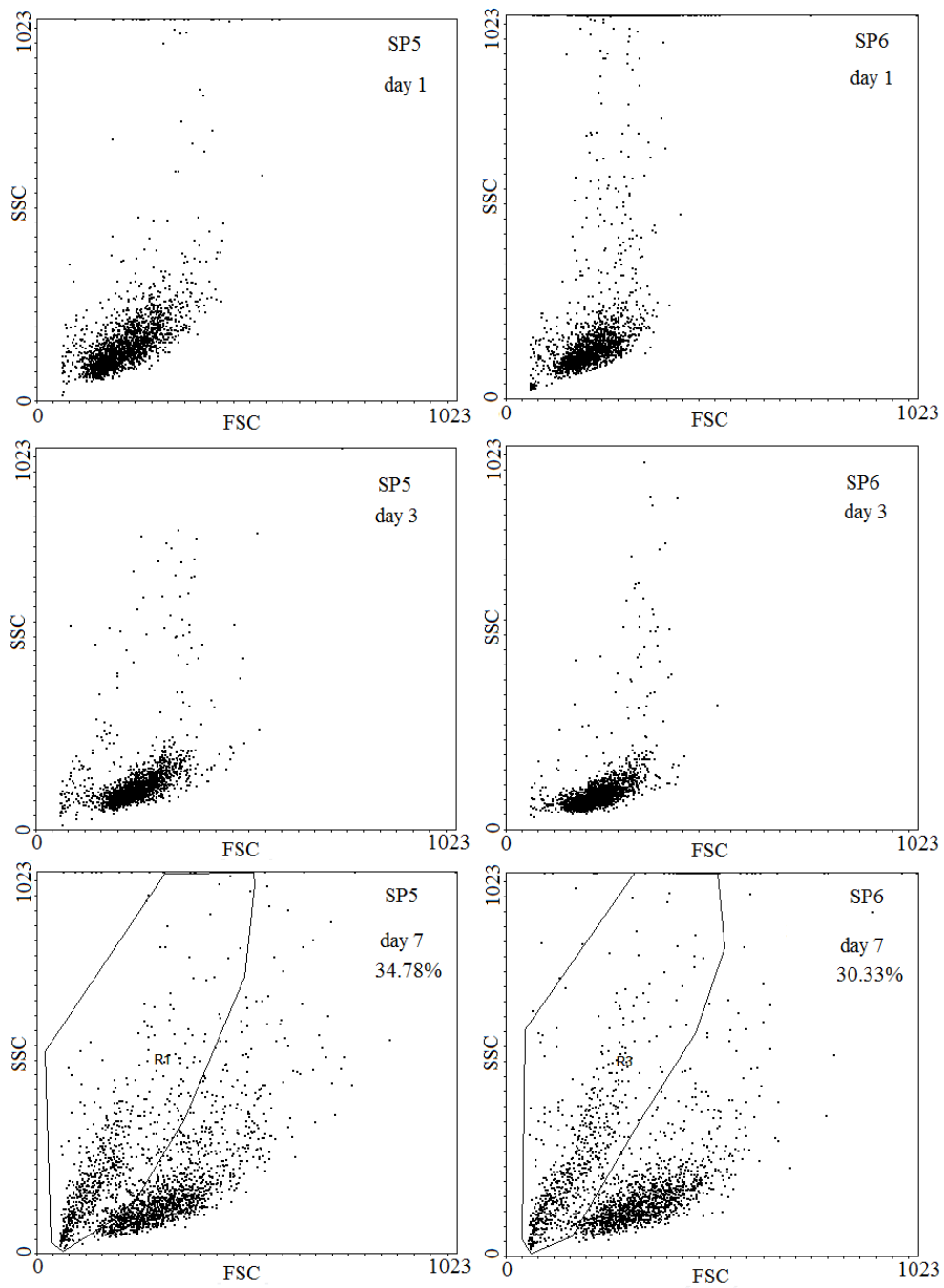
Figure 6.2: Bivariate distributions of cell samples for SSC vs. FSC in the low serum (SP5) and high serum culture (SP6)
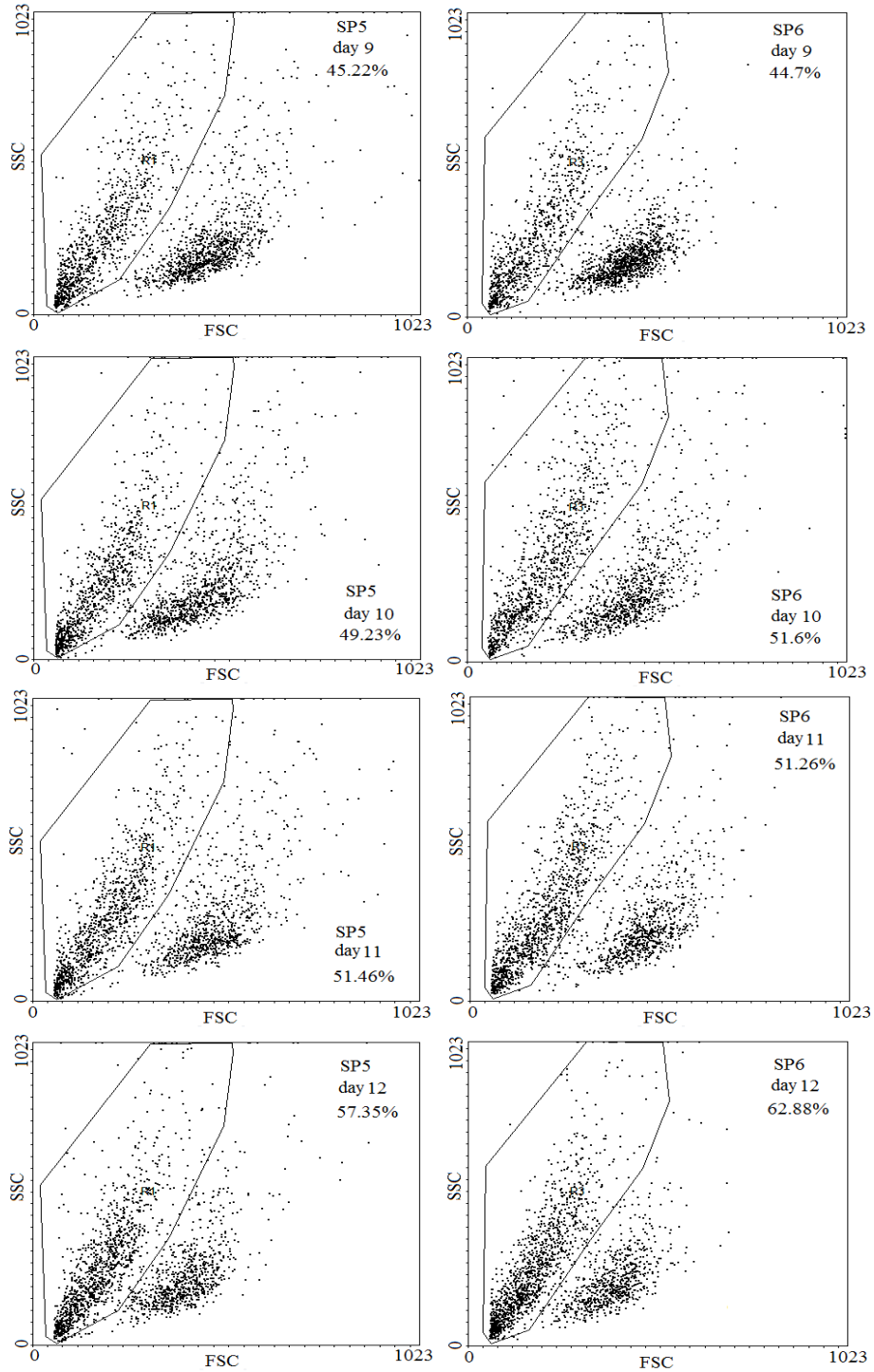
Figure 6.3: Bivariate distributions of cell samples for SSC vs. FSC in the low serum (SP5) and high serum culture (SP6)

In terms of caspase-9, as shown in Figure 6.4, the higher initial cell density cultures (SP7 and SP8) exhibited higher activation compared to the lower cell density cultures (SP5 and SP6). On the other hand the activation of caspase-9 was not significantly different among different serum levels in these higher cell density cultures (difference was approximately 5%). Considering caspase-3 activation (Figure 6.4), it was higher in the higher initial cell density cultures (SP7 and SP8) as compared to the lower cell density cultures (SP5 and SP6), but no significant difference was found among the higher initial cell density cultures in caspase-3 levels for different levels of serum. Comparing caspase-3 activation for different serum levels for the lower initial cell density cultures (SP5 and SP6), differences were observed indicating a slower activation of caspase-3 in SP6. Thus serum level affects caspase-3 activation dynamics, though the overall apoptosis level was found same by SSC-FSC plot in Figure 6.4A-B. An earlier experiment with 1% serum and low initial cell density (SP1), described in Chapter 4, was also compared with SP6 that was initiated with the same low density value but with 2 % serum. It was found from this comparison that the activation of caspase-9 and caspase-3 was similar for SP1 and SP6 thus corroborating that serum does not have a major effect on the dynamics of apoptosis for serum levels above 1% (SP6) (Figure 6.5).
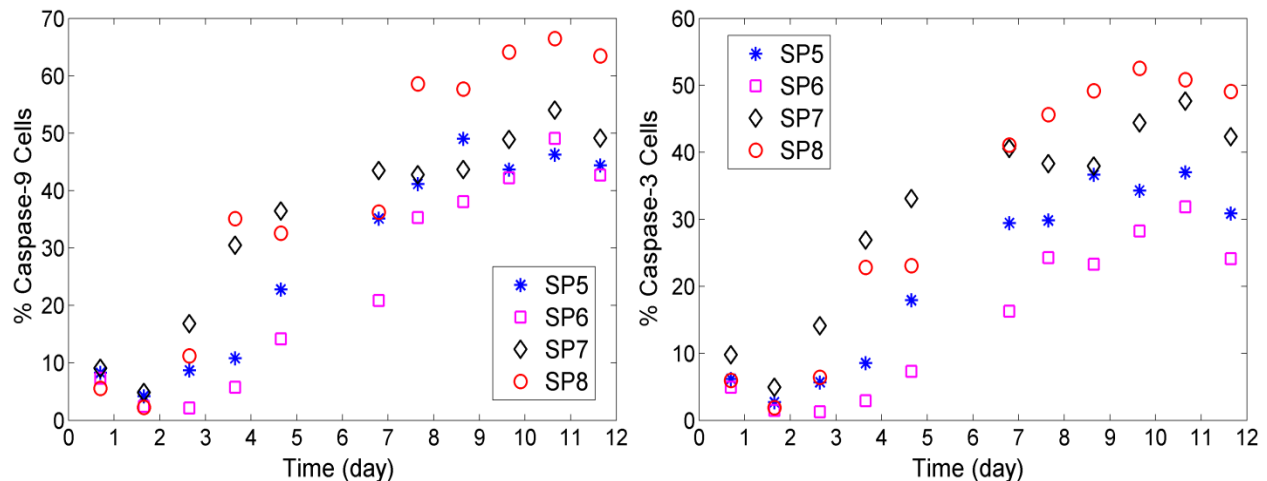
Figure 6.4: Caspase-9 and caspase-3 subpopulation progression in SP5, SP6, SP7 and SP8
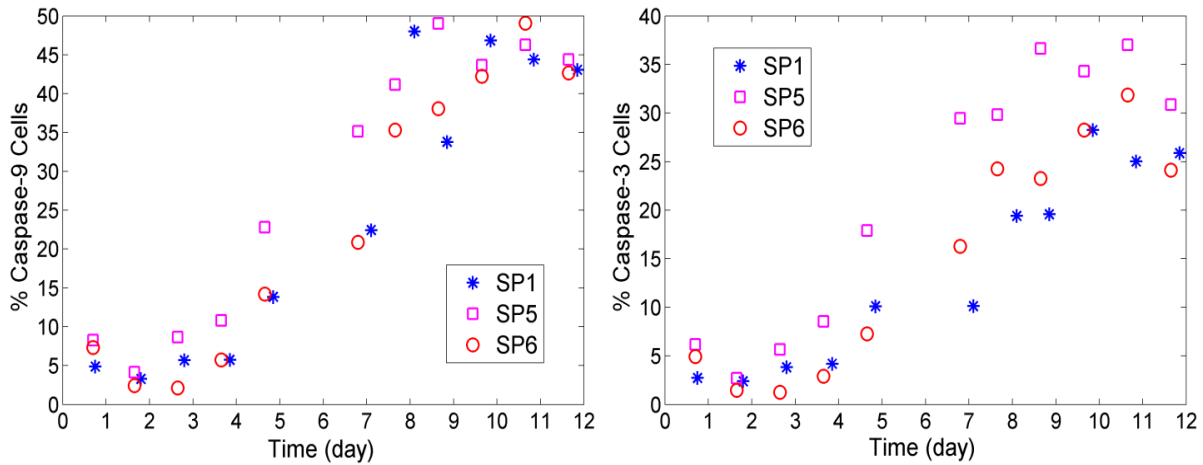
Figure 6.5: Caspase-9 and caspase-3 subpopulation progression in SP1, SP5 and SP6

Figure 6.6 shows the time course of glucose and glutamine consumption and lactate and ammonia production for the four experiments described in this chapter. While, comparing lower cell density cultures, serum level did not seem to affect specific glucose consumption rate for low serum level cultures SP5 (Table 6.1) and SP1 (Table 4.2) and was higher compared to higher serum level culture (SP6) (Table 6.1). Correspondingly, specific lactate production rates were similar for SP5 (Table 6.1) and SP1 (Table 4.2) and higher compared to the higher serum level and low cell density culture (SP6). Similar observations were made for different serum levels and higher cell density cultures SP7, SP8 (Table 6.1) and SP4 (Table 4.2).

Glutamine was depleted as the cell growth progressed. However, it was not completely depleted when the cell concentration reached its maximum for the higher cell density cultures with different serum levels (SP7 and SP8). In the lower initial cell density cultures (SP5 and SP6) with different serum levels, glutamine was almost depleted to zero because of the low initial glutamine levels used in these cultures (1mM). No difference was found in ammonia level for different levels of serum, but differences were observed for different initial cell density experiments.
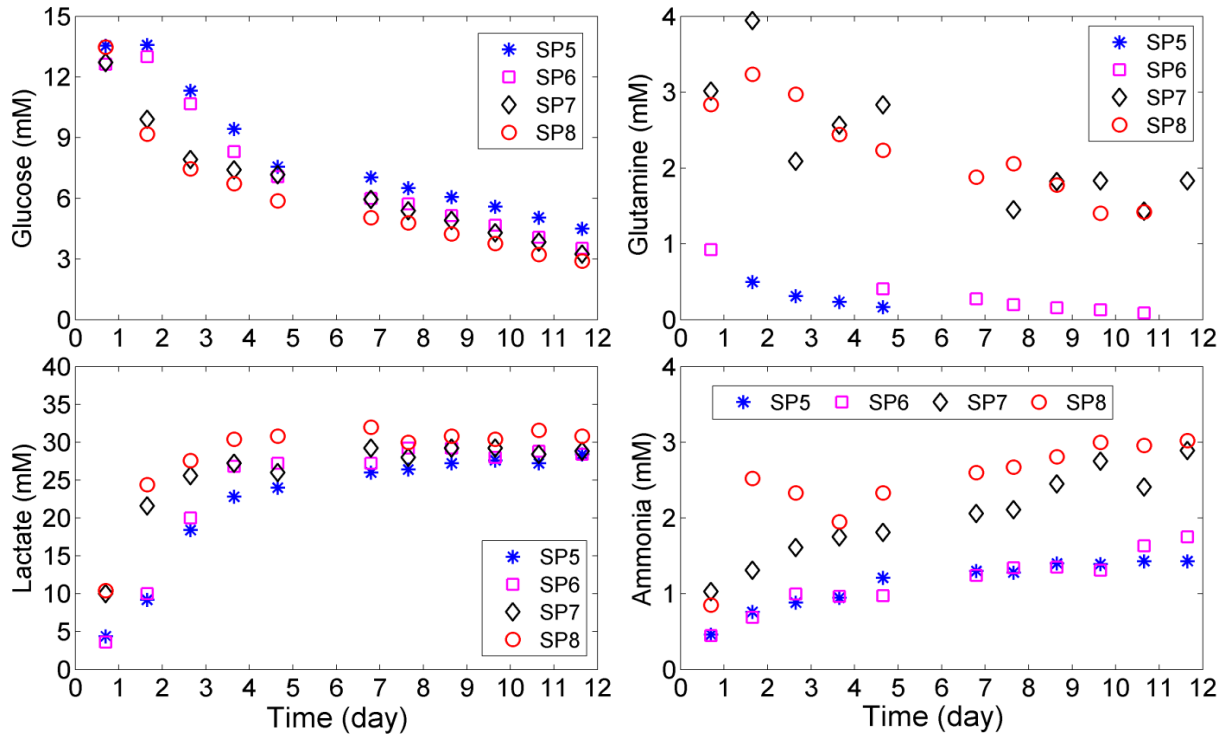
Figure 6.6: Time course of glucose, glutamine, lactate and ammonia evolution

The time evolution profile of mAb is shown in Figure 6.7. The concentration of mAb was not affected during the decline phase where mAb continued to be produced indicating that production is non-growth associated. A higher level of antibody was produced in the higher initial cell density culture.

The average specific mAb productivity rates (q_p) throughout the whole culture (calculated as shown in Appendix B) were determined for each culture. The plots of the time integral of viable cells i.e. $\int_0^t X_v \, dt$ vs. mAb concentration from which the q_p was calculated as slope are shown in Figure 6.8. A statistical test (F-test) was performed on experimental measurements of mAb concentration (Figure 6.8) to check if there was any difference in the q_p among SP5-8. With this test performed, it was found that there was no difference in the q_p among SP5-8 (Appendix C). The test results could be improved by increasing the degrees of freedom, thus increasing the number of mAb measurements. However, from the slopes

obtained by regression on these measurements (Figure 6.7), different values of q_p for SP5-8 were obtained. Based on these slopes a higher specific monoclonal antibody production rate was observed for the higher initial cell density cultures as compared to the lower initial cell density ones (Table 6.2). The antibody production rate was fairly constant throughout the culture regardless of cell density and serum level, although it was slightly higher during the decline phase corresponding to a slightly larger slope (Figure 6.8). It can be seen that for the lower initial cell density cultures the specific antibody production increased with serum level. Similar observation was found by (Dalili and Ollis, 1989) for hybridoma culture in T-flask level. However, in higher cell density cultures (SP7 and SP8), higher specific mAb productivity was found for SP7 where serum level was lower compared to SP8 (Table 6.2). Thus comparing specific mAb productivity for the similar initial cell density cultures but different serum levels, it can be observed that specific mAb productivity was higher for the culture exhibiting higher specific growth rate, regardless of serum level. Thus, according to the observation in Table 6.2, the mAb productivity appears to be positively correlated to specific growth rates but not to serum levels. Some previous investigations (Fox et al., 2004; Miller et al., 1987; Suzuki and Ollis, 1989) have reported increased specific antibody production rates with lower specific growth rates. Now this can be attributed to the type of cell line. Variability in the measurements of mAb concentration by ELISA can be observed. This variability can be due to inconsistency in standards, reagents or due to variability in handling, and analysis of data, and thus needs further improvement in the assay procedure.

Table 6.2: Specific mAb productivity in different cultures obtained from the slope of plots in Figure 6.7

	SP5	SP6	SP7	SP8
Initial cell density (10^6 cells/mL)	0.18	0.15	0.64	0.71
Specific growth rate (day $^{-1}$)	0.49	0.68	0.30	0.23
q_p (mM/10^6 cells/mL day)	3.45	4.1	5.8	4.35
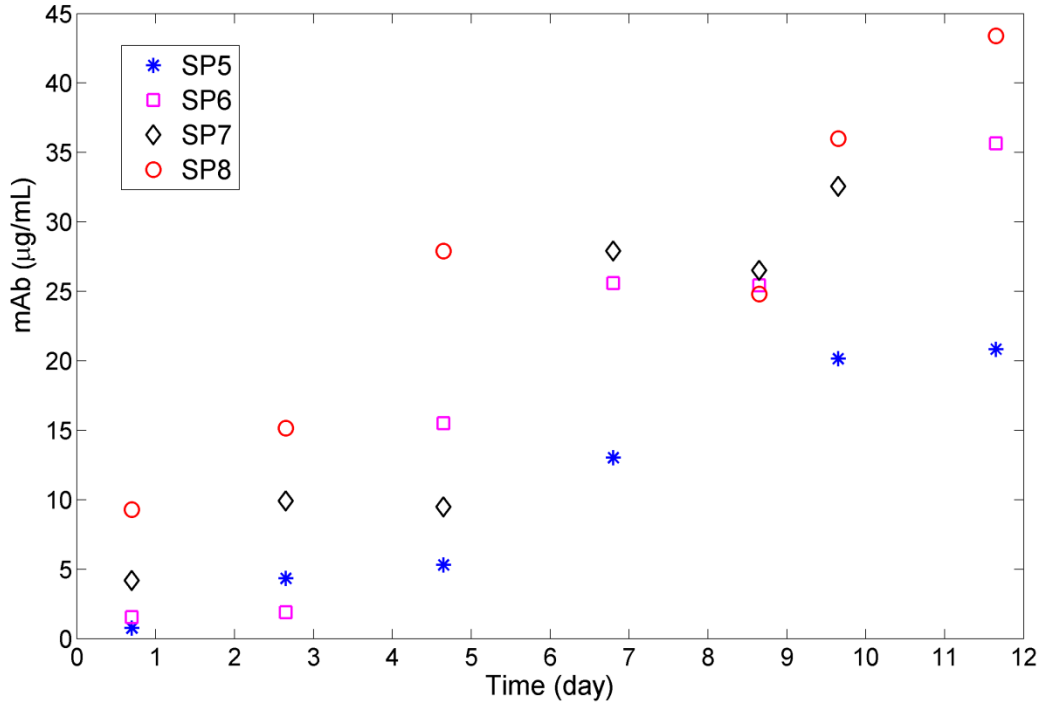
Figure 6.7: mAb concentration profiles in different serum level cultures
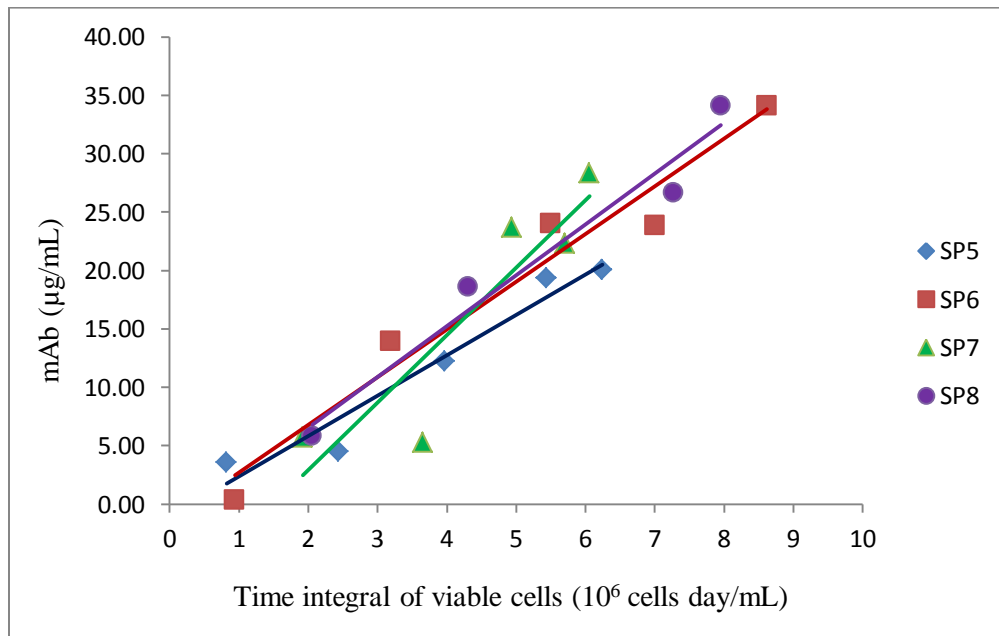
Figure 6.8: Specific mAb productivity in different serum level cultures

Chapter 7

Investigation of culture volume effect

7.1   Introduction

Chapter 6 described a series of experiments that were conducted with different serum levels and with different initial cell density cultures to elucidate whether growth arrest is caused by a limiting nutrient contained in serum. Since it was found from these experiments that growth arrest is not significantly affected by serum level, especially when this level is more than 1%, it was concluded that the limiting substrate is not in serum. Also, additional fed-batch experiments were conducted in a parallel study by Naderi, (2011) where medium was fed intermittently to the culture in order to test whether the limiting nutrient was contained in medium. Naderi found, even after feeding significant amounts of medium during the course of the experiments, no substantial improvements in terms of cell growth, maximum viable cell concentration, viability and mAb productivity. The possibility of toxicity effects due to lactate or ammonia accumulation was also ruled out as a cause for growth arrest since their concentrations were well below inhibitory levels at the moment of growth stoppage. Inhibitory levels were only reached towards the end of the experiments ($\sim$ 12-15 days).

Consequently, it was hypothesized that other factors like oxygen limitation or accumulation of toxic metabolite like CO_2 could be the cause of growth arrest and triggering of apoptosis during the early stages of the cultures ($\sim$3-4 days). It was hypothesized that CO_2 accumulation may occur due to slower release of CO_2 from the spinner into the atmosphere due to low surface area to culture volume ratio. To test this hypothesis experiments were conducted in spinners of different volumes and differences in growth and mAb productivity were investigated.

7.2   Materials and methods

Experimental design

Experiment was carried out with regular SFX-CHO medium supplemented with 1mM glutamine and 1% serum in 500 mL capacity spinner flasks. Four batch cultures were set up labeled SP9-12 with different working volumes: 150 mL, 250 mL, 375 mL and 500 mL respectively. All the spinners were inoculated with a common seed culture. The spinners were seeded without a previous centrifugation step as done in the earlier experiments described in Chapter 4 and 6. The same initial cell density of 0.25×10^6 cells/mL was used in all the different volume cultures.

Regular sampling was performed to monitor viable and dead cell concentration, pH, dissolved oxygen, glucose, lactate and ammonia.

7.3   Results and discussion

The progression of viable cell concentration with time in the different volumes is shown in Figure 7.1. As can be seen, the maximum viable cell concentration reached during the experiments was highest in the lower volume culture as compared to the other cultures. This figure clearly indicates that there is an inverse correlation between the cell density maxima and the volume of the culture. The viable cell concentration profile in 125 mL culture is somewhat similar to the profile obtained in the 250 mL culture. It appears that this similarity is due to the fact that in the 125 mL culture there was not enough room to fully accommodate the agitator within the broth and consequently, it remained partially outside the broth. This situation became more pronounced along the culture due to the loss of liquid following frequent sampling for analysis purposes. For this reason, the data collected for the 125 mL culture was not used in the following comparisons.

The maximum cell concentration reached in these experiments was approximately 1.6×10^6 cells/mL in the 250 mL, which was the lowest volume left after discarding the 125 mL experimental data for the reasons explained above. The dead cell concentration progression was similar in all volume cultures (within a 5% difference). Regarding the specific growth rates, calculated as the average specific growth rate during the exponential phase, the highest value was obtained in the lower volume experiment (250 mL, SP10); it was found to be 0.52 day^{-1} (Table 7.1), while the growth rates in the higher volume cultures, 375 mL and 500 mL, were smaller and similar to each other.
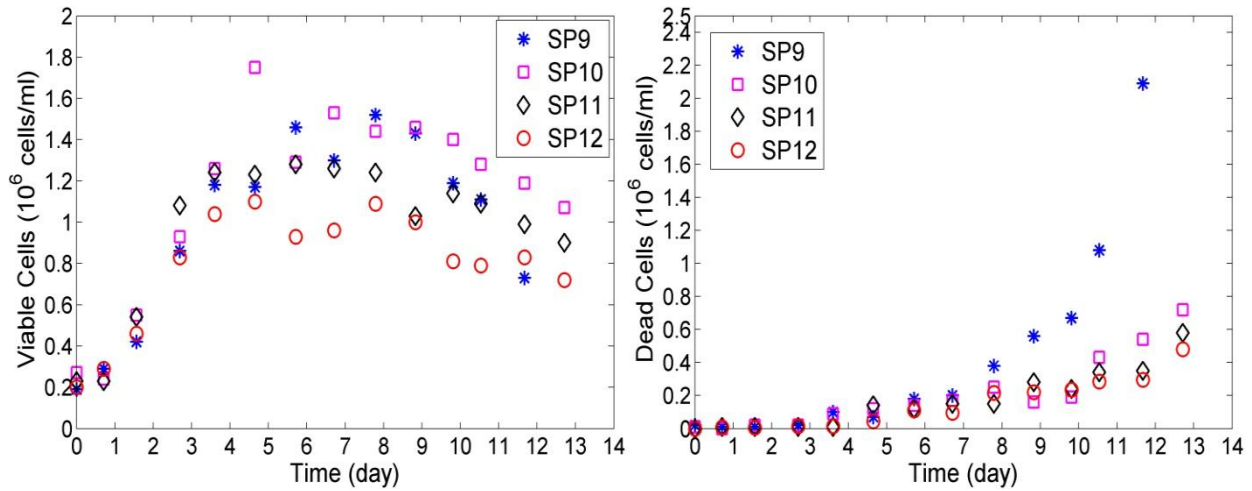
Figure 7.1: Viable and cell concentration profile in different volume culture

In order to assess the causes for growth arrest, pH was measured along the experiment. As can be seen from the pH profile (Figure 7.2), the drop in pH in the 500 mL culture was significantly more pronounced than in the 250 mL and 325 mL cultures. In the 500 mL experiment the pH dropped to a range of ~6.3-6.4 which has been reported to be inhibitory to cell growth (Link et al., 2004; Yoon et al., 2005). The steepest drop in pH occurred around the time when the cell concentrations reached their maximal values, thus suggesting an inhibitory effect of pH on cell growth, possibly due to CO_2 accumulation. Though the levels of CO_2 in the culture were not measured, it can be suggested that the slow removal of CO_2 due to mass transfer limitations and low driving force between the broth and the environment could lead to accumulation of CO_2 to inhibitory levels (Pattison et al., 2000). Thus, the lower cell density in the 500 mL culture, compared to the density observed in the 250 mL spinner, can be attributed to poorer CO_2 removal in the culture due to increased volume to mass transfer area ratio.

As stated above the possibility that either ammonia or lactate were inhibitory was also ruled out in the current experiments as the ammonia and lactate levels, shown in Figure 7.2, were similar in all the different volume cultures and was below the inhibitory levels reported in the literature (Figure 7.2). To confirm that growth arrest was not related to oxygen depletion, dissolved oxygen was measured during the experiments. The dissolved oxygen in all the cultures ranged between 40-80% (Figure 7.3), which is

96

sufficient for the cell growth and not in the limiting range that can lead to conditions of hypoxia (Ozturk and Palsson, 1990b; Shu and Liao, 2002; Trummer et al., 2006).

Figure 7.4A shows the time evolution of mAb concentration in each different volume. For the 250 mL culture, the final mAb concentration obtained was higher (46 µg/mL) than the higher volume cultures (500 mL and 375 mL), although there was no pronounced difference found in the specific mAb productivity between the different volumes (Table 7.1). The specific mAb productivity was determined from the slope of the mAb concentration and time integral of viable cells (Figure 7.4B) according to the calculations shown in Appendix B.

Table 7.1: Specific growth rates in different volume culture

	SP10	SP11	SP12
Culture volume (mL)	250	375	500
Specific growth rate (day $^{-1}$)	0.52	0.37	0.38
X_{max} (10^6 cells/mL)	1.75	1.28	1.10
q_p (mM/10^6 cells/mL day)	2.77	2.74	2.97
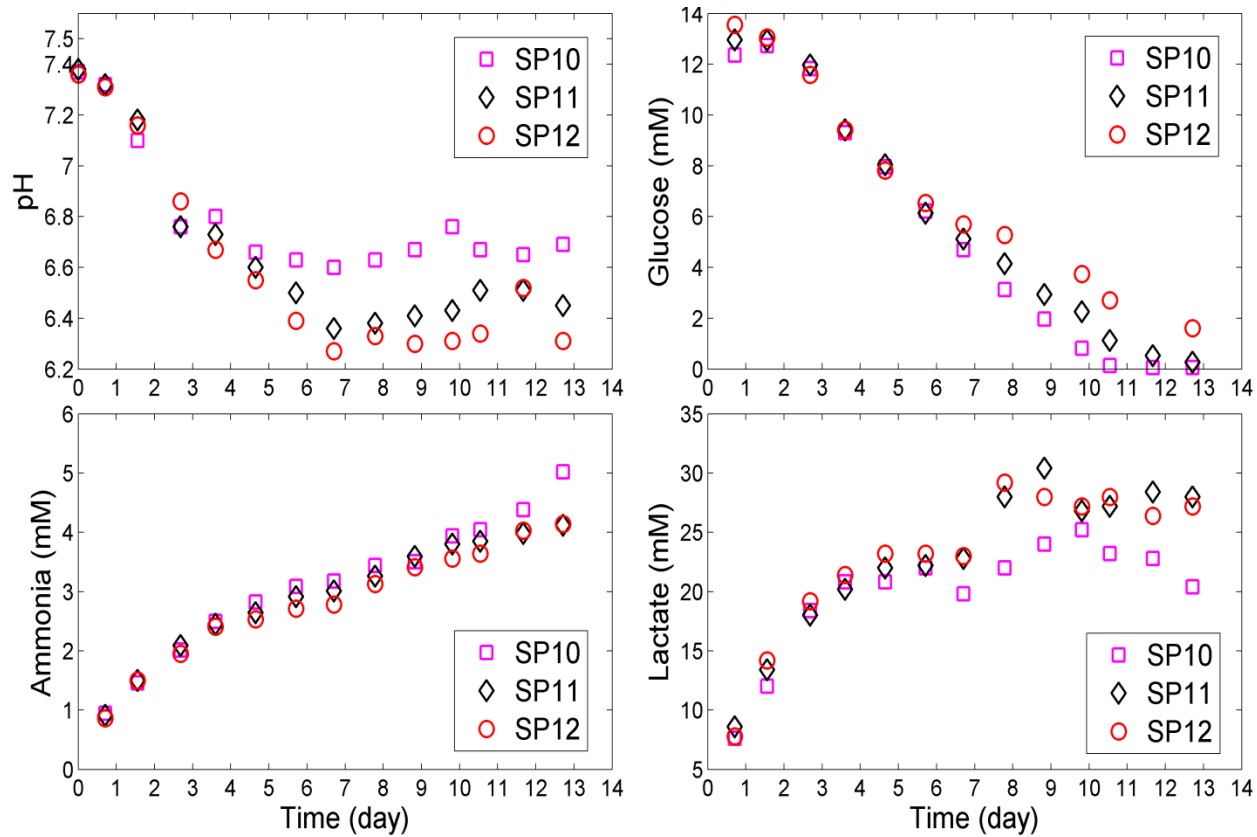
Figure 7.2: pH, glucose, ammonia and lactate concentration profile in different volume culture
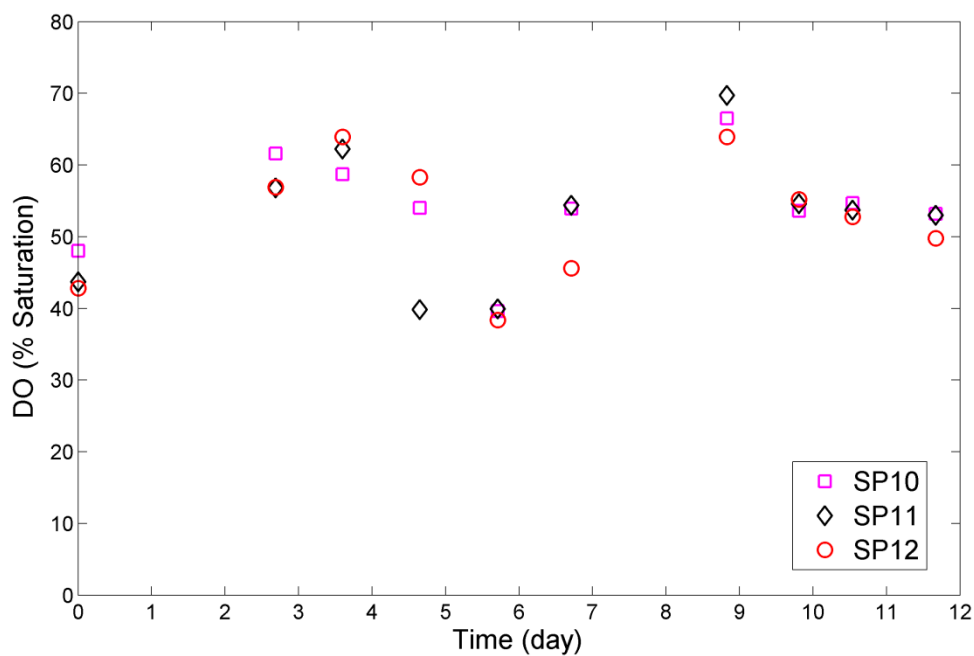
Figure 7.3: Time course of dissolved oxygen concentration in different volume culture

98
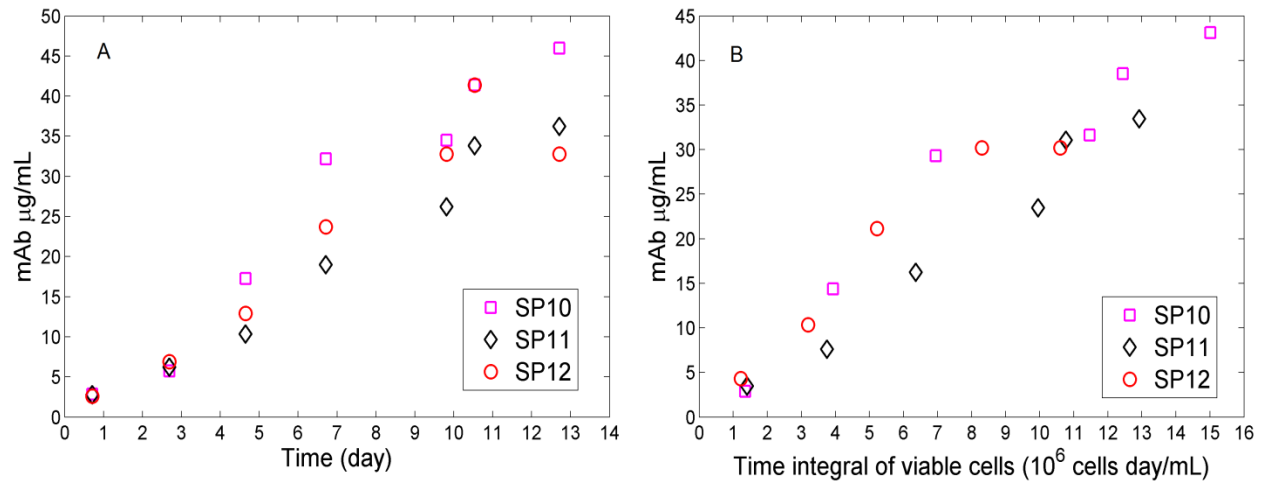
Figure 7.4: (A) Time course of mAb concentration (B) mAb concentration as a function of time integral of viable cells

Chapter 8

Integration of apoptosis and metabolic flux models to predict mAb production

8.1 Introduction

A key objective of the current research was to develop a comprehensive model of mAb production that will be used ultimately for optimizing culture conditions to maximize productivity. With this objective in mind it was necessary to integrate the population-based model of apoptotic progression (Chapter 5) with a model of extracellular metabolite concentration, since it will be the latter that can be manipulated for the purpose of optimization. This integrated model can provide a better understanding of cell behavior and help in devising strategies for delaying its onset. Since it was found in earlier phases of this work that mAb is non-growth associated, a model of both normal healthy and apoptotic cells is required to predict the mAb profile. Then, mAb productivity of the individual subpopulations in the apoptosis model was described separately. This chapter describes the integration of the metabolic flux model of extracellular metabolites with the population based model of apoptosis previously described in Chapter 5. Since it was found in Chapter 7, by experimenting with different culture volumes, that growth arrest is correlated to the accumulation of an inhibitory compound, the apoptosis model of Chapter 5 was slightly changed to incorporate this effect.

8.2   Materials and methods

The models to be integrated are described as follows

8.2.1 Metabolic flux model

During the early stage of culture, when cells are in an exponential growth phase, the majority of the cell population is composed of normal growing/dividing cells, although there are always a low number of apoptotic cells. At approximately day 3-4 growth arrest occurs resulting in normal growing cells shifting to a non-growing state (possibly due to G0 cell cycle phase arrest or G1 phase arrest at the G1/S checkpoint). On the other hand the sub-population of apoptotic cells continues to increase and reaches a maximum 3-4 days after the total cell density peaks, i.e. 6-7 days after the start of the culture. At the same time the apoptotic cell pool is slowly replaced by dead cells.

Recalling apoptosis population balance model developed in Chapter 5, the viable subpopulation was presented as

$$X_v = x_1 + x_2 + x_3 + x_4 + x_5$$

The subpopulation x_4 denotes caspase-3 active cells corresponding the late apoptosis phase, where cells exhibit blebbing onto the membrane surface and then disintegrate into apoptotic bodies. Due to the significant differences between these cells and the rest of the population, x_4 cells were considered as the true apoptotic cell subpopulation.

The metabolic flux model presented below (Figure 8.1) was developed by another PhD candidate (Naderi, 2011). The method is based on conducting a metabolic flux balance in which, following the calculation of fluxes, the reactions corresponding to the insignificant fluxes are eliminated from the network to simplify the model. Then, after assuming that there is no accumulation of intermediate metabolites, these intermediates are eliminated by combining reactions and obtaining a set of macro-reactions that relate nutrients to products as follows

$$Glc \rightarrow 2Lac \tag{8.1}$$
$$Glc \rightarrow 6CO_2 \tag{8.2}$$
$$Glu \rightarrow Lac + 2CO_2 + Amm \tag{8.3}$$
$$Asn \rightarrow Asp + Amm \tag{8.4}$$

$$Gln \rightarrow 2Amm + 5CO_2 \tag{8.5}$$

$$Ala \rightarrow 2Amm + 3CO_2 \tag{8.6}$$

$$Gln + 0.5Glc \rightarrow Glu + Ala \tag{8.7}$$

$$Asp \rightarrow Amm + 4CO_2 \tag{8.8}$$
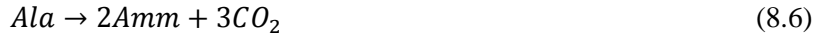
where Glc : Glucose, Lac : Lactate, Glu : Glutamate, Amm : Ammonia, Asn : Asparagine, Asp : Aspartate, Ala : Alanine

The reaction rates associated to these macro-reactions are formulated using Michaelis-Menten kinetics as per the following expression:

$$r_i(t) = a_{ig} \left[\prod_{i=1}^{n} \frac{m_i}{m_i + k_i} \right] X_g + a_{ing} \left[\prod_{i=1}^{n} \frac{m_i}{m_i + k_i} \right] X_{ng} \tag{8.9}$$

where $r_i(t)$ is the reaction rate for i^{th} reaction; m_i and k_i are the corresponding nutrient/metabolite concentration and half-saturation constant, respectively, X_g and X_{ng} are the viable growing and viable non-growing cell concentrations. As shown, the model provides two distinct terms for each metabolic rate: a "growth associated" term corresponding to growing cells (X_g) and a "non-growth associated" or maintenance term attributed to the population of non-growing cells (X_{ng}), which contains normal resting and apoptotic cells (x_4). To model the metabolite dynamics, it was assumed that growing cells, (X_g) and non-growing cells (X_{ng}), both normal and apoptotic, may metabolize nutrients at different rates. Thus a_{ig} and a_{ing} are the maximum rate at which the reaction can proceed.

Because of the higher substrate concentration in the exponential phase during which the majority of cells are growing, the nonlinear term associated to growth becomes close to unity, so Equation (8.9) was simplified to:

$$r_i(t) = a_{ig} X_g + a_{ing} \left[\prod_{i=1}^{n} \frac{m_i}{m_i + k_i} \right] X_{ng} \tag{8.10}$$
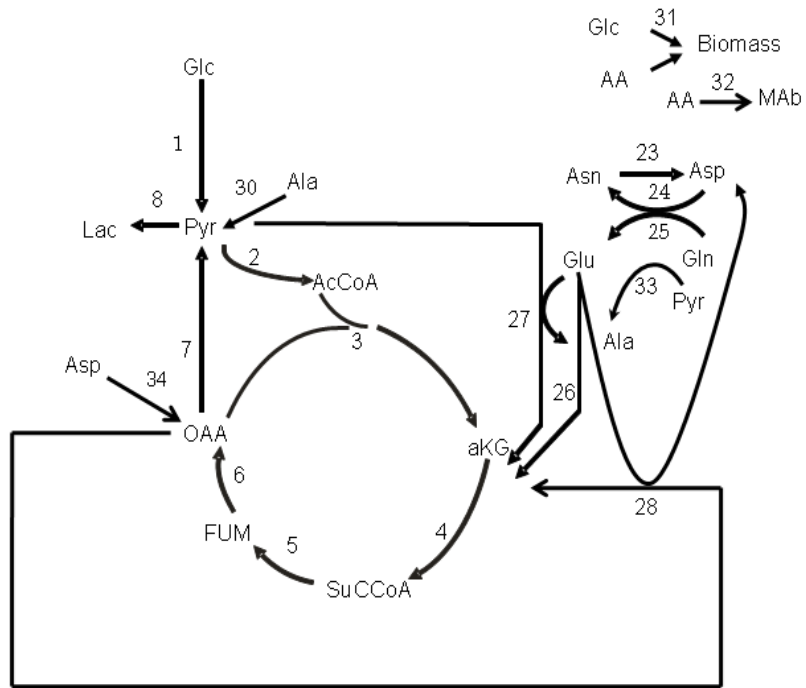
Figure 8.1: The metabolic network for the current CHO cell culture developed by Naderi, (2011)

As defined the Chapter 5, the term f_{gr} represents the fraction of dividing cells and defines the population of growing cells (X_g). Thus the term X_g was represented as

$$X_g = f_{gr}(X_v - x_4) \tag{8.11}$$

And the population of non-growing cells (X_{ng}) was represented as

$$X_{ng} = X_v - X_g \tag{8.12}$$

The metabolic model to be coupled with the apoptosis population balance model described in Chapter 5 is shown as follows

$$\frac{dGlc}{dt} = -a_{11}X_g - \left[\frac{a_1\,Glc}{k_{Glc}+Glc} + 0.5\frac{a_7\,Glc.Gln}{(k_{Glc}+Glc).(k_{Gln}+Gln)}\right]X_{ng} \tag{8.13}$$

$$\frac{dLac}{dt} = a_{22}X_g + \left[2.\frac{a_2\,Glc}{k_{Glc}+Glc} + \frac{a_3\,Glu}{k_{Glu}+Glu}\right]X_{ng} \tag{8.14}$$

$$\frac{dGln}{dt} = -a_{33}X_g - \left[\frac{a_5\,Gln}{k_{Gln5}+Gln} + \frac{a_7\,Glc.Gln}{(k_{Glc}+Glc).(k_{Gln}+Gln)}\right]X_{ng} \tag{8.15}$$

$$\frac{dGlu}{dt} = a_{44}X_g + \left[-\frac{a_3\,Glu}{k_{Glu}+Glu} + \frac{a_7\,Glc.Gln}{(k_{Glc}+Glc).(k_{Gln}+Gln)}\right]X_{ng} \tag{8.16}$$

$$\frac{dAsn}{dt} = -a_{55}X_g - \frac{a_4\,Asn}{k_{Asn}+Asn}\,X_{ng} \tag{8.17}$$

$$\frac{dAsp}{dt} = a_{66}X_g + \left[\frac{a_4\,Asn}{k_{Asn}+Asn} - \frac{a_8\,Asp}{k_{Asp}+Asp}\right]X_{ng} \tag{8.18}$$

$$\frac{dAla}{dt} = a_{77}X_g + \left[-\frac{a_6\,Ala}{k_{Ala}+Ala} + \frac{a_7\,Glc.Gln}{(k_{Glc}+Glc).(k_{Gln}+Gln)}\right]X_{ng} \tag{8.19}$$

$$\frac{dAmm}{dt} = a_{88}X_g + \left[\frac{a_3\,Glu}{k_{Glu}+Glu} + \frac{a_4\,Asn}{k_{Asn}+Asn} + 2\frac{a_5\,Gln}{k_{Gln5}+Gln} + \frac{a_6\,Ala}{k_{Ala}+Ala} + \frac{a_8\,Asp}{k_{Asp}+Asp}\right]X_{ng} \tag{8.20}$$

8.2.2 Apoptosis model of Chapter 5 modified to account for inhibitor accumulation

Based on the findings of Chapter 7 and as explained in the introduction of this chapter, growth arrest was found to be mostly correlated to inhibition possibly caused by carbon dioxide accumulation. Although carbon dioxide concentrations could not be measured, the model presented in Chapter 5 was modified to account for this inhibitory effect. It should be recalled that the model in Chapter 5 related the fraction of growing cells to the depletion of an unknown nutrient S. Since the experimental investigations with different serum levels and media addition did not confirm such depletion, an inhibition by a volume-dependent compound with concentration (I) was assumed instead. As illustrated previously in Chapter 7, this inhibitory agent could be attributed to the buildup of CO_2 during culture operation. It was thought that in order to improve productivity, this inhibitory effect could possibly be reduced by operating the culture in perfusion mode after the maximum cell concentration is reached, so that the CO_2 concentration is brought back below its inhibitory level following perfusion. Attempts were made toward this direction (Naderi, 2011). Accordingly, partial successive medium-replacement was performed after the maximum

cell concentration was reached, and fresh medium supplemented with serum and glutamine was fed to replace the volume that was removed. It was observed that the cell growth was renewed but it could not attain the same levels as before. Moreover, after each medium-replacement, the cell concentration maximum reached a lower level than the previous cell concentration maximum, and the maxima consistently decreased in all successive medium-replacement. This consistent decline in cell maxima observed by Naderi, (2011) seems to indicate an irreversible damage to the cells each time the cells are exposed to inhibitory effects of either pH or carbon dioxide. To model this inhibitory and irreversible effect on cell growth, the fraction of growing cells f_{gr} as represented in Equation (5.1) was modified by replacing the effect of unknown limiting nutrient (S), as follows

$$f_{gr} = 1 - e^{\frac{I-1}{k_I}} - k_a \int_0^t I dt \tag{8.21}$$

where I represents the inhibition factor concentration in the culture while k_I and k_a are the inhibitory and accumulation constants respectively. The integration term accounts for the accumulation effect of CO_2 causing irreversible cell damage and resulting in progressive reduction in the ability to grow following exposures to inhibitory levels of I. The net rate of production of I was expressed as follows

$$\frac{dI}{dt} = k_{i1}f_{gr}(X_v - x_4) + k_{i2}(1 - f_{gr})(X_v - x_4) + k_{i3}x_4 - k_{va}(I - I_\infty) \tag{8.22}$$

where k_{i1}, k_{i2} and k_{i3} are the specific CO_2 production rate by three subpopulations viz., normal growing, normal non-growing and apoptotic cells. The last term refers to the release of dissolved CO_2 of the culture to the environment. I_∞ would correspond to the CO_2 concentration in equilibrium with gas phase in headspace and k_{va} is a mass transfer coefficient that depends on the surface area of the culture with the environment and agitation rate.

The dependence of ammonia on specific death rate (μ_d) of caspase-3 active cells which not included in the earlier apoptosis model in Chapter 5, was included in the integrated model as follows

$$\mu_d = \frac{\mu_{dmax}}{1 + \left(\frac{K_{d_A}}{Amm}\right)^\gamma} \tag{8.23}$$

where μ_{dmax} is the maximum specific death rate, K_{d_A} is the constant for death by ammonia and γ is the nonlinearity dependence.

A mAb productivity model was also formulated. Initially it was assumed, for simplicity, that the dynamic model for mAb could be described by lumping the production rates of growing, resting and apoptotic cell populations, given by

$$\frac{dP}{dt} = q_p X_v \tag{8.24}$$

where P refers to mAb concentration and q_p is the specific production rate for both growing and non-growing cells. This relation was based on the assumption that the productivity of normal and apoptotic cells is equal. However, in later stages of the research, this assumption was further tested by assuming different productivity rates of normal and apoptotic cells.

A combined model coupling the extracellular metabolites balances (Equations 8.13-8.20), the apoptosis model described in Chapter 5 with the modification for f_{gr} (Equation 8.21) and the mAb productivity model (Equation 8.24) with incorporation of balance equation of inhibitory component (Equation 8.22) was formulated and calibrated with experiments. A schematic of the integrated model is shown in Figure 8.2. Initial guesses for parameter estimation were obtained by a genetic algorithm. In view of the nonlinearity of the resulting optimization problem, various initial guesses of parameters were provided for the minimization of the objective function (SSE). In each case, the final set of parameters obtained via the genetic algorithm was refined by subsequent application of a constrained nonlinear optimization function (MATLAB routine: *fmincon*). The integral in Equation (8.21) was evaluated by a trapezoidal rule while simulating the model. The model was implemented in MATLAB (Mathworks, USA) and the differential equations were integrated with the function *ode23s*. The parameters of the model were calculated with the *fmincon* optimization algorithm in MATLAB by minimizing the sum of square errors between model predictions and experimental data. The experiments described in Chapter 4, SP1 (lowest initial cell density culture) and SP4 (highest initial cell density culture), were used for fitting these parameters and the model was then validated with data from SP2-3 and SP5-8. The parameters associated with this integrated model obtained after minimizing objective function are shown in Appendix D.
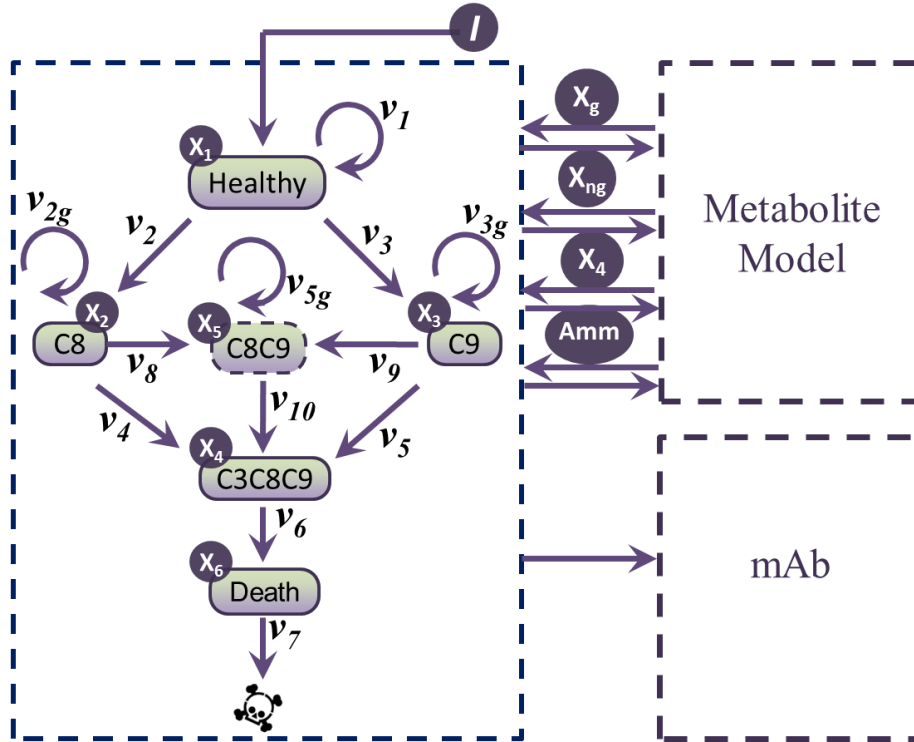
Figure 8.2: Combined model of apoptosis, metabolite and monoclonal antibody production for current CHO cell culture study. 'I' represents the inhibitory factor.

8.3 Results and discussion

The combined model, as shown in the Figure 8.2, involves interactions by which the two models, the apoptosis and metabolic flux model, were connected. These connections were established with X_g, X_{ng}, x_4 and Amm. The connections with X_g, and X_{ng} describes the metabolic flux model (Equations 8.13 - 8.20). The connection with x_4 comes from the Equation (8.11) and the connection with Amm comes from Equation (5.12). The effect of an unknown inhibitor as described by the balance Equation (8.22) is

incorporated in the f_{gr} term (Equation 8.21) which, in further, is incorporated in the apoptosis model in the growth rates of subpopulations x_1, x_2, x_3 and x_5 (Equations 5.2 - 5.5).

The fitting of the model with data from SP1 and SP4 is shown in Figure 8.3 for the different cell subpopulations. Figure 8.4 and Figure 8.5 show fitting of extracellular metabolites in SP1 and SP4 respectively. Model predictions for SP2-3 and SP5-8 are shown in Figure 8.6-14.

It was found that the comprehensive model is able to reasonably predict the concentrations of various subpopulations, nutrients, metabolites and mAb.

Model identifiability analysis was also performed on this integrated model to assess the confidence on parameter estimates. The steps described in Chapter 5 were followed. The ranking of identifiable parameters was pretty consistent with that found with the single apoptosis model developed in isolation as presented in Chapter 5. It was found in the integrated model that the parameter k_a associated with integration term to be highly identifiable followed by the parameter α associated with cell density dependence. The parameters q_p, a_1, a_4 and a_{11} were also found highly identifiable, while the least identifiable parameters were K_{d_A}, k_{i2}, I_∞, a_6, a_{55}, k_8, k_{i3}. The identifiability ranking of parameters corresponding to their identifiability scores is shown in Appendix E.
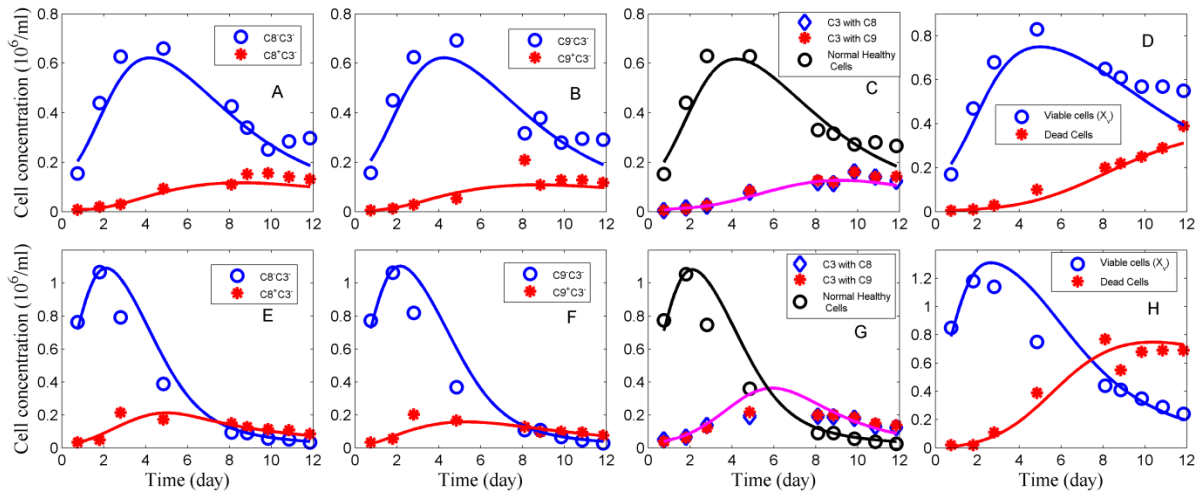
Figure 8.3: Comparison of experimental observations with simulated profiles of cell subpopulations. A-D: SP1 and E-H: SP4. The solid curves represent the simulated profiles and the data points represent the experimental observations.
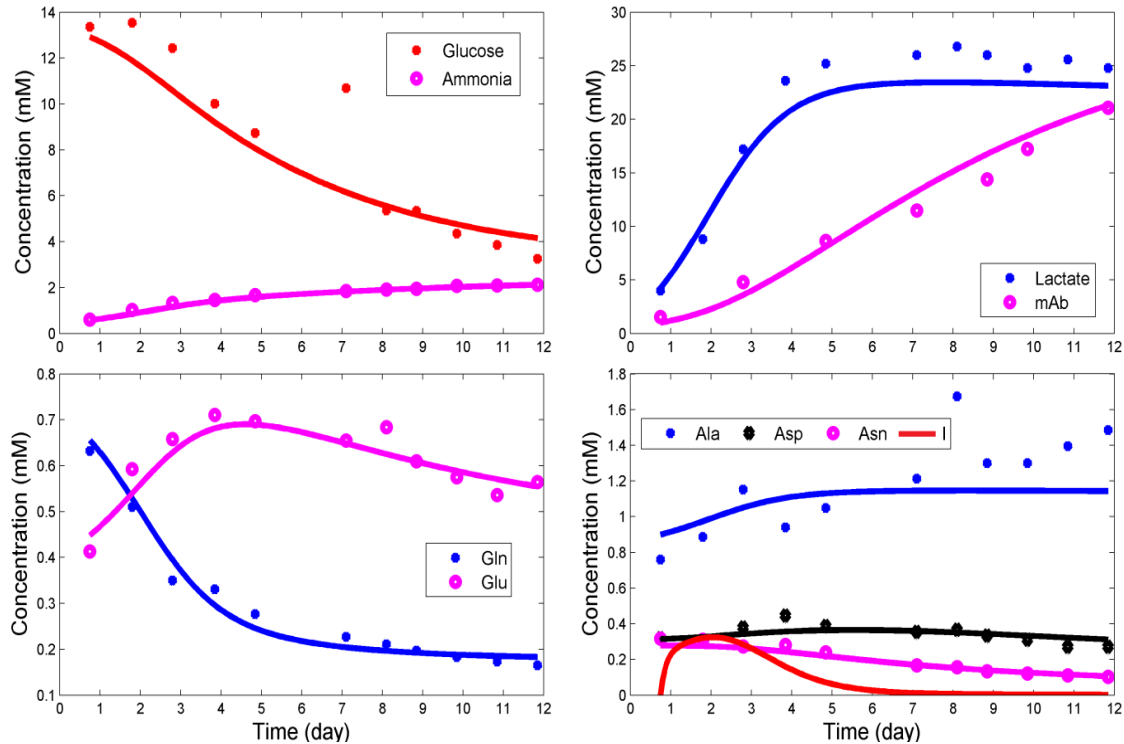
Figure 8.4: Comparison of experimental observations with simulated profiles of metabolites in SP1. The solid curves represent the simulated profiles and the data points represent the experimental observations. '*I*' represents the inhibitory factor.

Figure 8.5: Comparison of experimental observations with simulated profiles of metabolites in SP4. The solid curves represent the simulated profiles and the data points represent the experimental observations. '*I*' represents the inhibitory factor.

Figure 8.6: Comparison of experimental observations with simulated profiles of cell subpopulations. A-D: SP2 and E-H: SP3. The solid curves represent the simulated profiles and the data points represent the experimental observations.
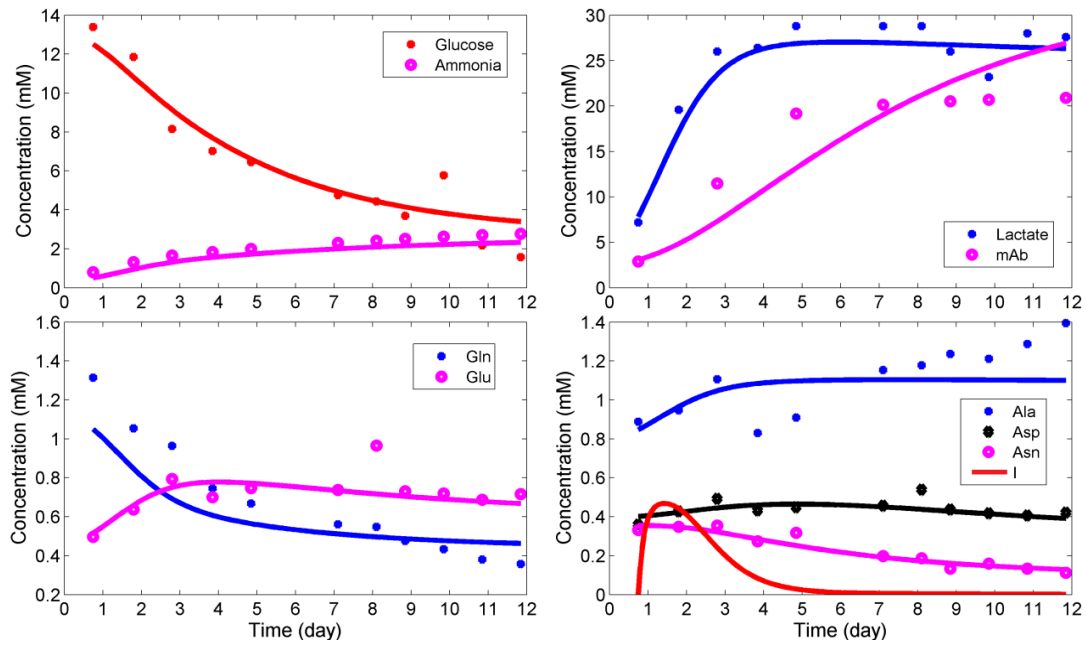
Figure 8.7: Comparison of experimental observations with simulated profiles of metabolites in SP2. The solid curves represent the simulated profiles and the data points represent the experimental observations. '*I*' represents the inhibitory factor.
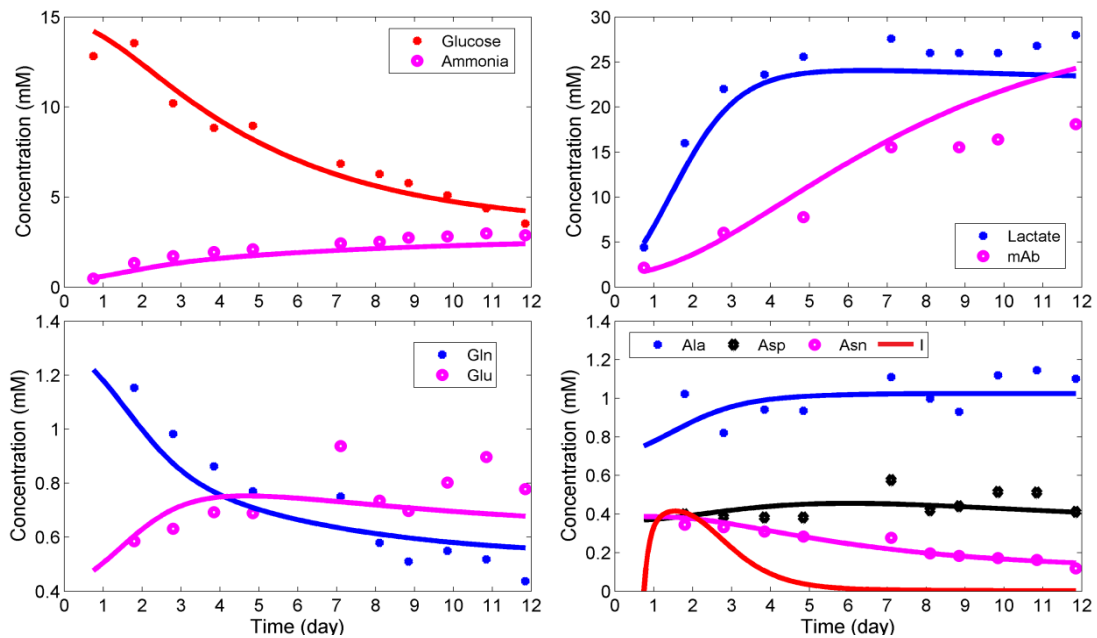
Figure 8.8: Comparison of experimental observations with simulated profiles of metabolites in SP3. The solid curves represent the simulated profiles and the data points represent the experimental observations. '*I*' represents the inhibitory factor.
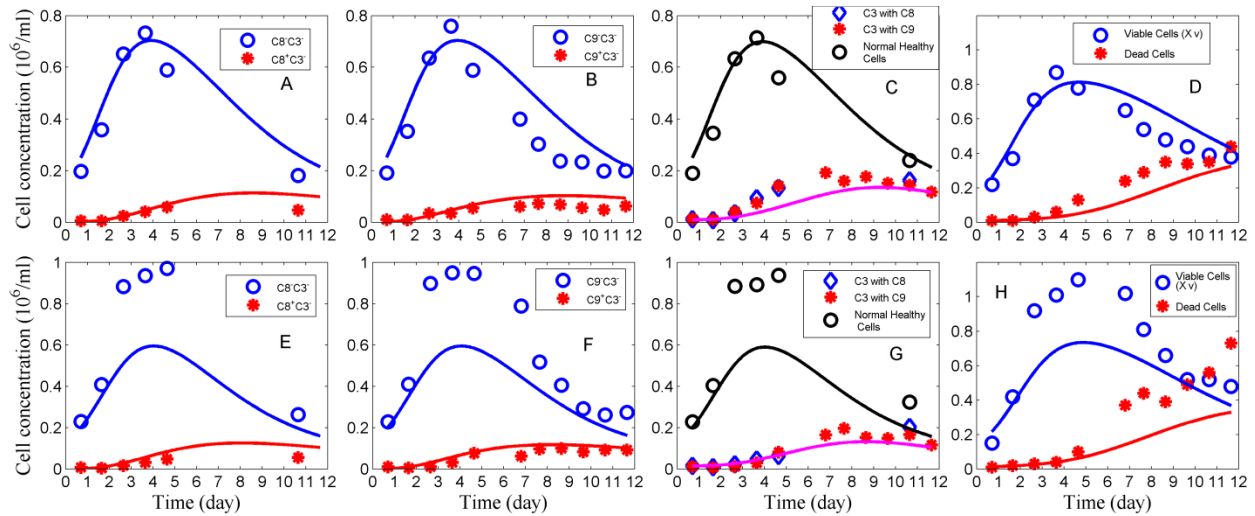
Figure 8.9: Comparison of experimental observations with simulated profiles of cell subpopulations. A-D: SP5 and E-H: SP6. The solid curves represent the simulated profiles and the data points represent the experimental observations.
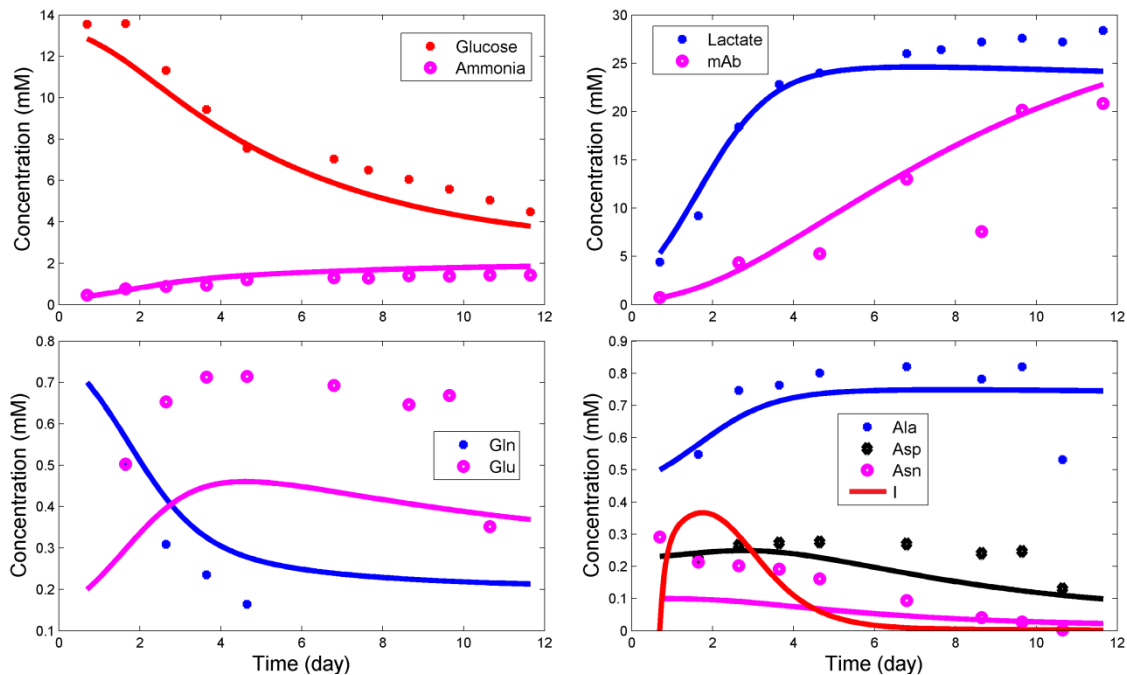
Figure 8.10: Comparison of experimental observations with simulated profiles of metabolites in SP5. The solid curves represent the simulated profiles and the data points represent the experimental observations. '*I*' represents the inhibitory factor.
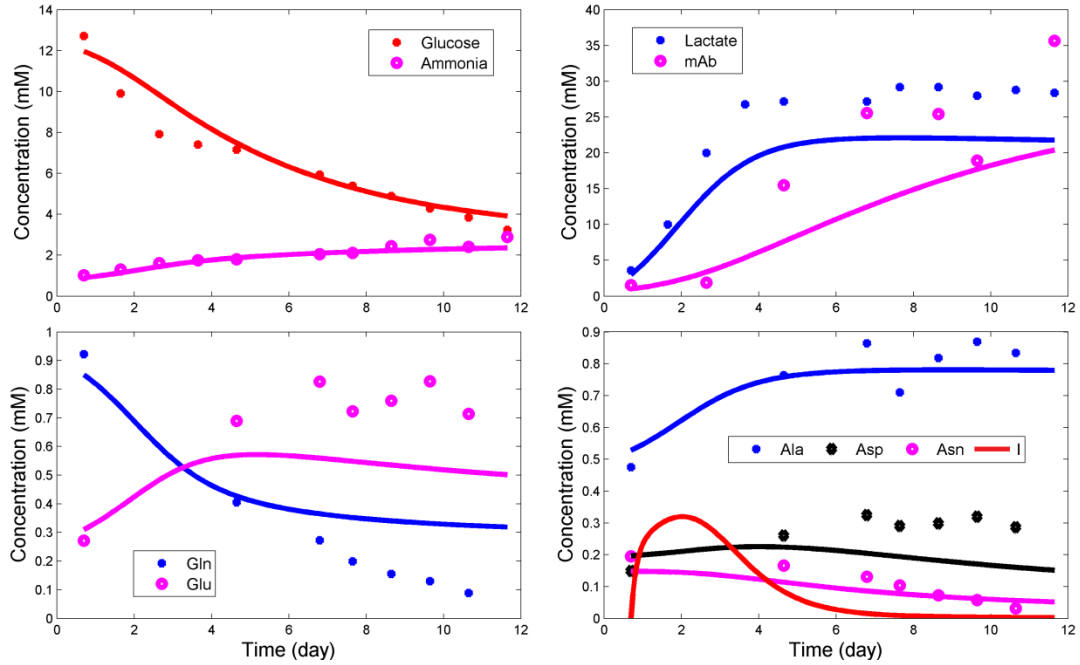
Figure 8.11: Comparison of experimental observations with simulated profiles of metabolites in SP6. The solid curves represent the simulated profiles and the data points represent the experimental observations. '*I*' represents the inhibitory factor.
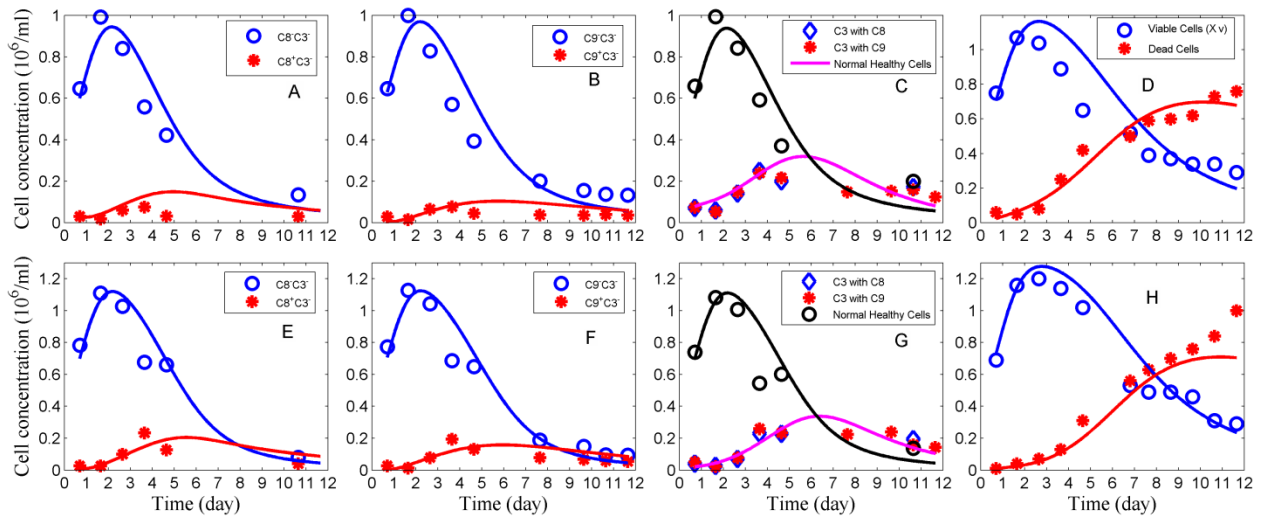
Figure 8.12: Comparison of experimental observations with simulated profiles of cell subpopulations. A-D: SP7 and E-H: SP8. The solid curves represent the simulated profiles and the data points represent the experimental observations.
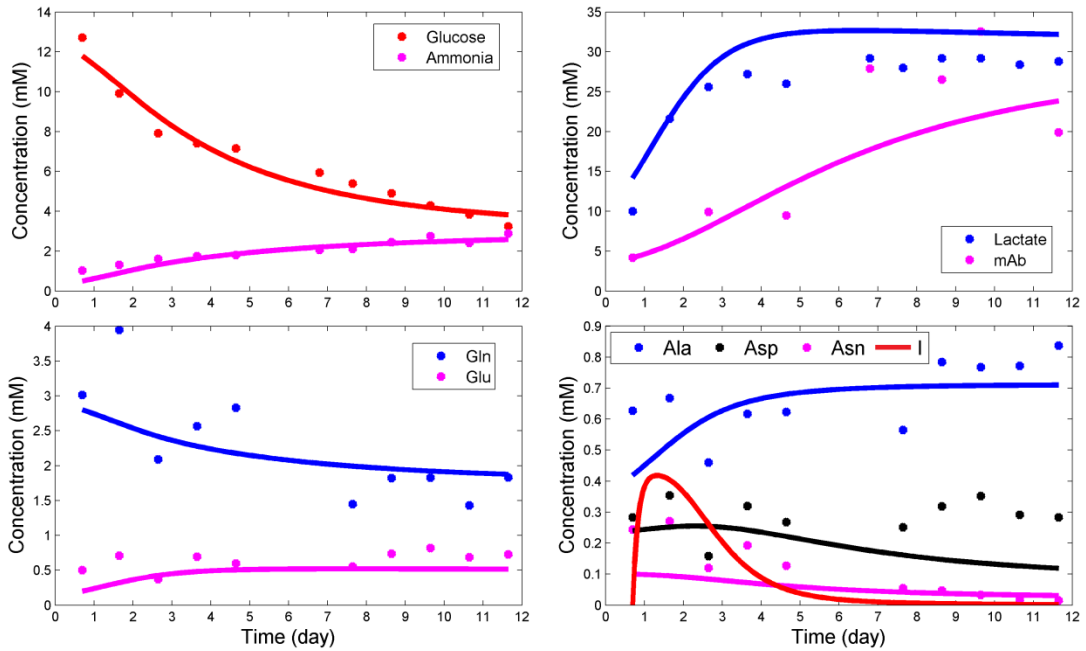
Figure 8.13: Comparison of experimental observations with simulated profiles of metabolites in SP7. The solid curves represent the simulated profiles and the data points represent the experimental observations. '*I*' represents the inhibitory factor.
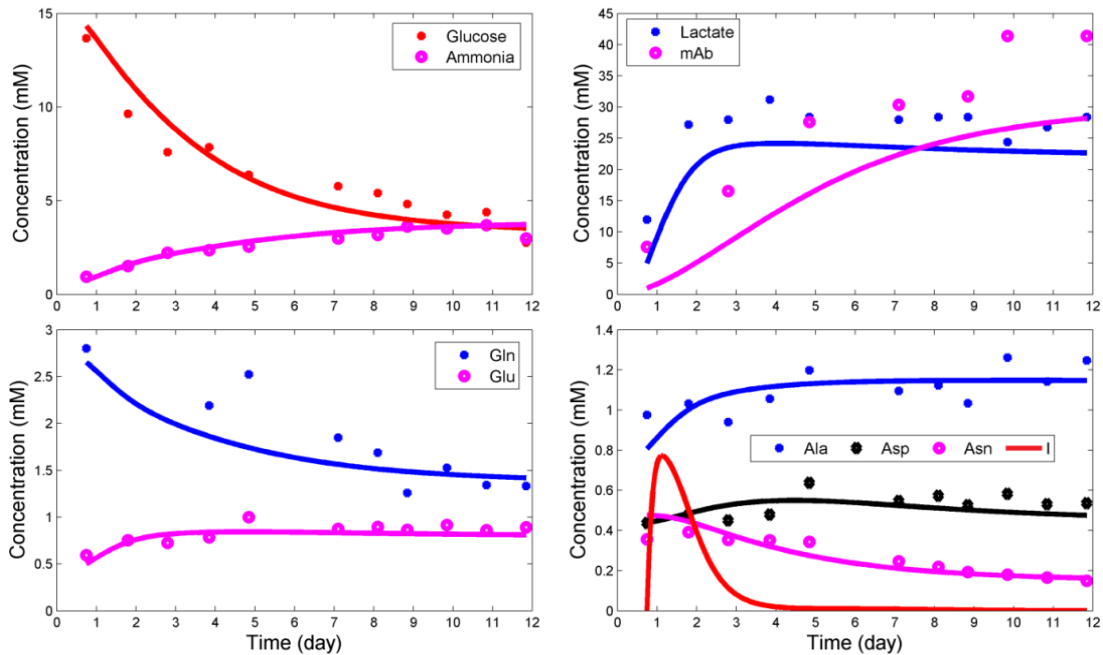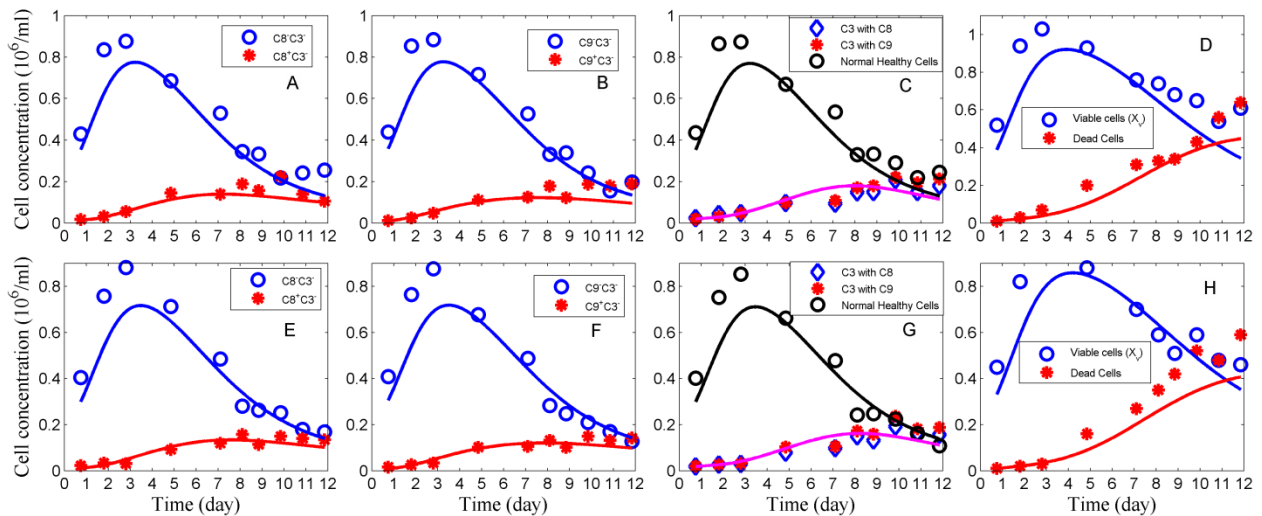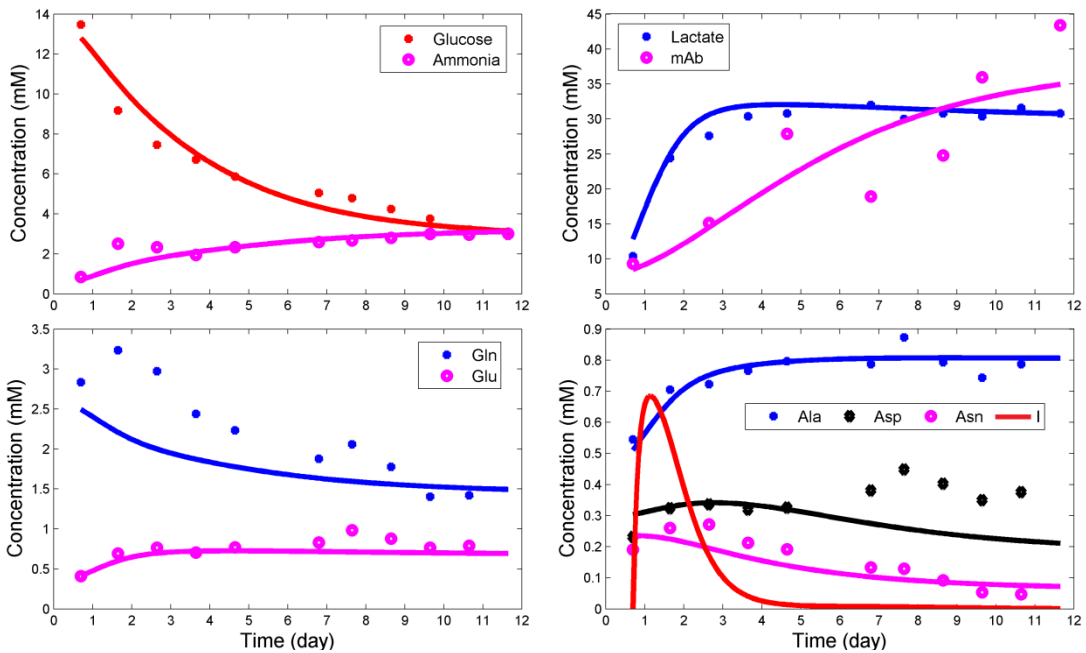

Figure 8.14: Comparison of experimental observations with simulated profiles of metabolites in SP8. The solid curves represent the simulated profiles and the data points represent the experimental observations. '*I*' represents the inhibitory factor.

114

Chapter 9

Investigation of cell growth and mAb productivity following medium-replacement

9.1 Introduction

The experiments described in this chapter were conducted to investigate whether medium-replacement of the cell culture can help to mitigate the inhibitory behavior observed during growth arrest. To this end Naderi, (2011) performed successive partial successive medium-replacements of 50 mL every time after cells reached a new maximum concentration in order to reduce the effect of CO_2 on growth. Naderi found that after each partial medium-replacement the cells concentration maximum was lower than the previous peak. This motivated to experiment with full medium-replacement to assess whether cell growth can be renewed thus resulting in higher cell density and mAb productivity as compared to a normal batch operation. This was also an attempt to test whether the trend toward reduced cell growth and apoptosis could be reversed before pH values dropped to non-optimal levels. To test whether pH effects could be mitigated, an additional experiment was performed in which pH was maintained at a value suitable for growth by addition of a base. The integrated model developed (as described in Chapter 8) which incorporates inhibitory effect 'I' was also used to predict the cell behavior in medium-replacement operation. The predictions were also compared with that obtained by integrated model which incorporated the effect of unknown nutrient 'S' as described in Chapter 5.

115

9.2   Materials and methods

All the cultures were grown in 500 mL spinner flask suspended in SFX-CHO medium supplemented with 1% serum and 1mM glutamine. A set of four different cultures labeled SP13-16 were prepared. The cultures were prepared without centrifugation (unlike the previous experiments described in Chapter 4 and 6 where centrifugation was done to achieve higher initial densities). All the cultures were seeded with the same initial cell density of 0.25×10^6 cells/mL.

The medium-replacement step was performed by centrifuging the cells, removing the spent medium and suspending the centrifuged cells in fresh SFX-CHO medium. Serum and glutamine in proportions to the cell density measured after the replacement step was added. This was done to avoid nutrient depletion for the increasing cell densities resulting after each successive medium-replacement step.

Culture SP13 was used as a control without any medium-replacement or pH adjustment.

The cultures labeled as SP14 and SP5 were used for medium-replacement. Full medium-replacement was performed in these cultures just after the density reached a maximum value. However, since it was impossible to know a priori the exact time where the maximum cell density occurred, it was decided to perfuse the culture after the cells dropped by an amount corresponding to approximately 25% of the cell maximum in the post-exponential phase. The culture in SP4 underwent a single full medium-replacement while that in SP15 was used to test two full medium-replacements where each one of these were performed after the cell density dropped by 25% with respect to the maximum density achieved before medium-replacement step. The first medium-replacement was performed on day ~8 (day 7.9) in both SP14 and SP15 and the second medium-replacement was performed in SP15 on day ~14.

The culture in the spinner labeled as SP16 was used for controlling the pH by base addition. 1N NaOH was used for this purpose. The pH was assessed, and whenever pH dropped below 6.9, base was added to bring it back to 7.1-7.15. Since it was not possible to monitor the pH online as the spinner was maintained inside the incubator, the amount of base to be added was determined by generating a titration curve. A previously made culture in the decline phase was used to generate this titration curve (The titration curve is shown in Appendix F).

Regular sampling was performed to monitor viable and dead cell concentration, pH, dissolved oxygen, glucose, lactate and ammonia. In addition apoptosis was assessed by measuring active caspase-3, capsase-8 and caspase-9 as per the methods described in Chapter 4.

116

9.3   Results and discussion

9.3.1 Culture growth

Viable and dead cell concentration profiles for the four cultures are shown in Figure 9.1 and Figure 9.2. It can be seen that in SP13, SP14 and SP15, the maximum cell concentration was reached at approximately day 4 and during this period the pH values dropped from 7.1 to ~6.4 (Figure 9.3). After the first full medium-replacement was implemented in SP14 and SP15 the cells exhibited additional growth but they could not attain the same maximum observed before medium-replacement. Similarly, after the second full medium-replacement was applied in SP15 some additional growth was observed in this spinner but the peak in cell density was smaller than the peak observed before the second medium-replacement.
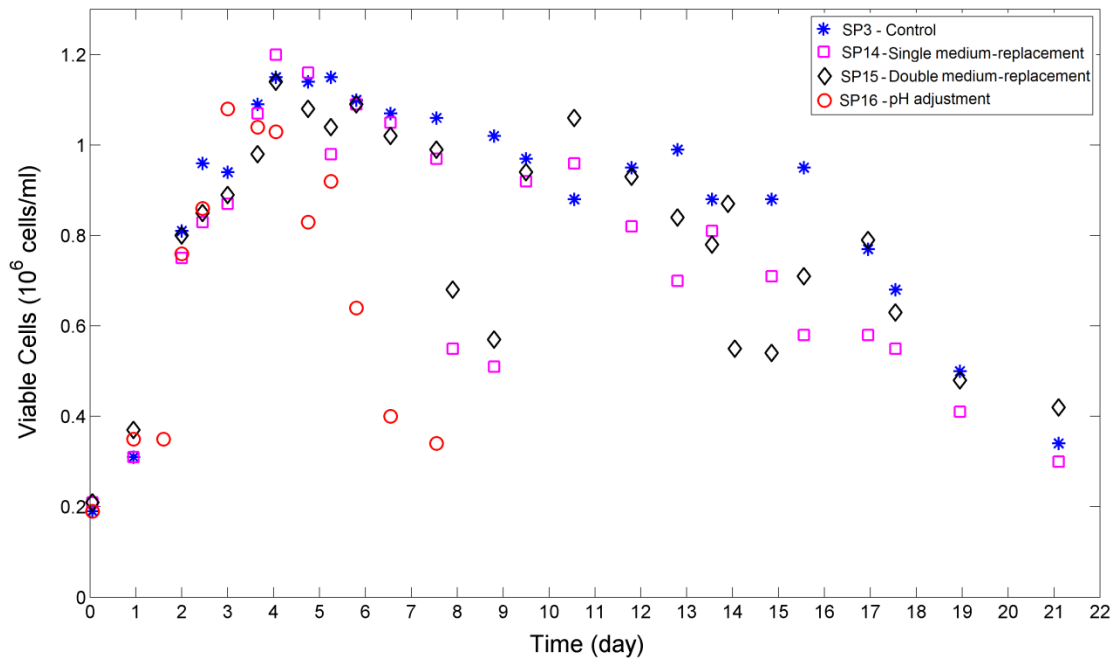
Figure 9.1: Viable cell concentration profile
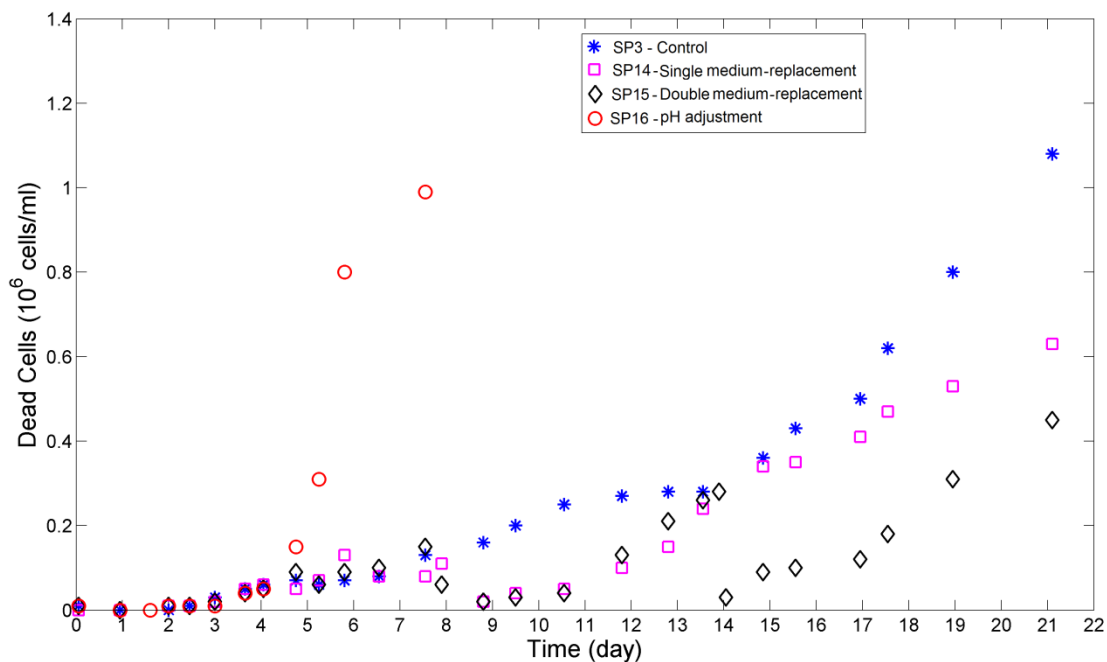
Figure 9.2: Dead cell concentration profile

The culture in SP16, where pH was controlled by base addition, exhibited significantly different behavior than the other three cultures. The specific growth rate in SP16 was significantly higher at approximately 0.55 per day (Table 9.1) and the maximal cell density was reached much faster in about three days and then the cells died rapidly (Figure 9.1 and Figure 9.2) due to glucose depletion to zero levels (Figure 9.4) (Table 9.2). The specific glucose consumption rate in SP16 was almost 3 fold higher than in the other three cultures.

Thus, maintaining the pH in the range of 7.1-7.15 helped in increasing specific growth rate but due to rapid depletion of glucose likely associated to higher metabolic activity, the culture could not attain the higher maximum cell concentration. It can be hypothesized that if initial glucose concentration had been higher, or if additional glucose had been added after depletion, the culture could have reached a higher maximum cell concentration than the other three cultures. Controlling glucose addition to avoid depletion while pH is controlled is left for future studies.

118

It was also observed that the higher glucose consumption rate in SP16 was accompanied by higher level of lactate production than in the other cultures (Figure 9.5) with an average specific production rate of 13.8 mM /10^6 cell/mL day (Table 9.2). This higher metabolic activity in terms of glucose consumption and lactate production can be possibly attributed to higher glycolytic activity of enzymes. It has been found that pH has a profound effect on metabolism. It has been observed that the decrease in pH led to decrease in both the glucose consumption rate and lactate production rate resulting in reduced metabolic activity with various cell lines (Birch and Edwards, 1980; Miller et al., 1988; Ozturk and Palsson, 1991; Reddy and Miller, 1994; Sauer et al., 2000). Thus, maintaining the pH in a range of 7.0-7.2 seems to promote normal metabolic activity thus corroborating that this range of pH values is optimal for growth.

Table 9.1: Specific growth rate in cultures

	SP13	SP14	SP15	SP16
Specific growth rate (day $^{-1}$) (calculated during exponential phase)	0.46	0.45 (before medium-replacement)	0.41 (before medium-replacement)	0.55
		0.79 (after first medium-replacement)	0.71 (after first medium-replacement)	
			0.16 (after second medium-replacement)	

119
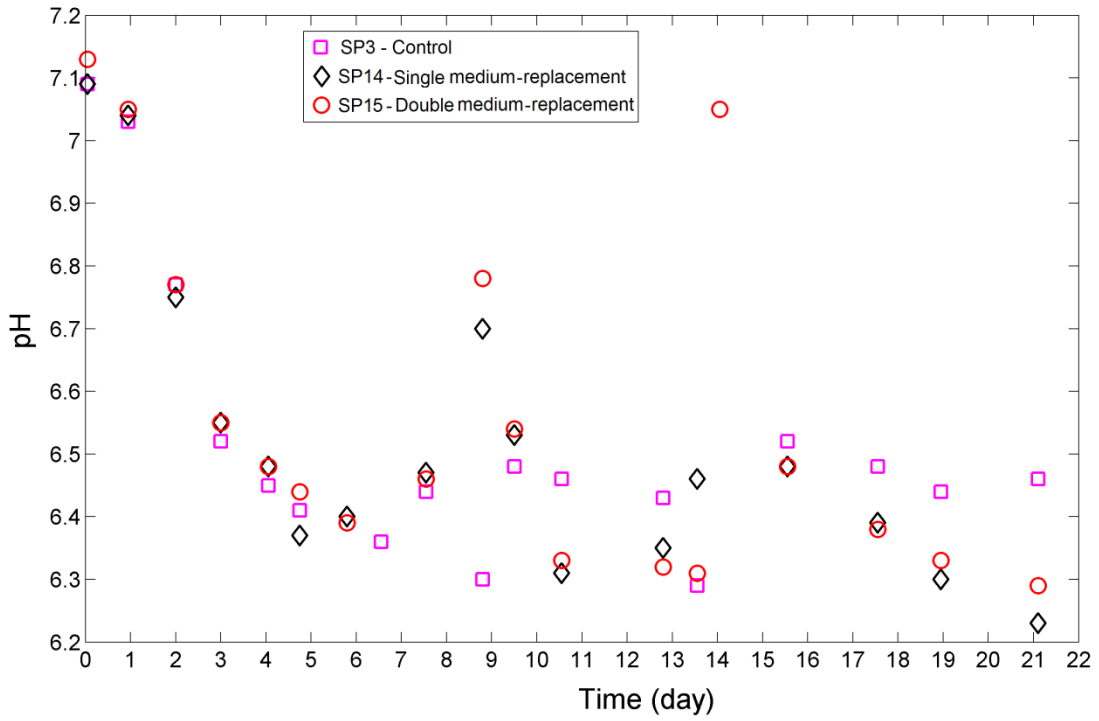
Figure 9.3: pH profile
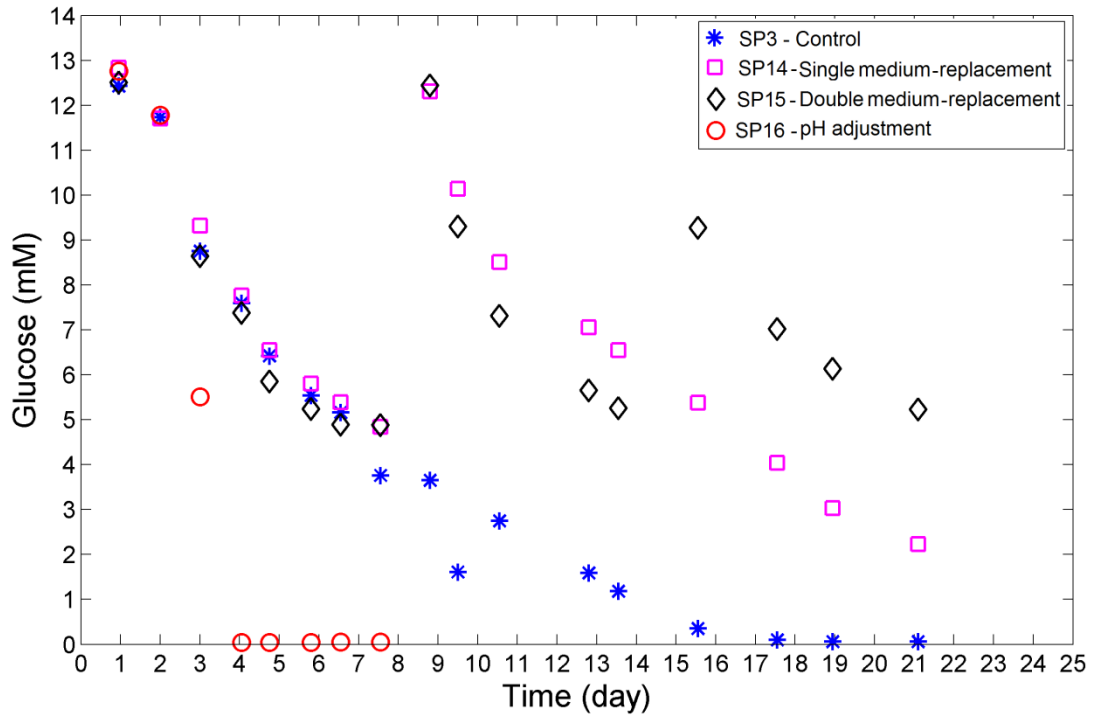
Figure 9.4: Glucose consumption
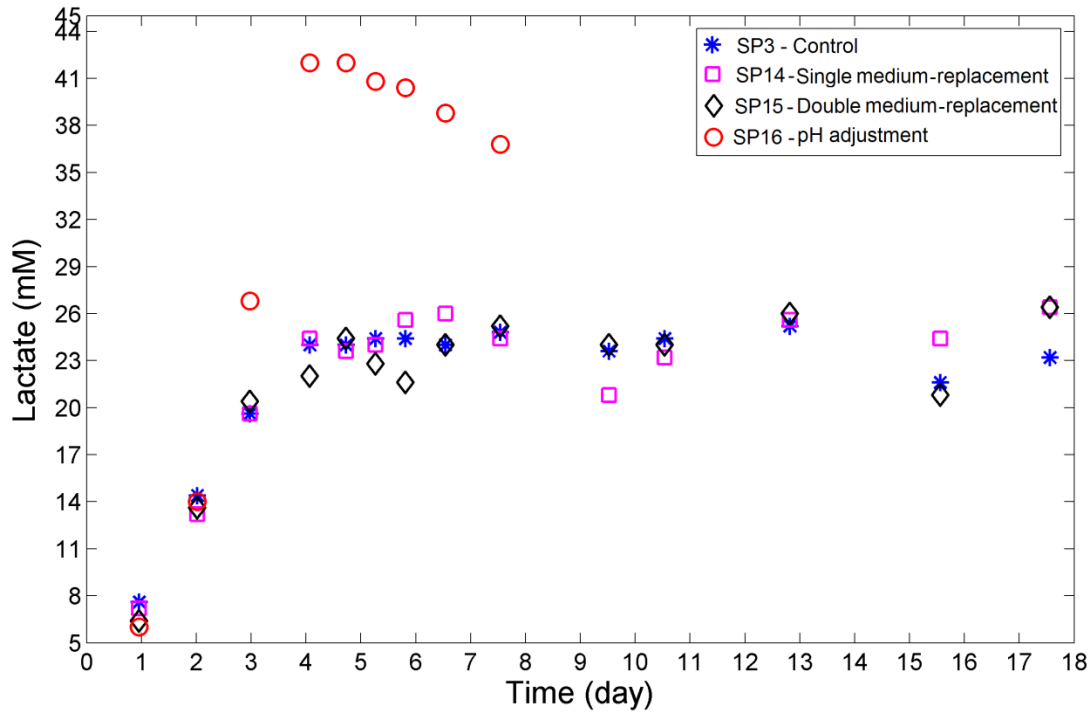
Figure 9.5: Lactate production

Table 9.2: Specific glucose consumption (q_{Glc}) and lactate production rate (q_{Lac})

	SP13	SP14	SP15	SP16
q_{Glc} (mM/10^6 cells/mL day) (calculated during exponential phase)	1.81	1.4 (before medium-replacement)	1.0 (before medium-replacement)	5.8
	-	1.39 (after first medium-replacement)	1.36 (after first medium-replacement)	-
			1.02 (after second medium-replacement)	
q_{Lac} (mM/10^6 cells/mL day) (calculated during first exponential phase)	4.8	4.4	1.9	13.8

Alternatively it can also be suggested that the optimal pH alters the cell membrane potential affecting glucose transport rate, thus increasing metabolic activity (Wilhelm et al., 1971). On the other hand the cultures SP3, SP14 and SP15 grew with approximately similar specific growth rates of 0.46, 0.45 and 0.41 per day (Table 9.1) and reached maximum cell concentrations of 1.15×10^6, 1.2×10^6 cells/mL and 1.14×10^6 cells/mL respectively. After the first medium-replacement, the specific growth rate increased almost two fold in SP4 and SP5 (Table 9.1). This again can be attributed to the optimal pH values attained after replenishing the spinner with fresh medium and with higher levels of glucose, glutamine and serum combined with the higher cell density in the spinner after medium-replacement as compared to the initial density at the start of the culture. A slightly higher specific glucose consumption rate was observed (Table 9.2) than before medium-replacement, resulting in rapid depletion of glucose (Figure 9.4). This higher glucose consumption rate was accompanied by a large increase in lactate production levels, both of which can be attributed to the high cell. The ammonia production rate was also increased after medium-replacement (Figure 9.6).

In the second medium-replacement implemented in SP15, the specific growth rate decreased considerably as compared to the growth observed after the first medium-replacement, resulting in a slight decrease in glucose consumption rate to 1.02 mM/10^6 cells/mL day. The ammonia production rate also decreased after the second medium-replacement. The decrease in specific growth rate can be attributed to accumulative damage from pH or CO_2 mentioned in Chapter 8. In principle, cells can remain indefinitely in a non-growing non-apoptotic state or switch into apoptosis at any time. Cells usually staying at the G1/S checkpoint (R1, as described in Chapter 2 in Figure 2.1) can eventually undergo cellular senescence and apoptosis. Once the cells reach critical levels of inhibitory stress due to for example pH drop or acidic environment, the cells cannot revert to normal growing conditions and they remain in this non-proliferative state for an indefinite amount of time or switch to apoptosis.

In eukaryotic cells, environmental stress related growth arrest has been found in previous studies to be related to depression of pH (Cipollaro et al., 1986) and/or elevated temperature (Rincheval et al., 2002) as the stress factors.
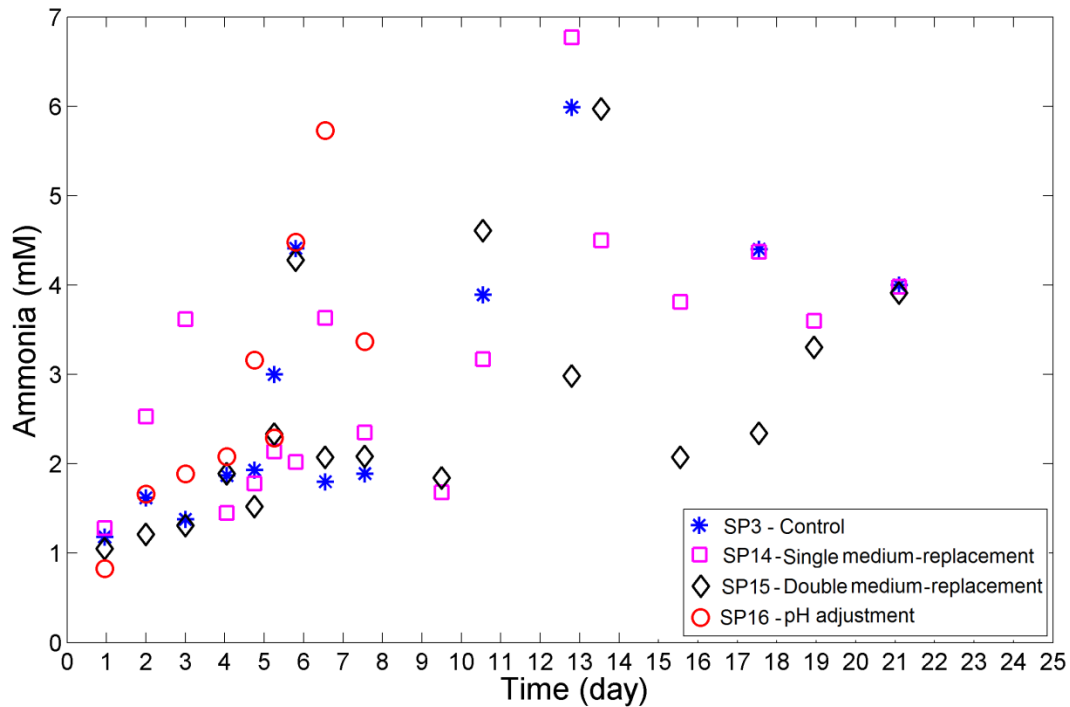
Figure 9.6: Ammonia progression

9.3.2 Apoptosis progression

Significant differences were observed in terms of capsase-8, caspase-9 and caspase-3 levels. Figure 9.7 shows the progression of these caspases in each one of the four cultures, while Figure 9.8 and Figure 9.9 compare the levels of each one of the caspases among the different cultures. It can be seen from Figure 9.7 that in all the cultures the proportion of caspase-9 cells were higher compared to caspase-8 and caspase-3 active cells. Apoptosis was minimal, as seen by minimal caspase active population, approximately during the first three days in all the cultures. However, due to progressive cell density increase, the pH in all cell cultures (SP13, SP14, SP15) except the one where pH was controlled (SP16) dropped to a value of 6.6 at approximately the time where the cell concentration reached a maximum value, After this time, cell viability started decreasing and the caspase-active populations started increasing at faster rate.

123
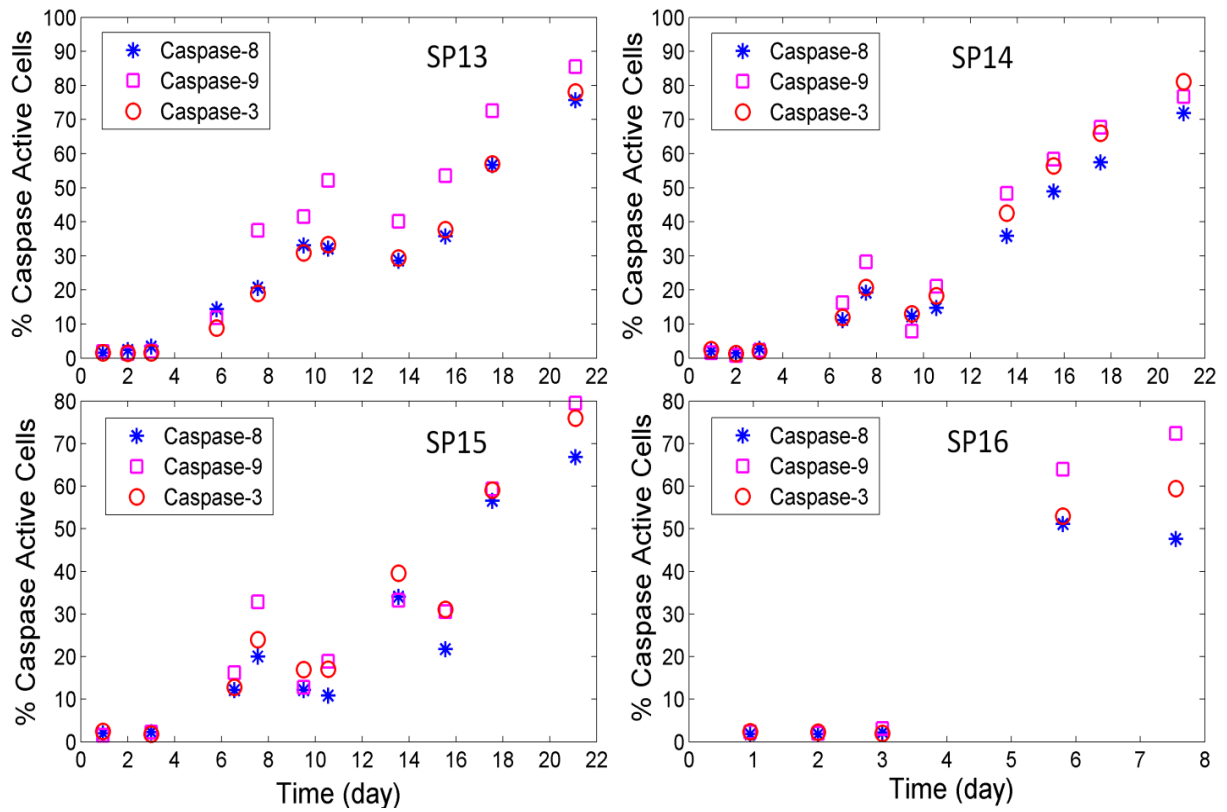
Figure 9.7: Comparison of percent caspase-8, caspases-9 and caspase-3 cells evolution in the culture
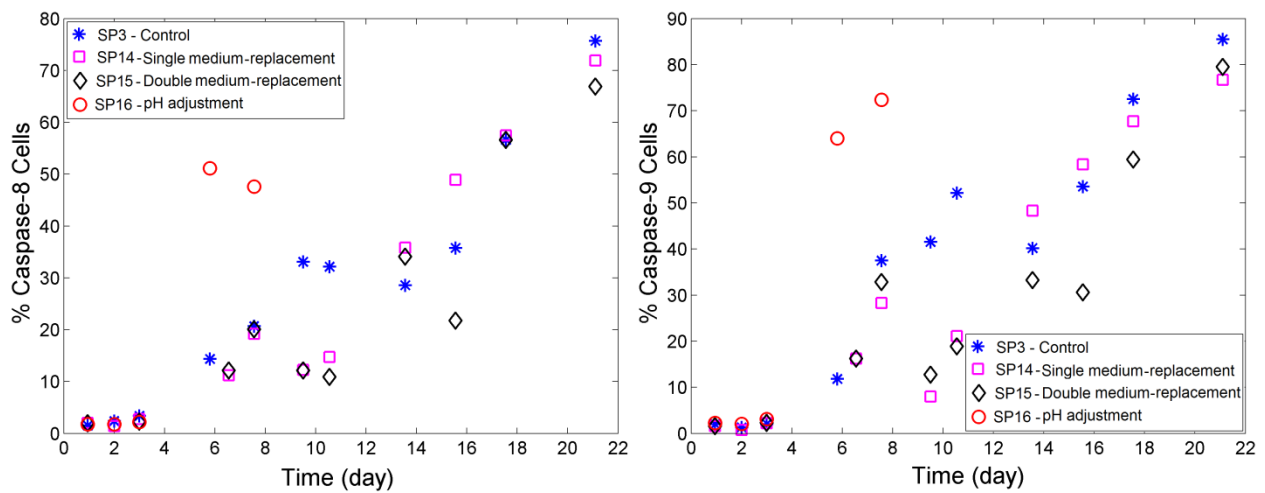
Figure 9.8: Percent caspase-8 and capsase-9 cells evolution
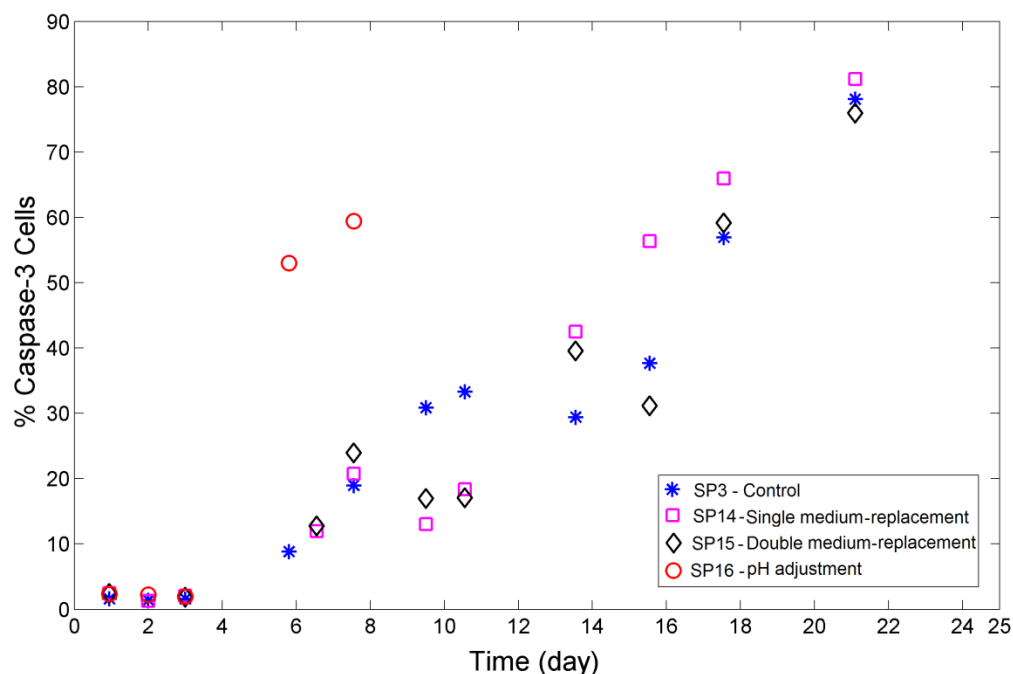
Figure 9.9: Percent caspase-3 cells evolution

It can be observed in SP13, the culture without medium-replacement or pH control, that the instantaneous caspase-9 active cell population levels after SP14 and SP15 underwent their first medium-replacement events were higher, possibly due to higher pH-related stress in SP13 as compared to SP14 and SP15. Thus, it appears that prolonged exposure of cells to this higher acidic environment also affected the evolution of apoptosis in SP13, leading to around 80% apoptotic population towards the end of this culture.

In SP16, the culture where pH was controlled by base addition, after day 3, the apoptotic cell population rapidly increased possibly due to near depletion glucose or excessive osmolality. Osmolality could not be measured directly. Instead, conductivity was recorded as an indirect measure of osmolality. No significant differences were found in conductivity levels in all the cultures; it remained at an average level of 13.3 mS/cm with a standard deviation of 0.3 units. Thus, the observed high rise in the apoptotic cell population in SP16 can primarily be attributed to glucose depletion to zero levels occurring at around day 3. As

mentioned in Chapter 2, nutrient depletion can lead to apoptosis due to DNA damage (Burhans et al., 2007) via the intrinsic pathway of apoptosis leading to caspase-9 activation. This is corroborated by the fact that the levels of caspase-9 active cells were higher in SP16 as compared to caspase-8 or caspase-3 active cell populations and rapidly reached to around 75% towards the end of culture. Also, the caspase-9 active cell population was higher in this culture compared to the corresponding populations in SP13, SP14 and SP15, due to the rapid depletion of glucose. It was also observed in SP16 that the caspase-8 and caspase-3 active cell populations were higher compared to those in SP13, SP14 and SP15 (Figure 9.8). This may be explained by the fact that there is feedback between the intrinsic and extrinsic apoptotic pathways thus high activation of caspase-9 may also cause activation of caspase-8 and vice versa (see model schematic in Figure 5.1, Chapter 5).

In SP14 and SP15, after medium-replacement, there was a slight decrease in proportion of caspase active cell populations due to loss of cells in centrifugation and then due to dilution into the fresh medium. It can be seen in Figures 9.8 and 9.9 that the medium-replacement did not really help in reviving the cells or in reducing the degree of apoptosis as compared to that in SP13, the negative control. The apoptosis progression in terms of the caspase-active cell populations was similar in all these cultures even after the medium-replacement event. This suggests that cell growth arrest occurring after a drop in pH before medium-replacement was not reversible. At the same time, the remaining normal non-apoptotic population attained rapid growth after medium-replacement following the replenishment of medium but due to the initial high density relative to the density at the beginning of the experiment, the build-up of CO_2 and drop in pH occurred faster which led them to become apoptotic earlier as compared to the period of growth before medium-replacement.

9.3.3 Monoclonal antibody production

The operation of the culture with successive medium-replacements had a profound effect on mAb production. Figure 9.10 shows differences in mAb production for these different cultures. In general, it can be seen that the rate of mAb production during the exponential and during the post-exponential phase are different as observed by the change in slopes after the end of the exponential phase. The pH-controlled culture in SP16 remained in exponential phase for the first three days and then entered a decline phase where mAb production suddenly increased, possibly due to higher production rates contributed by growth arrested and apoptotic cells. Similar observation was reported in other cultures as well (SP13, SP14 and SP15).

In SP13, the final mAb concentration obtained at the end of the operation (around 21 days) was approximately 90 µg/mL. When considering mAb production just before each medium-replacement event and after the end of culture, a total mAb yield of approximately 100 µg/mL in single medium-replacement culture (SP14) and 135 µg/mL in double medium-replacement (SP15) was attained. Thus operating the culture in medium-replacement mode and optimizing the time of replacement can enable significant improvements in mAb productivity. As can be seen in SP16, where the exponential phase lasted for approximately three days (Figure 9.1), there was a sudden increase in the mAb profile when the culture entered into the decline phase after three days of exponential phase. Similar observation can be made with regards to the culture in SP13, SP14 and SP15 where the exponential phase lasted up to four days (Figure 9.1). However the increase in mAb levels in the decline phase looks higher in SP16 than other cultures, indicating higher specific mAb productivity in SP16 compared to SP13, SP14 and SP15. The specific mAb productivity (calculated over the whole corresponding culture time) for SP13 (negative control) and SP16 (culture with pH control) is shown in Table 9.3. As can be seen from this table, the specific mAb productivity obtained for SP16 was 6.9 (mM/10^6 cells/mL day) while that for SP13 was 4.75 (mM/10^6 cells/mL day). The specific mAb productivity for SP14 and SP15 could not be calculated at this point because of insufficient data. As mentioned earlier in Chapter 5, variability in mAb assay by ELISA can be observed (particularly in SP3, Figure 9.10). And thus needs further improvement in the assay procedure.
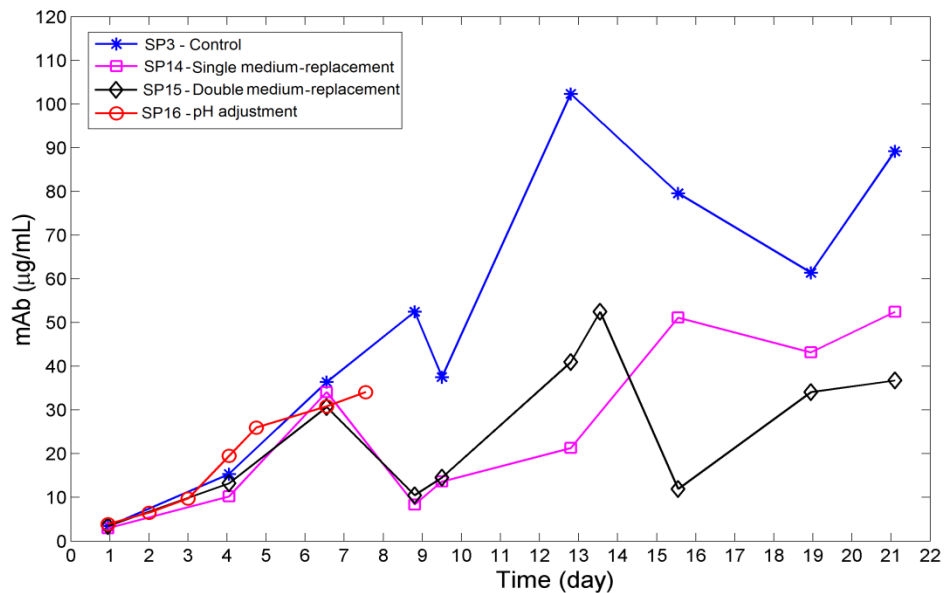
Figure 9.10: Effect of different culture operation modes on mAb production

Table 9.3: Specific mAb productivity in SP13 and SP16

	SP13	SP16
q_p (mM/10^6 cells/mL day)	4.75	6.9

9.3.4 Modeling

Finally, the predictive capabilities of the model that is described in Chapter 8 were tested by comparing model predictions and data for the experiments SP14 and SP15 described in this chapter. Initially the model was simulated with the same parameters' values obtained in the Chapter 8. However, using these parameters, the model underpredicted the normal healthy cell population data. A possible explanation for this lack of fit is that in SP13-16 the cells were grown without previous centrifugation of the seed culture possibly resulting in higher cell growth than those cultures used for fitting which underwent such centrifugation step. For this reason the parameter μ_g was varied for prediction of the data obtained in SP14-15. Also since there was change in specific growth rate in these cultures, there was also an observed change in mAb productivity. Accordingly, the specific mAb productivity q_p was also varied. Finally, to test the hypothesis of whether the different cell subpopulations (i.e. normal growing, normal non-growing and apoptotic) have different associated mAb production rate, different parameters were used for productivity as per the following equation:

$$\frac{dP}{dt} = q_{p_1}(x_1 + x_2 + x_3 + x_5) + q_{p_2}x_4$$

The sum $x_1 + x_2 + x_3 + x_5$ corresponds to normal growing and nongrowing cells as per the notation used in Chapter 5 and Chapter 8, and x_4 corresponds to apoptotic cells according to the same notation. After fitting of these individual specific mAb productivities it was observed that the model was able to predict all the state variables including mAb profile reasonably well. The predictions are shown in Figure 9.11 for

single medium-replacement experiment (SP15) and Figure 9.12 for double medium-replacement experiment (SP16).

Simulation parameters suggest that that the highest mAb production rate was obtained by caspase-3 active cells (x_4) (Appendix D).

When compared predictive capability of the integrated model which included inhibitory effect with the integrated model which included effect of unknown nutrient, it was found that both the models predict the medium-replacement experiments almost similarly, although there was a difference found in SSE. The SSE was found somewhat lower in integrated model which included inhibitory effect 'I' than that with unknown nutrient effect 'S'. The difference in SSE was around ~20%. However, Naderi et al., (2011) was found that for multiple partial medium-replacements, the cell maximum was progressively lower than the previous cell maximum following each medium-replacement event, which required the incorporation of the integration term in fgr to account for irreversible cell damage due to accumulation of CO_2.
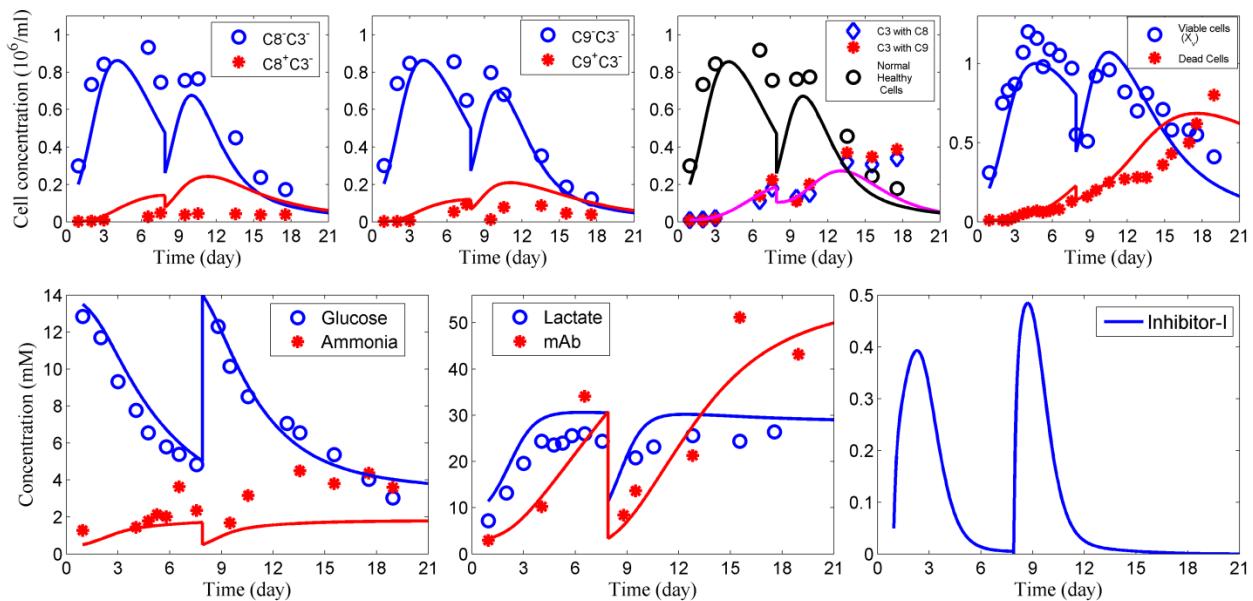
Figure 9.11: Comparison of experimental observations with simulated profiles of cell subpopulations, glucose, metabolites and mAb in single medium-replacement experiment (SP14). The solid curves represent the simulated profiles and the data points represent the experimental observations.
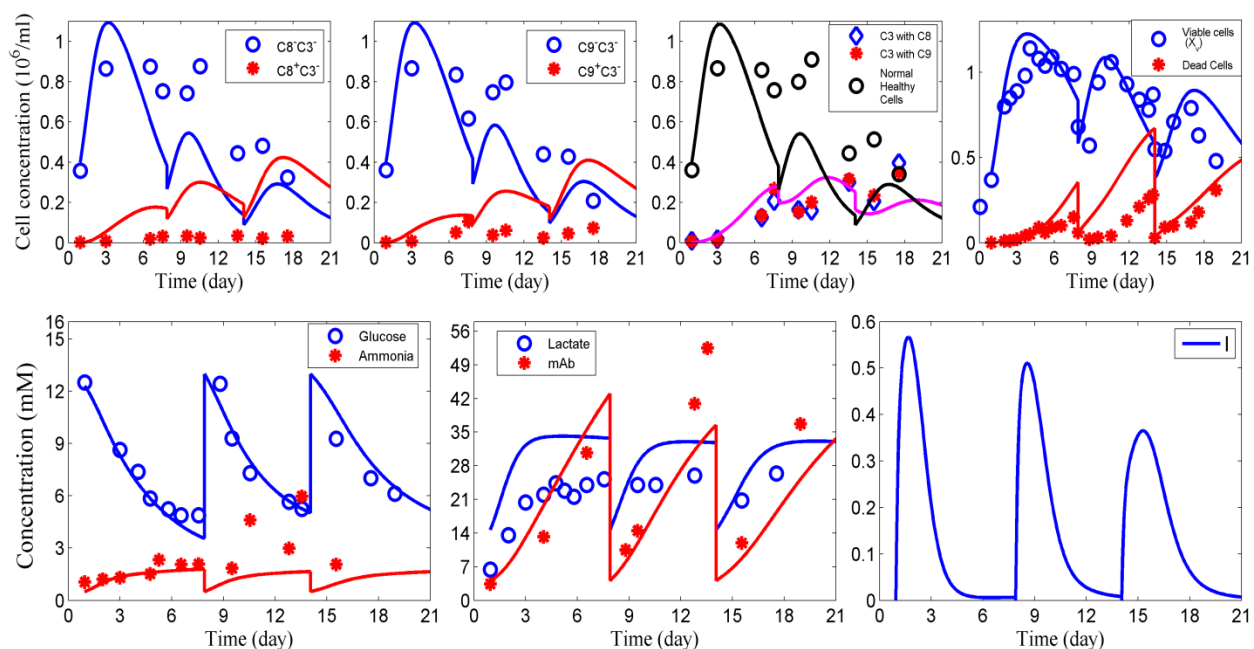
Figure 9.12: Comparison of experimental observations with simulated profiles of cell subpopulations, glucose, metabolites and mAb in double medium-replacement experiment (SP15). The solid curves represent the simulated profiles and the data points represent the experimental observations.

Chapter 10

Conclusions and recommendations

The overall goal of this thesis was to model the evolution of growth and apoptosis in CHO cell culture and assess their impact on monoclonal antibody productivity. Different factors contributing to growth and apoptosis were identified and their effects were quantified using the model. Based on general available knowledge of apoptotic pathways, the main factors studied were nutrient depletion effects in media and/or serum and cell-cell interactions effects related to cell density. The key novelty of this mathematical model is that it considers balances of both intracellular as well as extracellular species. Intracellular caspases were studied since they are good indicators of the active apoptotic pathways' occurring in process, e.g. caspase-8 is related to cell-cell interactions whereas caspase-9 levels are known to be related to either nutrient depletion or toxicants' levels. Furthermore, although mathematical models of intracellular species including caspases, have been proposed before in the literature (Eissing et al. 2004; Fussenegger et al. 2000; Spencer and Sorger, 2011), to the knowledge of the author these earlier reported models have never been verified by experimental data. In contrast, the current work proposes a novel population-balances' based model of caspases which has been calibrated and verified by flow cytometry measurements of caspases. Then, based on the identified model, the study suggests a direction towards a suitable operation of cell culture for maximized production of mAb.

The following conclusions refer to the quality of the model and the factors that seem to affect growth arrest and apoptosis as quantified by combining the model with experimental observations. Also, conclusions are given regarding limitations in the analytical techniques used to collect data and the impact of these limitations on the quality of the findings. Finally, different directions for future work are briefly outlined.

131

Model analysis: The original model was developed by considering a range of hypotheses (resulting in the 24 model variants discussed in Chapter 5) regarding CHO cell culture. The model revealed that growth arrest is mostly correlated to the buildup of an inhibitor in the culture. Furthermore, the fact that cultures of different volumes resulted in significant differences in maximal cell density led to the hypothesis that growth arrest is related to the accumulation of a gas that is inhibitory for growth and results in significant deviation of pH from its optimal range, possibly due to carbon dioxide. The model variant that was selected provides good agreement with the experimental observations of various cell subpopulations. The model also served to test the sensitivity of the process to different factors affecting growth arrest and apoptosis. For instance, the model sensitivity and identifiability analysis (Chapter 5) shows that the parameter associated with cell density dependence has a strong effect on the model behavior, indicating the prominent effect of cell density on apoptosis. The possibility of cell density dependence could not be avoided as removing this dependency in the model did not provide good fitting and prediction of state variables in the model. It is logical to assume that this significant dependence of the progression rate of apoptosis on cell density is related to cell-cell interactions (which were confirmed by preliminary Western blot measurements of FASL). Furthermore, the model shows that this interaction effect is mostly originating from caspase-3 active cells which initiate apoptotic signals further promoting apoptosis among healthy cells. The additional novel feature of the proposed model is that the population balances of intracellular caspases have been coupled to the evolution of the extracellular metabolites in the culture including nutrients and by-products. This coupling is essential if the model is to be used in the future for optimization since any optimal recipe will involve manipulation of extracellular culture conditions. The model of intracellular species categorizes the whole cell populations into different subpopulations based on caspase activity. To the author's knowledge is the first ever effort towards modeling these two domains simultaneously. The coupling of balances of intracellular species and extracellular species provides more insight into cell culture behavior as compared to modeling the extracellular species only and thus it is expected to be more reliable for the purpose of process optimization. This comprehensive model is found to predict cell subpopulations, metabolites, nutrients and product reasonably well. The analysis of the model shows the contribution to mAb production by different cell populations at different rates. The highest production rate appears to be contributed by capsase-3 active cells as shown in Chapter 9.

Sensitivity to cell density: Cell growth and apoptosis progression were found to be significantly affected by cell density. Though it was found from the volume experiment that inhibitory effects were the main trigger in affecting the cell growth, removing cell density dependence in simulation, led to inaccurate

predictions**.** Thus it was concluded that cell density has definitely an effect in addition to the observed inhibition effects related to culture volume.

Sensitivity to serum: Experiments with different levels of serum in low cell density cultures showed enhanced growth especially above 1% levels (Chapter 6). Higher initial serum concentration above 1% offered higher specific growth rate, thus obtaining higher maximum cell concentration. The lower maximum cell concentration in lower serum level below 1% as compared that in higher serum level of 2% in low cell density cultures can be attributed to the depletion of a nutrient (possibly some growth factor) present in serum. Whereas in higher initial cell density cultures, the similar maximum viable cell concentrations in different serum levels ranging from 0.5% to 4%, can be attributed to toxicity due to rapid pH drop possibly due to CO_2 accumulation because of high cell concentration. Higher specific growth rate resulted in higher specific mAb productivity. However, in Chapter 7, the correlation between productivity and growth was less conclusive since mAb productivity was found similar for different specific growth rate cultures (SP10-11). This may be attributed to the variability in ELISA method as described below and further studies are needed to investigate this correlation. Though different initial serum concentration for a given initial cell density did not have any effect on viability, it however affected apoptosis progression. For higher initial cell density, different levels of serum did not affect the progression of caspase-9 and caspase-3 (Chapter 6). However, for lower cell density, different levels of serum were found to have an effect on these caspases' cell populations. It can be hypothesized that for low levels of serum, some nutrient contained in the serum becomes depleted thus leading to lower cell growth and faster progression of apoptosis due to nutrient stress.

Reversibility in cell growth inhibition: In medium-replacement experiments it was found that the cells could not revert to previous growth ability following each medium-replacement event. This can be attributed to the combination of two effects: i - after each medium-replacement event the cell density is progressively larger thus causing faster accumulation of the inhibitory compound and ii - after cells are exposed to critical levels of an environmental stress, e.g. exposure to high levels of CO_2 accumulation, they cannot recover the ability to grow they had before that exposure. This acidic environment is detrimental to cell growth possibly due to DNA damage in cells which restricted cell growth and led to senescence or/and apoptosis thereafter. This was also observed in other studies (Jolly et al., 2004) where it was found that an acidic environment induced DNA damage. p53 is reported to regulate cell arrest in the G1/S checkpoint after DNA damage, however to the author's knowledge, there are no previous reports on whether DNA damaged cells revert to normal growth conditions after DNA repair by p53. As stated in the literature review, cells in G0/G1 (quiescent state) phase can remain in this state for an indefinite amount of time and can revert to normal conditions after suitable stimulation of environmental

133

conditions. On the other hand, the experimental measurements of caspases showed continued progression of percent caspase-active cells to the almost similar levels as those reached in the negative control culture (SP13) even after medium-replacements, supporting the hypothesis that the cells which have undergone DNA damage due to acidic environment may not have actually spent time in a growth arrest state (induced by p53) due to this damage, but switched to apoptosis more quickly. After the first medium-replacement, metabolic activity of cells is increased due to favorable pH conditions and cell density. However within the cell population which were already exposed to critical CO_2 levels from the earlier event (before medium- replacement) a large proportion of them switched to apoptosis, thus restricting the ability of cells in achieving the same cell concentration maxima as in the period before medium-replacement was done.

Sensitivity to culture volume: Cell behavior was found to be highly dependent on initial culture volume. Higher specific growth and higher maximum cell concentration were obtained with lower volume (Chapter 7). Thus, stoppage of growth seems to be correlated to the accumulation of a compound, possibly, CO_2 which accumulates within the culture due to lower surface to volume ratio. Accumulation of this compound was accompanied by a drop in pH which possibly inhibited cell growth by cell cycle arrest possibly at the G1/S checkpoint. Partial or full medium-replacement of this culture with supplementation of fresh medium was used to reduce the effect of CO_2 and thus pH. However, as observed in Chapter 9, although full medium-replacement could help in reviving cell growth to some extent, due to high cell density following each medium-replacement and subsequently high metabolic activity, the culture rapidly returned to undesirable conditions. Thus gradually the cells lost their ability for growth and the cell concentration maxima became lower after each medium-replacement event.

Sensitivity to nutrients and metabolites: In this study glucose and glutamine, although they were not limiting, were found to be essential for cell growth. The levels of glucose should not be too high so as to avoid high lactate concentration and osmolality, but should not be too low to avoid depletion that may initiate apoptotic cell death.

Sensitivity to pH control: As seen in Chapter 9, pH control by base addition resulted in higher cell growth as compared to cultures where pH was not controlled. Levels of pH 7.1-7.2 were optimal for growth but control of pH by base addition resulted in markedly high glucose consumption rate and corresponding higher lactate production rate.

Analytical methods: Although it was initially intended to measure the concentration of ligands such as FASL that mediate cell-cell communication related apoptosis, these measurements were not conclusive

due to background noise or nonspecific binding in the western blot technique used for that purpose. Signal to noise ratio in the western blot technique for measuring FASL activity can be improved by using CHO version of primary antibody, by manipulating blocking time and protein concentration loaded into gel and by optimizing the concentration of primary and secondary antibody.

Recommendations and Future Work

- Testing cell reversibility following exposure to non-optimal levels of pH or to glucose depletion conditions. Irreversibility in cell growth inhibition was found to be important in medium-replacement experiments. This subject could be investigated through operation of continuous reactors and by correlating time of exposure to unfavorable conditions with irreversibilities.

- Glucose resulted in high buildup of lactate which may be inhibitory. Thus, future work should investigate the use of other slower utilized carbon sources galactose or fructose, which considerably reduces formation of lactate. However, these carbon sources might result in slower cell growth because of slower utilization. Similarly glutamine concentration should be manipulated to avoid excessive buildup of ammonia.

- The faster depletion of glucose in the pH controlled experiment was followed by very steep decrease in cell viability. Future work should study pH controlled fed-batch operation where glucose is fed continuously to avoid depletion while avoiding excessive lactate buildup or high osmolality.

- The medium-replacement was found to be beneficial for growth and mAb productivity. It is suggested to investigate the implementation of an optimal schedule of medium-replacements to maximize productivity. The model developed in this work is an ideal tool to perform such optimization task.

- The sensitivity of growth to volume also encourages implementation of monitoring CO_2 levels for optimal process operation and implementation of strategies for its faster removal from a suspension culture. For industrial bioreactors, the requirement of large headspace or an open system with continuous flow of air becomes necessary. This should ensure that CO_2 produced by cells satisfactorily diffuse from culture medium without accumulation and thus subsequence drop in pH. In laboratory reactors (spinner flasks), a simple approach could be leveling off the CO_2 level slowly inside the incubator before the cells reach the maximal density.

- Since pH is an important factor in controlling cell growth, attention should be given to reduce the effect of pH. A way to reduce the effect of pH, is to use a medium of higher buffering capacity that will sustain any large changes in pH.

Appendices

Appendix A

Derivatization reaction in HPLC separation of amino acids
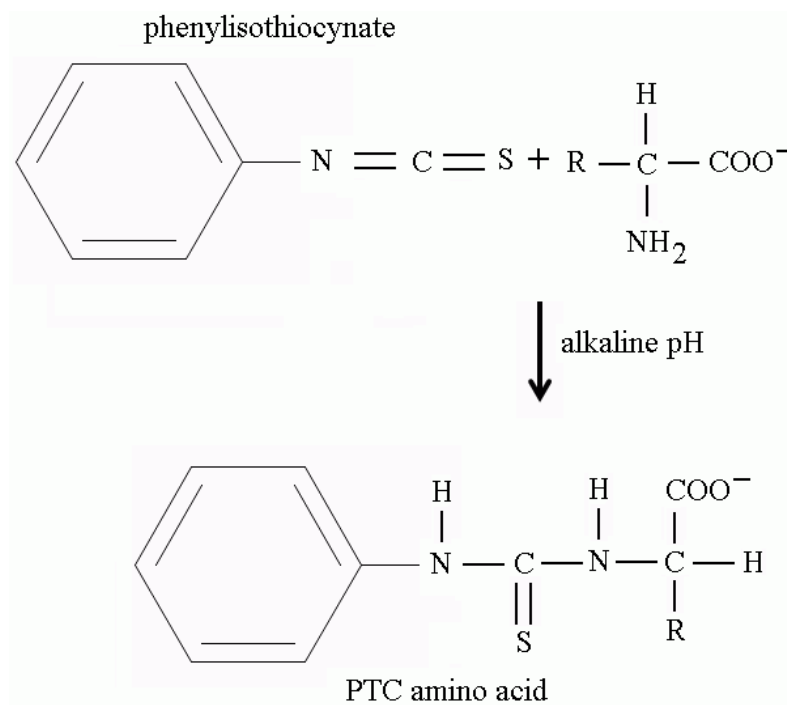
Derivatization reaction of PITC (phenylisothiocyanate) with amino acid forming PTC (phenylthiocarbamyl) (Butler and Dawson, 1992)

Appendix B

Calculation of the specific depletion and production rates

The specific consumption and production rates can be denoted as follows

$$\frac{dC}{dt} = q_c X_v$$

where C represents a nutrient/metabolite/product (glucose, lactate or mAb) concentration

$$\Delta C = q_c \int_0^t X_v \, dt$$

The quantity q_c over the whole culture period was calculated from the slope of the plot of ΔC vs. time integral of viable cells (TIV), $\int_0^t X_v \, dt$. The viable cell concentration being a continuous function, the quantity $\int_0^t X_v \, dt$ was evaluated at each sample point φ by the trapezoidal rule as follows

$$TIV(\varphi) = \sum_{i=1}^{\varphi} \frac{X_{v(i)} + X_{v(i-1)}}{2} (t_i - t_{i-1})$$

where i represents all the sample points

MATLAB function was used to evaluate the trapezoid to calculate the TIV.

Appendix C

Statistical test for q_p among serum level experiments

A sample was generated by calculating instantaneous slopes of the plot of time integral of viable cells and mAb concentration (Figure 6.8) in each experiment SP5-8. The variability associated with these slopes corresponding to each experiment were compared each other by F-test. Following shows the results of the test at a significance level of 5%.

	F_{obs}	F_{test}
SP5-SP6	3.11	9.27 (df2/df1-3/2)
SP5-SP7	2.42	9.5 (df2/df1-3/2)
SP5-SP8	1.10	9.5 (df2/df1-3/2)
SP6-SP7	7.55	19 (df2/df1-2/2)
SP6-SP8	2.82	19 (df2/df1-2/2)
SP7-SP8	2.67	19 (df2/df1-2/2)

Appendix D

Parameter estimates of the integrated model

Apoptosis Model				Metabolic Flux Model			
Parameter	Value	Parameter	Value	Parameter	Value	Parameter	Value
μ_g	0.71	k_{10}	0.16	a_1	0.38	a_{44}	0.34
μ_e	1.34	α	1.28	a_2	0.0003	a_{55}	1×10^{-5}
μ_i	0.05	k_I	0.07	a_3	0.0243	a_{66}	0.04
μ_{dmax}	0.99	k_{i1}	8.98	a_4	0.12	a_{77}	0.27
k_4	2.8	k_{i2}	0.001	a_5	1.48	a_{88}	0.97
k_5	4.5	k_{i3}	0.50	a_6	1.34×10^{-5}	k_{Glc}	2.41
k_8	0.0013	k_{lys}	0.09	a_7	0.071	k_{Gln}	0.509
k_9	5.13	I_∞	0.001	a_8	0.024	k_{Gln5}	4.968
γ	0.03	k_{va}	7.99	q_p	3.15	k_{Glu}	0.223
K_{d_A}	6.05	k_a	0.99	a_{11}	3.48	k_{Asn}	0.096
q_{p1}	4.4 (single medium-replacement) 5.1 (double medium-replacement)			a_{22}	22.1	k_{Asp}	0.0605
q_{p2}	9.9 (single medium-replacement) 8.0 (double medium-replacement)			a_{33}	0.45	k_{Ala}	0.109

Appendix E

Identifiability analysis of parameter estimates of the integrated model

Parameter	Sensitivity score	Identifiability score	Parameter	Sensitivity score	Identifiability score
k_a	15.95	9416.05	a_7	0.103	0.31
α	7.69	2079.34	a_{77}	0.089	0.27
μ_g	2.33	84.52	a_{33}	0.099	0.24
μ_i	1.91	50.71	a_{11}	0.110	0.13
μ_d	2.91	43.28	k_{i1}	0.299	0.012
k_4	1.26	29.80	a_3	0.049	0.010
μ_e	3.61	8.16	a_{66}	0.020	0.007
q_p	0.46	7.70	γ	0.040	0.001
a_1	0.42	5.98	k_{va}	0.272	3.02E-05
a_4	0.419	5.62	a_2	0.0008	8.29E-06
a_{22}	0.413	5.48	k_I	0.109	7.11E-06
k_9	0.553	5.20	k_{i3}	0.003	5.27E-06
k_5	0.975	2.69	k_8	0.001	2.49E-06
a_5	0.441	2.10	a_{55}	8.19E-05	5.73E-08
k_{10}	0.803	1.73	a_6	8.6E-05	2.41E-08
a_{88}	0.522	1.37	I_∞	0.0004	8.83E-10
a_8	0.185	1.10	k_{i2}	2E-05	3.36E-11
k_{lys}	0.197	0.94	K_{d_A}	0.038	3.4E-12
a_{44}	0.173	0.80			

Appendix F

Titration curve

The following observation indicates titration curve generated in 250 mL of culture in decline phase by addition of 1N NaOH (base) for adjusting pH in culture medium. Following observations were extrapolated for 500 mL culture volume.

Volume of base added (µL)	pH of culture after addition of base	Total volume of base for a given pH value to reach (µL)
0	6.54	0
2	6.55	2
5	6.55	7
10	6.56	17
20	6.57	37
40	6.6	77
50	6.63	127
70	6.67	197
90	6.73	287
100	6.79	387
100	6.84	487
100	6.9	587
100	6.96	687
100	7.01	787
100	7.06	887
100	7.12	987
100	7.17	1087
100	7.23	1187
100	7.27	1287
100	7.32	1387

Titration curve

y = 0.0006x + 6.5565
R² = 0.9985

pH

Volume of 1N NaOH (μL)
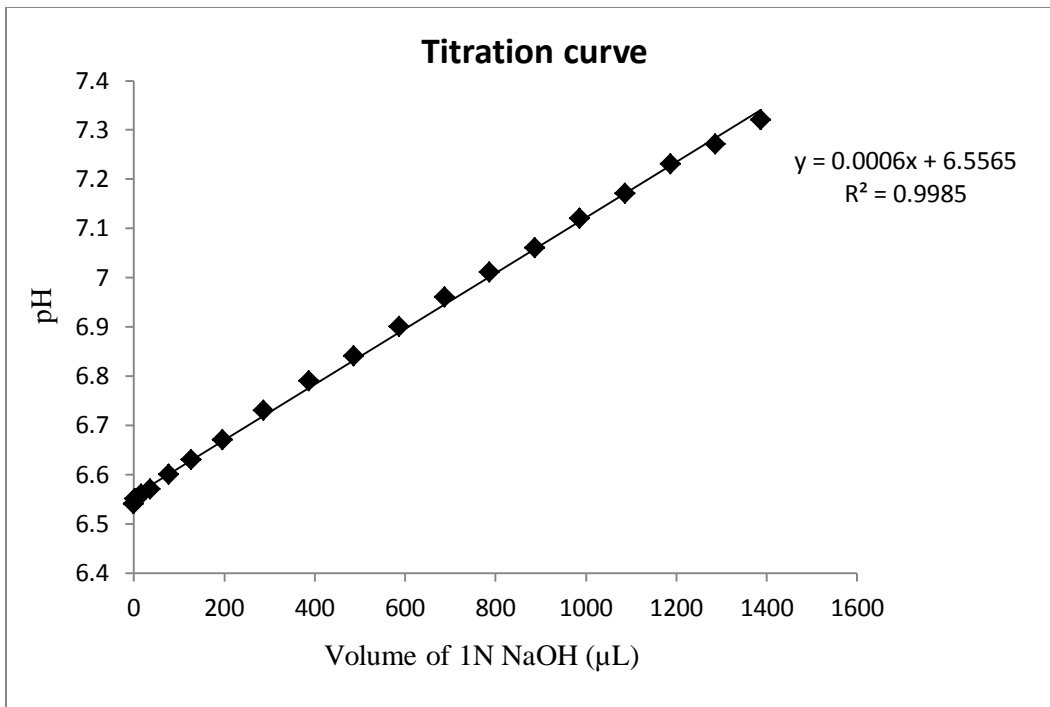
Bibliography

Aggarwal, B.B. (2003). Signalling pathways of the TNF superfamily: a double-edged sword. Nat Rev Immunol *3*, 745-756.

Akaike, H. (1973). Information theory as an extension of the maximum likelihood principle. . In Second International Symposiumon Information Theory, B.C. Petrov, F, ed. (Budapest: Akademiai), pp. 267-281.

Al-Rubeai, M. (1997). Apoptosis and cell culture technology. Adv Biochem Biotechnol *59*, 225-249.

Al-Rubeai, M., Emery, A.N., and Chalder, S. (1991). Flow cytometric study of cultured mammalian cells. J Biotechnol *19*, 67-81.

Al-Rubeai, M., and Ishaque, A. (1998). Use of intracellular pH and annexin-V flow cytometric assays to monitor apoptosis and its suppression by bcl-2 over-expression in hybridoma cell culture. J Immunol Methods *221*, 43-57.

Al-Rubeai, M., Leelavatcharamas, V., and Emery, A.N. (1999). Use of cell cycle analysis to characterise growth and interferon-gamma production in perfusion culture of CHO cells. Cytotechnology *30*, 59-69.

Andersen, D.C., and Reilly, D.E. (2004). Production technologies for monoclonal antibodies and their fragments. Curr Opin Biotech *15*, 456-462.

Arden, N., and Betenbaugh, M.J. (2004). Life and death in mammalian cell culture: strategies for apoptosis inhibition. Trends Biotechnol *22*, 174-180.

Arden, N., Majors, B.S., Ahn, S., Oyler, G., and Betenbaugh, M.J. (2006). Inhibiting the Apoptosis Pathway Using MDM2 in Mammalian Cell Cultures. Biotechnol Bioeng *97*, 601 – 614.

Ashkenazi, A., and Dixit, V.M. (1998). Death receptors: signaling and modulation. Science *281*, 1305-1308.

Aunins, J.G., and Henzler, H.-J. (1993). Aeration in Cell Culture Bioreactors. In Biotechnology: A Multi-volume Comprehensive Treatise (Vol 3), Bioprocessing (Weinheim, Germany, VCH Verlag).

Avgerinos, G.C., Drapeau, D., Socolow, J.S., Mao, J., Hsiao, K., and Broeze, R.J. (1990). Spin Filter Perfusion System for High-Density Cell-Culture - Production of Recombinant Urinary Type Plasminogen-Activator in Cho Cells. Bio-Technol *8*, 54-58.

Bachinger, T., Riese, U., Eriksson, R., and Mandenius, C.F. (2000). Monitoring cellular state transitions in a production-scale CHO-cell process using an electronic nose. Journal of Biotechnology *76*, 61-71.

Bagci, E.Z., Vodovotz, Y., Billiar, T.R., Ermentrout, G.B., and Bahar, I. (2006). Bistability in apoptosis: Roles of Bax, Bcl-2, and mitochondrial permeability transition pores. Biophys J *90*, 1546-1559.

Bailey, J.E., Zanghi, J.A., and Fussenegger, M. (1999). Serum protects protein-free competent Chinese hamster ovary cells against apoptosis induced by nutrient deprivation in batch culture. Biotechnology and Bioengineering *64*, 108-119.

Bakalczuk, G., Jakiel, G., Rolinski, J., and Podhorecka, M. (2003). The flow cytometry study of Annexin-V binding by human spermatozoa – is it a marker of apoptosis? . Central Eur J Immunol *28* 19–22.

Banik, G.G., and Heath, C.A. (1995). Hybridoma Growth and Antibody-Production as a Function of Cell-Density and Specific Growth-Rate in Perfusion Culture. Biotechnology and Bioengineering *48*, 289-300.

Bao, Q., and Shi, Y. (2007). Apoptosome: a platform for the activation of initiator caspases. Cell Death Differ *14*, 56-65.

Baserga, R. (1985). The Biology of Cell Reproduction (Cambridge, Massachusetts, Harvard University Press).

Beck, J.V., and Arnold, K. (1977). Parameter Estimation in Engineering and Science (John Wiley & Sons).

Benford, H.L., McGowan, N.W., Helfrich, M.H., Nuttall, M.E., and Rogers, M.J. (2001). Visualization of bisphosphonate-induced caspase-3 activity in apoptotic osteoclasts in vitro. Bone *28*, 465-473.

Bentele, M., Lavrik, I., Ulrich, M., Stosser, S., Heermann, D.W., Kalthoff, H., Krammer, P.H., and Eils, R. (2004). Mathematical modeling reveals threshold mechanism in CD95-induced apoptosis. J Cell Biol *166*, 839-851.

Bi, J.X., Buhr, P., Zeng, A.P., and Wirth, M. (2003). Human c-fos promoter mediates high-level, inducible expression in various mammalian cell lines. Biotechnology and Bioengineering *81*, 848-854.

Bibila, T.A., and Robinson, D.K. (1995). In Pursuit of the Optimal Fed-Batch Process for Monoclonal-Antibody Production. Biotechnol Progr *11*, 1-13.

Bidlingmeyer, B.A., Cohen, S.A., and Tarvin, T.L. (1984). Rapid analysis of amino acids using pre-column derivatization. J Chromatogr *336*, 93-104.

Birch, J.R., and Edwards, D.J. (1980). The effect of pH on the growth and carbohydrate metabolism of a lymphoblastoid cell line. Dev Biol Stand *46*, 59-63.

Birch, J.R., and Racher, A.J. (2006). Antibody production. Adv Drug Deliver Rev *58*, 671-685.

Boedecker, B.G.D., Newcomb. R., Yuan, P., Braufman, A., Kelsey, W. (1994). Production of recombinant factor VIII from perfusion cultures. In Animal cell technology: products of today, prospects

for tomorrow, R.E. Spier, Griffiths, J.B., Berthold, W., ed. (Butterworth Heinemann, Oxford), pp. 580-583.

Bonarius, H.P.J., Hatzimanikatis, V., Meesters, K.P.H., deGooijer, C.D., Schmid, G., and Tramper, J. (1996). Metabolic flux analysis of hybridoma cells in different culture media using mass balances. Biotechnology and Bioengineering *50*, 299-318.

Brekke, O.H., and Sandlie, I. (2003). Therapeutic antibodies for human diseases at the dawn of the twenty-first century. Nat Rev Drug Discov *2*, 52-62.

Broker, L.E., Kruyt, F.A.E., and Giaccone, G. (2005). Cell death independent of caspases: A review. Clinical Cancer Research *11*, 3155-3162.

Brun, R., Kuhni, M., Siegrist, H., Gujer, W., and Reichert, P. (2002). Practical identifiability of ASM2d parameters--systematic selection and tuning of parameter subsets. Water Res *36*, 4113-4127.

Burger, W.B., and Burge, M. (2008). Digital Image Processing - An Algorithmic Introduction using Java (New York, USA, Springer Publishing Co.).

Burhans, W.C., Weinberger, M., Feng, L., Paul, A., Smith, D.L., Hontz, R.D., Smith, J.S., Vujcic, M., Singh, K.K., and Huberman, J.A. (2007). DNA Replication Stress Is a Determinant of Chronological Lifespan in Budding Yeast. Plos One *2*.

Burnham, K.P., and Anderson, D.R. (2004). Multimodel inference - understanding AIC and BIC in model selection. Sociol Method Res *33*, 261-304.

Butler, M. (2005). Animal cell cultures: recent achievements and perspectives in the production of biopharmaceuticals. Appl Microbiol Biotechnol *68*, 283-291.

Butler, M., Dawson, M. (1992). Cell Culture (Oxford, UK, Bios Scientific Publishers Ltd. and Academic Press).

Cai, K., Ren, C., and Yu, Z. (2010). Nickel-induced apoptosis and relevant signal transduction pathways in Caenorhabditis elegans. Toxicol Ind Health *26*, 249-256.

Carrondo, M.J.T., Cruz, H.J., and Moreira, J.L. (1999). Metabolic shifts by nutrient manipulation in continuous cultures of BHK cells. Biotechnology and Bioengineering *66*, 104-113.

Chanas-Sacre, G., Rogister, B., Moonen, G., and Leprince, P. (2000). Radial glia phenotype: Origin, regulation, and transdifferentiation. J Neurosci Res *61*, 357-363.

Chattopadhyay, S., Yamashita, M., Zhang, Y., and Sen, G.C. (2011). The IRF-3/Bax-Mediated Apoptotic Pathway, Activated by Viral Cytoplasmic RNA and DNA, Inhibits Virus Replication. J Virol *85*, 3708-3716.

Chen, C., Cui, J., Lu, H., Wang, R., Zhang, S., and Shen, P. (2007b). Modeling of the role of a Bax-activation switch in the mitochondrial apoptosis decision. Biophys J *92*, 4304-4315.

Chen, C., Cui, J., Zhang, W., and Shen, P. (2007a). Robustness analysis identifies the plausible model of the Bcl-2 apoptotic switch. Febs Lett *581*, 5143-5150.

Chittenden, T., Flemington, C., Houghton, A.B., Ebb, R.G., Gallo, G.J., Elangovan, B., Chinnadurai, G., and Lutz, R.J. (1995). A Conserved Domain in Bak, Distinct from BH1 and BH2, Mediates Cell-Death and Protein-Binding Functions. Embo J *14*, 5589-5596.

Choi, H.S., Han, S., Yokota, H., and Cho, K.H. (2007). Coupled positive feedbacks provoke slow induction plus fast switching in apoptosis. Febs Lett *581*, 2684-2690.

Cipollaro, M., Corsale, G., Esposito, A., Ragucci, E., Staiano, N., Giordano, G.G., and Pagano, G. (1986). Sublethal pH decrease may cause genetic damage to eukaryotic cell: a study on sea urchins and Salmonella typhimurium. Teratog Carcinog Mutagen *6*, 275-287.

Cockett, M.I., Bebbington, C.R., and Yarranton, G.T. (1990). High-Level Expression of Tissue Inhibitor of Metalloproteinases in Chinese Hamster Ovary Cells Using Glutamine-Synthetase Gene Amplification. Bio-Technol *8*, 662-667.

Cohen, G.M. (1997). Caspases: the executioners of apoptosis. Biochem J *326 (Pt 1)*, 1-16.

Crompton, M. (1999). The mitochondrial permeability transition pore and its role in cell death. Biochem J *341 (Pt 2)*, 233-249.

Cui, J., Chen, C., Lu, H., and Shen, P. (2008). Modelling of the mitochondrial apoptosis network. Int J Bioinform Res Appl *4*, 172-187.

Dalili, M., and Ollis, D.F. (1989). Transient Kinetics of Hybridoma Growth and Monoclonal-Antibody Production in Serum-Limited Cultures. Biotechnology and Bioengineering *33*, 984-990.

Dally, H., and Hartwig, A. (1997). Induction and repair inhibition of oxidative DNA damage by nickel(II) and cadmium(II) in mammalian cells. Carcinogenesis *18*, 1021-1026.

Darzynkiewicz, Z., Juan, G., Li, X., Gorczyca, W., Murakami, T., and Traganos, F. (1997). Cytometry in cell necrobiology: analysis of apoptosis and accidental cell death (necrosis). Cytometry *27*, 1-20.

De Jong, H. (2002). Modeling and simulation of genetic regulatory systems: A literature review. J Comput Biol *9*, 67-103.

Deo, Y.M., Mahadevan, M.D., and Fuchs, R. (1996). Practical considerations in operation and scale-up of spin-filter based bioreactors for monoclonal antibody production. Biotechnol Progr *12*, 57-64.

DeTremblay, M., Perrier, M., Chavarie, C., and Archambault, J. (1992). Optimization of Fed-Batch Culture of Hybridoma Cells Using Dynamic-Programming - Single and Multi Feed Cases. Bioprocess Eng *7*, 229-234.

Dezengotita, V.M., Kimura, R., and Miller, W.M. (1998). Effects of CO_2 and osmolality on hybridoma cells: growth, metabolism and monoclonal antibody production. Cytotechnology *28*, 213-227.

DeZengotita, V.M., Schmeizer, A.E., and Miller, W.M. (2002). Characterization of hybridoma cell response to elevated pCO_2 and osmolality: Intracellular pH, cell size, apoptosis and metabolis. Biotechnol Bioeng *77*, 369-380.

Dorka, P., Fischer, C., Budman, H., and Scharer, J. (2009). Metabolic flux-based modeling of mAb production during batch and fed-batch operations. Bioproc Biosyst Eng *32*, 183-196.

Droin, N., Cathelin, S., Jacquel, A., Guery, L., Garrido, C., Fontenay, M., Hermine, O., and Solary, E. (2008). A role for caspases in the differentiation of erythroid cells and macrophages. Biochimie *90*, 416-422.

Eissing, T., Conzelmann, H., Gilles, E.D., Allgower, F., Bullinger, E., and Scheurich, P. (2004). Bistability analyses of a caspase activation model for receptor-induced apoptosis. J Biol Chem *279*, 36892-36897.

Elias, C.B., Zeiser, A., Bedard, C., and Kamen, A.A. (2000). Enhanced growth of Sf-9 cells to a maximum density of 5.2 x 10(7) cells per mL and production of beta-galactosidase at high cell density by fed batch culture. Biotechnol Bioeng *68*, 381-388.

Emery, A.N., Jan, D.C.H., and Alrubeai, M. (1995). Oxygenation of Intensive Cell-Culture System. Appl Microbiol Biot *43*, 1028-1033.

Even, M.S., Sandusky, C.B., and Barnard, N.D. (2006). Serum-free hybridoma culture: ethical, scientific and safety considerations. Trends Biotechnol *24*, 105-108.

Follstad, B.D., Balcarcel, R.R., Stephanopoulos, G., and Wang, D.I.C. (1999). Metabolic flux analysis of hybridoma continuous culture steady state multiplicity. Biotechnology and Bioengineering *63*, 675-683.

Fox, S.R., Patel, U.A., Yap, M.G.S., and Wang, D.I.C. (2004). Maximizing interferon-gamma production by Chinese hamster ovary cells through temperature shift optimization: Experimental and modeling. Biotechnology and Bioengineering *85*, 177-184.

Frame, K.K., and Hu, W.S. (1991). Kinetic-Study of Hybridoma Cell-Growth in Continuous Culture .2. Behavior of Producers and Comparison to Nonproducers. Biotechnology and Bioengineering *38*, 1020-1028.

Franek, F., and Dolnikova, J. (1991). Nucleosomes occurring in protein-free hybridoma cell culture. Evidence for programmed cell death. Febs Lett *284*, 285-287.

Fussenegger, M., and Bailey, J.E. (1998). Molecular regulation of cell-cycle progression and apoptosis in mammalian cells: Implications for biotechnology. Biotechnol Progr *14*, 807-833.

Fussenegger, M., Bailey, J.E., and Varner, J. (2000). A mathematical model of caspase function in apoptosis. Nature Biotechnology *18*, 768-774.

Gadkar, K.G., Gunawan, R., and Doyle, F.J. (2005a). Iterative approach to model identification of biological networks. Bmc Bioinformatics *6*.

Gadkar, K.G., Varner, J., and Doyle, F.J., 3rd (2005b). Model identification of signal transduction networks from data using a state regulator problem. Syst Biol (Stevenage) *2*, 17-30.

Gandor, C., Leist, C., Fiechter, A., and Asselbergs, F.A.M. (1995). Amplification and expression of recombinant genes in serum-independent Chinese hamster ovary cells. Febs Lett *377*, 290-294.

Gao, J.Y., Gorenflo, V.M., Scharer, J.M., and Budman, H.M. (2007). Dynamic metabolic modeling for a MAB bioprocess. Biotechnol Progr *23*, 168-181.

Geffen, D. (2008). Parameter Identifiability of Biochemical Reaction Networks in Systems Biology. In Department of Chemical Engineering (Kingston, Queen's University).

Gheshlaghi, R., Scharer, J.M., Moo-Young, M., and Douglas, P.L. (2008). Application of statistical design for the optimization of amino acid separation by reverse-phase HPLC. Anal Biochem *383*, 93-102.

Giuliano, M., Lauricella, M., Vassallo, E., Carabillo, M., Vento, R., and Tesoriere, G. (1998). Induction of apoptosis in human retinoblastoma cells by topoisomerase inhibitors. Invest Ophthalmol Vis Sci *39*, 1300-1311.

Goldstein, J.C., Waterhouse, N.J., Juin, P., Evan, G.I., and Green, D.R. (2000). The coordinate release of cytochrome c during apoptosis is rapid, complete and kinetically invariant. Nat Cell Biol *2*, 156-162.

Golstein, P. (1997). Cell death: TRAIL and its receptors. Curr Biol *7*, R750-753.

Golstein, P., Ojcius, D.M., and Young, J.D.E. (1991). Cell-Death Mechanisms and the Immune-System. Immunol Rev *121*, 29-65.

Goswami, J., Sinskey, A.J., Steller, H., Stephanopoulos, G.N., and Wang, D.I.C. (1999). Apoptosis in batch cultures of Chinese Hamster Ovary cells. Biotechnology and Bioengineering *62*, 632-640.

Gottlieb, R.A. (1996). Cell acidification in apoptosis. Apoptosis *1*, 40.

Goudar, C.T., Joeris, K., Konstantinov, K.B., and Piret, J.M. (2005). Logistic equations effectively model Mammalian cell batch and fed-batch kinetics by logically constraining the fit. Biotechnol Prog *21*, 1109-1118.

Goudar, C.T., Matanguihan, R., Long, E., Cruz, C., Zhang, C., Piret, J.M., and Konstantinov, K.B. (2006). Decreased pCO_2 accumulation by eliminating bicarbonate addition to high celldensity cultures. Biotechnol Bioeng *96*, 1107-1117.

Gozuacik, D., and Kimchi, A. (2004). Autophagy as a cell death and tumor suppressor mechanism. Oncogene *23*, 2891-2906.

Gray, D.R., Chen, S., Howarth, W., Inlow, D., and Maiorella, B.L. (1996). CO_2 in large-scale and high-density CHO cell perfusion culture. Cytotechnology *22*, 65-78.

Han, Y.K., Kim, Y.G., Kim, J.Y., and Lee, G.M. (2010). Hyperosmotic Stress Induces Autophagy and Apoptosis in Recombinant Chinese Hamster Ovary Cell Culture. Biotechnology and Bioengineering *105*, 1187-1192.

Hansen, H.A., and Emborg, C. (1994). Influence of ammonium on growth, metabolism, and productivity of a continuous suspension Chinese hamster ovary cell culture. Biotechnol Prog *10*, 121-124.

Hardy, K., and Stark, J. (2002). Mathematical models of the balance between apoptosis and proliferation. Apoptosis *7*, 373-381.

Harrington, H.A., Ho, K.L., Ghosh, S., and Tung, K.C. (2008). Construction and analysis of a modular model of caspase activation in apoptosis. Theor Biol Med Model *5*, 26.

Hartwell, L.H., and Kastan, M.B. (1994). Cell cycle control and cancer. Science *266*, 1821-1828.

Hassell, T., Gleave, S., and Butler, M. (1991). Growth-Inhibition in Animal-Cell Culture - the Effect of Lactate and Ammonia. Appl Biochem Biotech *30*, 29-41.

Hawkins, E.D., Turner, M.L., Dowling, M.R., van Gend, C., and Hodgkin, P.D. (2007). A model of immune regulation as a consequence of randomized lymphocyte division and death times. P Natl Acad Sci USA *104*, 5032-5037.

Heidemann, R., Lutkemeyer, D., Buntemeyer, H., and Lehmann, J. (1998). Effects of dissolved oxygen levels and the role of extra- and intracellular amino acid concentrations upon the metabolism of mammalian cell lines during batch and continuous cultures. Cytotechnology *26*, 185-197.

Hooks, M.A., Wade, C.S., and Millikan, W.J. (1991). Muromonab Cd-3 - a Review of Its Pharmacology, Pharmacokinetics, and Clinical Use in Transplantation. Pharmacotherapy *11*, 26-37.

Houweling, A.C., Philippens, M.E., Dijkema, T., Roesink, J.M., Terhaard, C.H., Schilstra, C., Ten Haken, R.K., Eisbruch, A., and Raaijmakers, C.P. (2010). A comparison of dose-response models for the parotid gland in a large group of head-and-neck cancer patients. Int J Radiat Oncol Biol Phys *76*, 1259-1265.

Hu, W.S., Europa, A.F., Gambhir, A., and Fu, P.C. (2000). Multiple steady states with distinct cellular metabolism in continuous culture of mammalian cells. Biotechnology and Bioengineering *67*, 25-34.

Hua, F., Cornejo, M.G., Cardone, M.H., Stokes, C.L., and Lauffenburger, D.A. (2005). Effects of Bcl-2 levels on Fas signaling-induced caspase-3 activation: molecular genetic tests of computational model predictions. J Immunol *175*, 985-995.

Huber, H.J., Rehm, M., Plchut, M., Dussmann, H., and Prehn, J.H. (2007). APOPTO-CELL--a simulation tool and interactive database for analyzing cellular susceptibility to apoptosis. Bioinformatics *23*, 648-650.

Huerta, S., Goulet, E.J., Huerta-Yepez, S., and Livingston, E.H. (2007). Screening and detection of apoptosis. J Surg Res *139*, 143-156.

Hurvich, C.M., and Tsai, C.L. (1989). Regression and Time-Series Model Selection in Small Samples. Biometrika *76*, 297-307.

Hwang, S.O., and Lee, G.M. (2008). Nutrient deprivation induces autophagy as well as apoptosis in Chinese hamster ovary cell culture. Biotechnology and Bioengineering *99*, 678-685.

Ibuki, Y., Naitou, H., Ohashi, N., and Goto, R. (2005). Proteome analysis of UV-B-induced anti-apoptotic regulatory factors. Photochem Photobiol *81*, 823-829.

Ishioka, S., Ezaka, Y., Umemura, K., Hayashi, T., Endo, T., and Saito, T. (2007). Proteomic analysis of mechanisms of hypoxia-induced apoptosis in trophoblastic cells. Int J Med Sci *4*, 36-44.

Ishizaki, Y., Burne, J., and Raff, M.C. (1994). Autocrine signlas enables chondrocytes to survive in the culture. J Cell Biol *126*, 13-20.

Jo, E.C., Kim, D.I., and Moon, H.M. (1993). Step-Fortifications of Nutrients in Mammalian-Cell Culture. Biotechnology and Bioengineering *42*, 1218-1228.

Jolly, A.J., Wild, C.P., and Hardie, L.J. (2004). Acid and bile salts induce DNA damage in human oesophageal cell lines. Mutagenesis *19*, 319-324.

Kay, S.M. (1993). Fundamentals of Statistical Signal Processing, Estimation Theory, Englewood Cliffs, NJ, Prentice-Hall.

Kim, K., Lee, S.H., Seo, Y.R., Perkins, S.N., and Kasprzak, K.S. (2002). Nickel(II)-induced apoptosis in murine T cell hybridoma cells is associated with increased Fas ligand expression. Toxicol Appl Pharm *185*, 41-47.

Kimura, R., and Miller, W.M. (1996). Effects of elevated pCO(2) and/or osmolality on the growth and recombinant tPA production of CHO cells. Biotechnology and Bioengineering *52*, 152-160.

King, D.J. (1998). Preparation, structure and function of monoclonal antibodies. Applications And Engineering Of Monoclonal Antibodies, CRC, UK, 1-25.

Kluck, R.M., Bossy-Wetzel, E., Green, D.R., and Newmeyer, D.D. (1997). The release of cytochrome c from mitochondria: a primary site for Bcl-2 regulation of apoptosis. Science *275*, 1132-1136.

Kohler, G., and Milstein, C. (1975). Continuous Cultures of Fused Cells Secreting Antibody of Predefined Specificity. Nature *256*, 495-497.

Kumar, N., Gammell, P., Meleady, P., Henry, M., and Clynes, M. (2008). Differential protein expression following low temperature culture of suspension CHO-K1 cells. BMC Biotechnol *8*, 42.

Kuwana, T., Mackey, M.R., Perkins, G., Ellisman, M.H., Latterich, M., Schneiter, R., Green, D.R., and Newmeyer, D.D. (2002). Bid, Bax, and lipids cooperate to form supramolecular openings in the outer mitochondrial membrane. Cell *111*, 331-342.

Lai, R., and Jackson, T.L. (2004). A mathematical model of receptor-mediated apoptosis: dying to know why fasl is a trimer. Math Biosci Eng *1*, 325-338.

Laken, H.A., and Leonard, M.W. (2001). Understanding and modulating apoptosis in industrial cell culture. Curr Opin Biotechnol *12*, 175-179.

Lao, M.S., and Toth, D. (1997). Effects of ammonium and lactate on growth and metabolism of a recombinant Chinese hamster ovary cell culture. Biotechnol Prog *13*, 688-691.

Lavrik, I.N., Golks, A., Riess, D., Bentele, M., Eils, R., and Krammer, P.H. (2007). Analysis of CD95 threshold signaling - Triggering of CD95 (FAS/APO-1) at low concentrations primarily results in survival signaling. J Biol Chem *282*, 13664-13671.

Lee, E. (2002). Kinetic analysis of the effect of cell density on hybridoma cell growth in batch culture. Biotechnology and Bioprocess Engineering *7*, 117-120.

Lee, J.C., Chang, H.N., and Oh, D.J. (2005). Recombinant antibody production by perfusion cultures of rCHO cells in a depth filter perfusion system. Biotechnol Progr *21*, 134-139.

Lee, Y.Y., Yap, M.G.S., Hu, W.S., and Wong, K.T.K. (2003). Low-glutamine fed-batch cultures of 293-HEK serum-free suspension cells for adenovirus production. Biotechnol Progr *19*, 501-509.

Legewie, S., Bluthgen, N., and Herzel, H. (2006). Mathematical modeling identifies inhibitors of apoptosis as mediators of positive feedback and bistability. Plos Comput Biol *2*, e120.

Leist, M., and Jaattela, M. (2001). Four deaths and a funeral: from caspases to alternative mechanisms. Nat Rev Mol Cell Biol *2*, 589-598.

Letai, A., Bassik, M.C., Walensky, L.D., Sorcinelli, M.D., Weiler, S., and Korsmeyer, S.J. (2002). Distinct BH3 domains either sensitize or activate mitochondrial apoptosis, serving as prototype cancer therapeutics. Cancer Cell *2*, 183-192.

Li, X., Traganos, F., Melamed, M.R., and Darzynkiewicz, Z. (1995). Single-step procedure for labeling DNA strand breaks with fluorescein- or BODIPY-conjugated deoxynucleotides: detection of apoptosis and bromodeoxyuridine incorporation. Cytometry *20*, 172-180.

Link, T., Backstrom, M., Graham, R., Essers, R., Zorner, K., Gatgens, J., Burchell, J., Taylor-Papadimitriou, J., Hansson, G.C., and Noll, T. (2004). Bioprocess development for the production of a recombinant MUC1 fusion protein expressed by CHO-K1 cells in protein-free medium. Journal of Biotechnology *110*, 51-62.

Linz, M., Zeng, A.P., Deckwer, W. D. (1999). Induction kinetics of apoptosis in mammalian cell cultures, Animal Cell Technology: Products from Cells, Cells as Products. Kluwer Academic Publishers,Netherland, 127-129.

Liu, L., Chahroudi, A., Silvestri, G., Wernett, M.E., Kaiser, W.J., Safrit, J.T., Komoriya, A., Altman, J.D., Packard, B.Z., and Feinberg, M.B. (2002). Visualization and quantification of T cell-mediated cytotoxicity using cell-permeable fluorogenic caspase substrates. Nat Med *8*, 185-189.

Ljunggren, J., and Haggstrom, L. (1994). Catabolic control of hybridoma cells by glucose and glutamine limited fed batch cultures. Biotechnol Bioeng *44*, 808-818.

Lloyd, D.R., Holmes, P., Jackson, L.P., Emery, A.N., and Al-Rubeai, M. (2000). Relationship between cell size, cell cycle and specific recombinant protein productivity. Cytotechnology *34*, 59-70.

Lorz, C., Ortiz, A., Justo, P., Gonzalez-Cuadrado, S., Duque, N., Gomez-Guerrero, C., and Egido, J. (2000). Proapoptotic Fas ligand is expressed by normal kidney tubular epithelium and injured glomeruli. J Am Soc Nephrol *11*, 1266-1277.

Majno, G., and Joris, I. (1995). Apoptosis, oncosis, and necrosis. An overview of cell death. Am J Pathol *146*, 3-15.

Malhotra, R., Lin, Z., Vincenz, C., and Brosius, F.C., 3rd (2001). Hypoxia induces apoptosis via two independent pathways in Jurkat cells: differential regulation by glucose. Am J Physiol Cell Physiol *281*, C1596-1603.

Mangalampalli, V.R.M., Mowry, M.C., Lipscomb, M.L., James, R.I., Johnson, A.K., and Kompala, D.S. (2002). Increased production of a secreted glycoprotein in engineered CHO cells through amplification of a transcription factor. Cytotechnology *38*, 23-35.

Manns, J., Daubrawa, M., Driessen, S., Paasch, F., Hoffmann, N., Loffler, A., Lauber, K., Dieterle, A., Alers, S., Iftner, T.*, et al.* (2011). Triggering of a novel intrinsic apoptosis pathway by the kinase inhibitor staurosporine: activation of caspase-9 in the absence of Apaf-1. Faseb J *25*, 3250-3261.

Mathieu, C., Jozan, S., Mazars, P., Come, M.G., Moisand, A., and Valette, A. (1995). Density-dependent induction of apoptosis by transforming growth factor-beta 1 in a human ovarian carcinoma cell line. Exp Cell Res *216*, 13-20.

Meikrantz, W., and Schlegel, R. (1995). Apoptosis and the cell cycle. J Cell Biochem *58*, 160-174.

Mercille, S., and Massie, B. (1994a). Induction of apoptosis in nutrient-deprived cultures of hybridoma and myeloma cells. Biotechnol Bioeng *44*, 1140-1154.

Mercille, S., and Massie, B. (1994b). Induction of apoptosis in oxygen-deprived cultures of hybridoma cells. Cytotechnology *15*, 117-128.

Merten, O.-W., Palfi, G. E., Klement, G., Steindl, F. (1987). Specific kinetic patterns of production of monoclonal antibodies in batch cultures and consequences on fermentation processes In Modern Approaches to Animal Cell Technology, R.E.a.G. Spier, J. B., ed. (Oxford: Butterworth).

Miao, H.Y., Dykes, C., Demeter, L.M., and Wu, H.L. (2009). Differential Equation Modeling of HIV Viral Fitness Experiments: Model Identification, Model Selection, and Multimodel Inference. Biometrics *65*, 292-300.

Miller, W.M., Blanch, H.W., and Wilke, C.R. (1988). A Kinetic-Analysis of Hybridoma Growth and Metabolism in Batch and Continuous Suspension-Culture - Effect of Nutrient Concentration, Dilution Rate, and Ph. Biotechnology and Bioengineering *32*, 947-965.

Miller, W.M., Wilke, C.R., and Blanch, H.W. (1987). Effects of Dissolved-Oxygen Concentration on Hybridoma Growth and Metabolism in Continuous Culture. J Cell Physiol *132*, 524-530.

Moles, C.G., Mendes, P., and Banga, J.R. (2003). Parameter estimation in biochemical pathways: a comparison of global optimization methods. Genome Res *13*, 2467-2474.

Moore, A., Donahue, C.J., Bauer, K.D., and Mather, J.P. (1998). Simultaneous measurement of cell cycle and apoptotic cell death. Methods Cell Biol *57*, 265-278.

Mortimore, G.E., and Poso, A.R. (1988). Amino-Acid Control of Intracellular Protein-Degradation. Method Enzymol *166*, 461-476.

Moser, A. (1985). Kinetics of batch fermentations. In Biotechnology, H.J.a.R. Rehm, G., ed. (CH Verlagsgesellschaft mbH, Federal Republic of Germany), p. 253.

Motulsky, H., and Christopoulos, A. (2004). Fitting models to biological data using linear and nonlinear regression. A practical approach guide to curve fitting (New York, Oxford University Press, Inc.).

Naderi, S. (2011). Metabolic Analysis of a CHO Cell Line in Batch and Fed-batch Culture. PhD Thesis. Chemical Engineering Department (University of Waterloo, Canada).

Naderi, S., Meshram, M., Wei, C., McConkey, B., Ingalls, B., Budman, H., and Scharer, J. (2011). Development of a mathematical model for evaluating the dynamics of normal and apoptotic Chinese hamster ovary cells. Biotechnol Prog *27*, 1197-1205.

Nakabayashi, J., and Sasaki, A. (2006). A mathematical model for apoptosome assembly: the optimal cytochrome c/Apaf-1 ratio. J Theor Biol *242*, 280-287.

Newland, M., Kamal, M.N., Greenfield, P.F., and Nielsen, L.K. (1994). Ammonia inhibition of hybridomas propagated in batch, fed-batch, and continuous culture. Biotechnol Bioeng *43*, 434-438.

Nguang, S.K., Chen, L.Z., and Chen, X.D. (2001). Optimisation of fed-batch culture of hybridoma cells using genetic algorithms. Isa T *40*, 381-389.

Nyberg, G.B., Balcarcel, R.R., Follstad, B.D., Stephanopoulos, G., and Wang, D.I.C. (1999). Metabolic effects on recombinant interferon-gamma glycosylation in continuous culture of Chinese hamster ovary cells. Biotechnology and Bioengineering *62*, 336-347.

Oda, E., Ohki, R., Murasawa, H., Nemoto, J., Shibue, T., Yamashita, T., Tokino, T., Taniguchi, T., and Tanaka, N. (2000). Noxa, a BH3-only member of the Bcl-2 family and candidate mediator of p53-induced apoptosis. Science *288*, 1053-1058.

Osman, J.J., Birch, J., and Varley, J. (2001). The response of GS-NS0 myeloma cells to pH shifts and pH perturbations. Biotechnol Bioeng *75*, 63-73.

Osman, J.J., Birch, J., and Varley, J. (2002). The response of GS-NS0 myeloma cells to single and multiple pH perturbations. Biotechnol Bioeng *79*, 398-407.

Overbeeke, R., Steffens-Nakken, H., Vermes, I., Reutelingsperger, C., and Haanen, C. (1998). Early features of apoptosis detected by four different flow cytometry assays. Apoptosis *3*, 115-121.

Ozturk, S.S., and Hu, W.H. (2006). Cell culture technology for pharmaceutical and cell-based therapies (Boca Raton, FL, CRC Press, Taylor &Francis Group).

Ozturk, S.S., and Palsson, B.O. (1990a). Effect of Initial Cell-Density on Hybridoma Growth, Metabolism, and Monoclonal-Antibody Production. Journal of Biotechnology *16*, 259-278.

Ozturk, S.S., and Palsson, B.O. (1990b). Effects of Dissolved-Oxygen on Hybridoma Cell-Growth, Metabolism, and Antibody-Production Kinetics in Continuous Culture. Biotechnol Progr *6*, 437-446.

Ozturk, S.S., and Palsson, B.O. (1991). Growth, metabolic, and antibody production kinetics of hybridoma cell culture: 1. Analysis of data from controlled batch reactors. Biotechnol Prog *7*, 471-480.

Ozturk, S.S., Riley, M.R., and Palsson, B.O. (1992). Effects of Ammonia and Lactate on Hybridoma Growth, Metabolism, and Antibody-Production. Biotechnology and Bioengineering *39*, 418-431.

Pallavicini, M.G., Deteresa, P.S., Rosette, C., Gray, J.W., and Wurm, F.M. (1990). Effects of Methotrexate on Transfected DNA Stability in Mammalian-Cells. Mol Cell Biol *10*, 401-404.

Pardee, A.B. (1974). A restriction point for control of normal animal cell proliferation. Proc Natl Acad Sci U S A *71*, 1286-1290.

Park, S.H., and Ryu, D.D.Y. (1994). Cell-Cycle Kinetics and Monoclonal-Antibody Productivity of Hybridoma Cells during Perfusion Culture. Biotechnology and Bioengineering *44*, 361-367.

Pattison, R.N., Swamy, J., Mendenhall, B., Hwang, C., and Frohlich, B.T. (2000). Measurement and control of dissolved carbon dioxide in mammalian cell culture processes using an in situ fiber optic chemical sensor. Biotechnol Prog *16*, 769-774.

Pavlou, A.K. (2003). Marketspace. Trends in biotherapeutics. J Commercial Biotechnology *9*, 358-363.

Pereira, N.A., and Song, Z. (2008). Some commonly used caspase substrates and inhibitors lack the specificity required to monitor individual caspase activity. Biochem Biophys Res Commun, *377*.

Petricciani, J.C. (1995). The acceptability of continuous cell lines: a personal and historical perspective,In: Beuvery EC, Gruffith JB, Ziejlemarker WP, eds. Animal Cell Technology: Developments towards the 21st Century (Dordrecht: Kluwer Academic Publishers).

Phillips, H.J. (1973). Dye exclusion tests for cell viability. In Tissue culture: methods and applications (New York, USA, Academic Press), p. 406.

Polyak, K., Kato, J.Y., Solomon, M.J., Sherr, C.J., Massague, J., Roberts, J.M., and Koff, A. (1994). p27(Kip1), a Cyclin-Cdk Inhibitor, Links Transforming Growth-Factor-Beta and Contact Inhibition to Cell-Cycle Arrest. Gene Dev *8*, 9-22.

Ramirez, O.T., and Mutharasan, R. (1990). Cell Cycle-Dependent and Growth Phase-Dependent Variations in Size Distribution, Antibody Productivity, and Oxygen-Demand in Hybridoma Cultures. Biotechnology and Bioengineering *36*, 839-848.

Rangamani, P., and Sirovich, L. (2007). Survival and apoptotic pathways initiated by TNF-alpha: modeling and predictions. Biotechnol Bioeng *97*, 1216-1229.

Rao, R.V., Castro-Obregon, S., Frankowski, H., Schuler, M., Stoka, V., del Rio, G., Bredesen, D.E., and Ellerby, H.M. (2002). Coupling endoplasmic reticulum stress to the cell death program. An Apaf-1-independent intrinsic pathway. J Biol Chem *277*, 21836-21842.

Ray, N.G., Karkare, S.B., and Runstadler, P.W. (1989). Cultivation of Hybridoma Cells in Continuous Cultures - Kinetics of Growth and Product Formation. Biotechnology and Bioengineering *33*, 724-730.

Reddy, S., and Miller, W.M. (1994). Effects of abrupt and gradual osmotic stress on antibody production and content in hybridoma cells that differ in production kinetics. Biotechnol Prog *10*, 165-173.

Rehm, M., Dussmann, H., Janicke, R.U., Tavare, J.M., Kogel, D., and Prehn, J.H. (2002). Single-cell fluorescence resonance energy transfer analysis demonstrates that caspase activation during apoptosis is a rapid process. Role of caspase-3. J Biol Chem *277*, 24506-24514.

Rehm, M., Huber, H.J., Dussmann, H., and Prehn, J.H. (2006). Systems analysis of effector caspase activation and its control by X-linked inhibitor of apoptosis protein. Embo J *25*, 4338-4349.

Rincheval, V., Renaud, F., Lemaire, C., Godefroy, N., Trotot, P., Boulo, V., Mignotte, B., and Vayssiere, J.L. (2002). Bcl-2 can promote p53-dependent senescence versus apoptosis without affecting the G1/S transition. Biochem Bioph Res Co *298*, 282-288.

Robinson, D.K., Chan, C.P., Yu Lp, C., Tsai, P.K., Tung, J., Seamans, T.C., Lenny, A.B., Lee, D.K., Irwin, J., and Silberklang, M. (1994). Characterization of a recombinant antibody produced in the course of a high yield fed-batch process. Biotechnol Bioeng *44*, 727-735.

Saeki, K., Yuo, A., Kato, M., Miyazono, K., Yazaki, Y., and Takaku, F. (1997). Cell density-dependent apoptosis in HL-60 cells, which is mediated by an unknown soluble factor, is inhibited by transforming growth factor beta1 and overexpression of Bcl-2. J Biol Chem *272*, 20003-20010.

Sanfeliu, A., and Stephanopoulos, G. (1999). Effect of glutamine limitation on the death of attached Chinese hamster ovary cells. Biotechnology and Bioengineering *64*, 46-53.

Sauer, P.W., Burky, J.E., Wesson, M.C., Sternard, H.D., and Qu, L. (2000). A high-yielding, generic fed-batch cell culture process for production of recombinant antibodies. Biotechnology and Bioengineering *67*, 585-597.

Schimmer, A.D. (2004). Inhibitor of apoptosis proteins: translating basic knowledge into clinical practice. Cancer Res *64*, 7183-7190.

Schmelzer, A.E., and Miller, W.M. (2002). Effects of osmoprotectant compounds on NCAM polysialylation under hyperosmotic stress and elevated pCO(2). Biotechnol Bioeng *77*, 359-368.

Schulte, M., Reiss, K., Lettau, M., Maretzky, T., Ludwig, A., Hartmann, D., de Strooper, B., Janssen, O., and Saftig, P. (2007). ADAM10 regulates FasL cell surface expression and modulates FasL-induced cytotoxicity and activation-induced cell death. Cell Death Differ *14*, 1040-1049.

Schulze-Osthoff, K., Ferrari, D., Los, M., Wesselborg, S., and Peter, M.E. (1998). Apoptosis signaling by death receptors. Eur J Biochem *254*, 439-459.

Schwarz, G. (1978). Estimating the dimensions of a model. Annals of Statistics *6*, 461–464.

Sen, S.M., Bagci, E.Z., and Camurdan, M.C. (2011). Bistability analysis of an apoptosis model in the presence of nitric oxide. Bull Math Biol *73*, 1952-1968.

155

Sherr, C.J., and Roberts, J.M. (1999). CDK inhibitors: positive and negative regulators of G1-phase progression. Genes Dev *13*, 1501-1512.

Shiao, Y.H., Lee, S.H., and Kasprzak, K.S. (1998). Cell cycle arrest, apoptosis and p53 expression in nickel(II) acetate-treated Chinese hamster ovary cells. Carcinogenesis *19*, 1203-1207.

Shu, C.H., and Liao, C.C. (2002). Optimization of L-phenylalanine production of Corynebacterium glutamicum under product feedback inhibition by elevated oxygen transfer rate. Biotechnology and Bioengineering *77*, 131-141.

Shuller, M., Kargi, F. (2002). Biopeocess Engineering, Basic Concepts, 2nd edition edn (Upper Saddle River, NJ, PH PTR).

Simpson, N.H., Singh, R.P., Perani, A., Goldenzon, C., and Al-Rubeai, M. (1998a). In hybridoma cultures, deprivation of any single amino acid leads to apoptotic death, which is suppressed by the expression of the bcl-2 gene. Biotechnology and Bioengineering *59*, 90-98.

Simpson, N.H., Singh, R.P., Perani, A., Goldenzon, C., and Al-Rubeai, M. (1998b). In hybridoma cultures, deprivation of any single amino acid leads to apoptotic death, which is suppressed by the expression of the bcl-2 gene. Biotechnol Bioeng *59*, 90-98.

Singh, R.P., Al-Rubeai, M., Gregory, C.D., and Emery, A.N. (1994). Cell death in bioreactors: a role for apoptosis. Biotechnol Bioeng *44*, 720-726.

Spencer, S.L., and Sorger, P.K. (2011). Measuring and Modeling Apoptosis in Single Cells. Cell *144*, 926-939.

Stucki, J.W., and Simon, H.U. (2005). Mathematical modeling of the regulation of caspase-3 activation and degradation. J Theor Biol *234*, 123-131.

Sugimoto, M., Martin, N., Wilks, D.P., Tamai, K., Huot, T.J., Pantoja, C., Okumura, K., Serrano, M., and Hara, E. (2002). Activation of cyclin D1-kinase in murine fibroblasts lacking both p21(Cip1) and p27(Kip1). Oncogene *21*, 8067-8074.

Susin, S.A., Lorenzo, H.K., Zamzami, N., Marzo, I., Snow, B.E., Brothers, G.M., Mangion, J., Jacotot, E., Costantini, P., Loeffler, M.*, et al.* (1999). Molecular characterization of mitochondrial apoptosis-inducing factor. Nature *397*, 441-446.

Suzuki, E., and Ollis, D.F. (1989). Cell-Cycle Model for Antibody-Production Kinetics. Biotechnology and Bioengineering *34*, 1398-1402.

Tang, Y.J., Ohashi, R., and Hamel, J.F.P. (2007). Perfusion culture of hybridoma cells for hyperproduction of IgG(2a) monoclonal antibody in a wave bioreactor-perfusion culture system. Biotechnol Progr *23*, 255-264.

Trampler, F., Sonderhoff, S.A., Pui, P.W., Kilburn, D.G., and Piret, J.M. (1994). Acoustic cell filter for high density perfusion culture of hybridoma cells. Biotechnology (N Y) *12*, 281-284.

Trummer, E., Fauland, K., Seidinger, S., Schriebl, K., Lattenmayer, C., Kunert, R., Vorauer-Uhl, K., Weik, R., Borth, N., Katinger, H., *et al.* (2006). Process parameter shifting: Part I. Effect of DOT, pH, and temperature on the performance of Epo-Fc expressing CHO cells cultivated in controlled batch bioreactors. Biotechnology and Bioengineering *94*, 1033-1044.

Vayttaden, S.J., Ajay, S.M., and Bhalla, U.S. (2004). A spectrum of models of signaling pathways. Chembiochem *5*, 1365-1374.

Ventura, B.D., Lemerle, C., Michalodimitrakis, K., and Serrano, L. (2006). From in vivo to in silico biology and back. Nature *443*, 527-533.

Vermes, I., Haanen, C., and Reutelingsperger, C. (2000). Flow cytometry of apoptotic cell death. J Immunol Methods *243*, 167-190.

Vriezen, N., and van Dijken, J.P. (1998). Fluxes and enzyme activities in central metabolism of myeloma cells grown in chemostat culture. Biotechnology and Bioengineering *59*, 28-39.

Wei, Y.Y., Naderi, S., Meshram, M., Budman, H., Scharer, J.M., Ingalls, B.P., and McConkey, B.J. (2011). Proteomics analysis of chinese hamster ovary cells undergoing apoptosis during prolonged cultivation. Cytotechnology.

Weinberger, M., Feng, L., Paul, A., Smith, D.L., Hontz, R.D., Smith, J.S., Vujcic, M., Singh, K.K., Huberman, J.A., and Burhans, W.C. (2007). DNA Replication Stress Is a Determinant of Chronological Lifespan in Budding Yeast. Plos One *2*.

Wiersma, E. (2000). Expression and characterization of human IgG specific for the RhD antigen. In Final Project Report (Toronto, Cangene Corporation), pp. 23.

Wilhelm, G., Schulz, J., and Hofmann, E. (1971). pH-dependence of aerobic glycolysis in ehrlich ascites tumour cells. Febs Lett *17*, 158-162.

Wlaschin, K.F., and Hu, W.S. (2006). Fedbatch culture and dynamic nutrient feeding. Adv Biochem Eng Biotechnol *101*, 43-74.

Wolf, B.B., and Green, D.R. (1999). Suicidal tendencies: apoptotic cell death by caspase family proteinases. J Biol Chem *274*, 20049-20052.

Wurm, F.M. (2004). Production of recombinant protein therapeutics in cultivated mammalian cells. Nature Biotechnology *22*, 1393-1398.

Xie, L., Nyberg, G., Gu, X., Li, H., Mollborn, F., and Wang, D.I. (1997). Gamma-interferon production and quality in stoichiometric fed-batch cultures of Chinese hamster ovary (CHO) cells under serum-free conditions. Biotechnol Bioeng *56*, 577-582.

Xie, L., and Wang, D.I. (1994). Fed-batch cultivation of animal cells using different medium design concepts and feeding strategies. Biotechnol Bioeng *43*, 1175-1189.

Xie, L., and Wang, D.I. (1996). High cell density and high monoclonal antibody production through medium design and rational control in a bioreactor. Biotechnol Bioeng *51*, 725-729.

Xie, L.Z., and Wang, D.I.C. (1997). Integrated approaches to the design of media and feeding strategies for fed-batch cultures of animal cells. Trends Biotechnol *15*, 109-113.

Yang, J.D., Angelillo, Y., Chaudhry, M., Goldenberg, C., and Goldenberg, D.M. (2000). Achievement of high cell density and high antibody productivity by a controlled-fed perfusion bioreactor process. Biotechnology and Bioengineering *69*, 74-82.

Yang, M., and Butler, M. (2000). Effects of ammonia on CHO cell growth, erythropoietin production, and glycosylation. Biotechnol Bioeng *68*, 370-380.

Yao, K.Z., Shaw, B.M., Kou, B., McAuley, K.B., and Bacon, D.W. (2003). Modeling ethylene/butene copolymerization with multi-site catalysts: Parameter estimability and experimental design. Polym React Eng *11*, 563-588.

Yoon, S.K., Choi, S.L., Song, J.Y., and Lee, G.M. (2005). Effect of culture pH on erythropoietin production by chinese hamster ovary cells grown in suspension at 32.5 and 37.0 degrees C. Biotechnology and Bioengineering *89*, 345-356.

Yoshikawa, K. (2000). Cell cycle regulators in neural stem cells and postmitotic neurons. Neurosci Res *37*, 1-14.

Zha, J., Weiler, S., Oh, K.J., Wei, M.C., and Korsmeyer, S.J. (2000). Posttranslational N-myristoylation of BID as a molecular switch for targeting mitochondria and apoptosis. Science *290*, 1761-1765.

Zhang, F., Sun, X.M., Yi, X.P., and Zhang, Y.X. (2006). Metabolic characteristics of recombinant Chinese hamster ovary cells expressing glutamine synthetase in presence and absence of glutamine. Cytotechnology *51*, 21-28.

Zhang, X., Li, J., Sejas, D.P., and Pang, Q. (2005). The ATM/p53/p21 pathway influences cell fate decision between apoptosis and senescence in reoxygenated hematopoietic progenitor cells. J Biol Chem *280*, 19635-19640.

Zhang, X.D., Gillespie, S.K., and Hersey, P. (2004). Staurosporine induces apoptosis of melanoma by both caspase-dependent and -independent apoptotic pathways. Mol Cancer Ther *3*, 187-197.

Zhou, R., Mazurchuk, R.V., Tamburlin, J.H., Harrold, J.M., Mager, D.E., and Straubinger, R.M. (2010). Differential pharmacodynamic effects of paclitaxel formulations in an intracranial rat brain tumor model. J Pharmacol Exp Ther *332*, 479-488.

Zhu, M.M., Goyal, A., Rank, D.L., Gupta, S.K., Vanden Boom, T., and Lee, S.S. (2005). Effects of elevated pCO_2 and osmolality on growth of CHO cells and production of antibody-fusion protein B1: a case study. Biotechnol Prog *21*, 70-77.

Zong, W.X., Li, C., Hatzivassiliou, G., Lindsten, T., Yu, Q.C., Yuan, J., and Thompson, C.B. (2003). Bax and Bak can localize to the endoplasmic reticulum to initiate apoptosis. J Cell Biol *162*, 59-69.